THE UNIVERSITY OF CHICAGO

THE IMPACT OF SUBSTRATE INTERACTION IN DIRECTED SELF-ASSEMBLY OF SYMMETRIC DIBLOCK COPOLYMER THIN FILMS

A DISSERTATION SUBMITTED TO

THE FACULTY OF THE INSTITUTE FOR MOLECULAR ENGINEERING

IN CANDIDACY FOR THE DEGREE OF

DOCTOR OF PHILOSOPHY

BY

ROBERT SEIDEL

CHICAGO, ILLINOIS

DECEMBER 2015

To my Anya, without whom none of this would have any meaning,

and to Joseph, who brightens my every day

TABLE OF CONTENTS

List of Tables

List of Figures

List of Abbreviations and Symbols

χ: Flory-Huggins interaction parameter

AFM: atomic force microscopy

BCP: block copolymer

DSA: directed self-assembly

FOV: field of view

GISAXS: grazing incidence small-angle x-ray scattering

HVM: high-volume manufacturing

L_0: natural periodicity of a block copolymer

L_S: pitch of chemical pattern

LbL: layer-by-layer

LER: line edge roughness

LiNe flow: Liu-Nealey flow

-NH_2: primary amine (functionality)

OAI: off-axis illumination

-OH: hydroxyl (functionality)

PMMA: poly(methyl methacrylate)

PS: polystyrene

P(S-*b*-MMA): poly(styrene-*block*-methyl methacrylate)

P(S-*r*-MMA): poly(styrene-*random*-methyl methacrylate)

R2R: roll-to-roll processing

SEM: scanning electron microscope

SiN: silicon nitride

W: guide stripe width

WCA: water contact angle

X-PMMA: crosslinked poly(methyl methacrylate)

X-PS: crosslinked polystyrene

ACKNOWLEDGMENTS

It's been a long road getting here, and I wouldn't have made it without the help of countless other individuals who have supported me as mentors, guides, collaborators, and friends. I don't know where I'd be without them.

My parents Mark and Catherine gave me a warm, loving home and an example which I strive to emulate. They always put their children first, and I am only now beginning to fully appreciate the many years of tireless effort they put into raising the six of us. My father was a special inspiration for my graduate work, as I distinctly remember the pride I felt when he earned his PhD in engineering at the end of my 3rd grade school year. Somehow I always knew that I'd follow in his footsteps, though I little dreamed of the effort it would entail. To think that he did it all while raising us older four and that my mother worked to provide for us at the same time gives me newfound respect for everything they did. Mom and Dad, thank you. Of course, growing up as the oldest of six brought its own joys and struggles, but my younger siblings made and continue to make me a better person. Ruthanna, Timothy, αδ. Γαβριηλία (Christina), John, and Stephen: you guys are great and I look forward to many more happy memories with you.

Family has always been an important part of my life and my many relatives have always been there to support me in any way possible even without being asked. I had the great privilege of knowing all four of my grandparents quite well, and each of them left me an indelible mark in raising me. My aunts and uncles in the Seidel and Mamalakis clans, along with my 50-odd cousins, have been there to laugh and cry and worry and exult with me. They were instrumental in getting me down the home stretch and now share in my relief and satisfaction in finishing.

To my PhD advisor and graduate mentor of the last five years, Professor Paul Nealey, I owe an immense debt of gratitude. He was patient and encouraging even when my results were less

than hoped for; thanks to his efforts and through his collaborations, I was able to gain valuable perspective and experience, and if I don't go far with where he's gotten me it will be entirely my own fault. I have been especially lucky to work with his close friend Professor Juan de Pablo, whom I consider a second mentor from working with him both directly and through his students. Professor Matt Tirrell at the University of Chicago and Professors David Lynn, Mark Ediger, and Michael Graham at the University of Wisconsin, Madison were a further source of wonderful help and insight. Truly, I have been privileged to stand on the shoulders of giants.

Of course, just getting into graduate school would not have been possible without the help of many other teachers over the years. Professors C. Grant Willson, Nicholas Peppas, Venkat Ganesan, Thomas Truskett, and many more were instrumental in shaping my path in college.

On a more personal note, my life over the years has been enriched by the friendship of countless people: old and young, guys and gals, classmates or coworkers or fellow parishioners. I can't thank each of you by name, but a few of you deserve especial recognition for the special times we've shared as students. In no particular order and at the risk of omitting some good friends, Aaron Fluitt, Tyler Roberts, Daman Khaira, Ben Wilson, and Peter Mushenheim from my entering class at UW and several of you in continuation at UChicago, what a wild ride! And now we're all at the finish line and going our separate ways, but I hope our future paths cross early and often. Congratulations on graduation and good luck in your futures, not that any of you need it.

Life in the Nealey lab is always interesting, and the people who make up the group are what got me through the low points. I am especially grateful to Chris Thode, Charlie Liu, Shengjiang Ji, Paulina Rincon, Hyo Seon Suh, and Lingshu Wan for passing along their experience and wisdom and to Jiaxing Ren, Xuanxuan Chen, Yu Kambe, and Moshe Dolejsi for the pleasure of

working alongside you on various projects. Good luck in your studies! A big thank-you as well to Adam Broderick, Matt Carter, and Grant Garner for your generous help in our collaborative work.

Let's see, am I forgetting anyone? Oh, well, I guess there's Lance. ☺ Roommate for years, coworker at imec, fellow-presenter at conferences, and travel partner across the world, you mentored me on subjects from juggling bean bags and attempting to unicycle to polymer physics and cutting-edge commercial technology. Good luck in Boise!

During my 18 months at imec in Leuven, Belgium, I learned so much from so many friends that it would be impossible to name you all: Roel Gronheid, along with Todd, Hari, Jan, Alex, Ainhoa, Kathleen, Safak, Yu-Tsung, Doni, BT, Yi, Youngjun….the list goes on. Arjun Singh deserves a special shout-out: his keen insight delivered with that unique charm of a devastatingly biting wit is a memory I'll always genuinely cherish.

Finally, in the spirit of saving the best for last, there are three people whom I lean on more than anything, who help and support me without fail, who bring strength and color to my life at the toughest times, and who are always shaping me into a better person. My Γέροντα, Fr. Dositheos, abbot of Holy Archangels Monastery and my spiritual father, turned my life around when I needed it most; God alone knows what his prayers and guidance mean to me. Even closer to me is my daily joy and constant support, my dearest wife Anya. How can I ever begin to thank you for your tireless, uncomplaining, selfless devotion to our family? I love you more than even I know, and that love deepens every day. The past three years have been full of amazing memories, and I look forward to many more happy years with you. And finally, the fatling, mijn Jozefke, little Joseph, whose unflagging energy, contagious smile, and unconditional love motivate me in so many ways. May you always brighten my days as you do now, and may you preserve your joy, peace, and sanity by never embarking on a PhD.

ABSTRACT

Block copolymers (BCP) are a class of materials that have attracted significant attention due to their ability to self-assemble into dense arrays of nanoscale features. These materials are being investigated for their use in applications such as nanolithography, but for commercial implementation require the ability to control or direct the self-assembly process. Chemoepitaxial directed self-assembly (DSA) is one avenue to achieving this control, where a BCP thin film self-assembles in the presence of precisely defined chemical boundary conditions. In such a process, the equilibrium structure of the BCP film and the kinetic pathways it evolves along to reach equilibrium are both a function of the thermodynamic landscape, which is in turn controlled by the chemical pattern. This thesis contributes to the significant body of work attempting to detail the relationship between chemical pattern parameters and the thermodynamics of assembly (both kinetic and equilibrium). We restrict our investigation to the assembly of lamellae-forming diblock copolymers on line/space chemical patterns that employ density multiplication, with a focus on developing technology for nanopatterning beyond the resolution limit of traditional lithography. In the first chapter we introduce the fundamental ideas of BCP DSA and develop the concepts of free energy balance that are crucial to framing the discussion in the following chapters. The second chapter explores using poly(methyl methacrylate) as a guide material and shows how the greater strength of guiding interaction for this system has the ability to guide complex, frustrated non-bulk morphologies. The third chapter develops a novel concept of using process conditions to generate so-called ‘three-tone’ chemical patterns with multiple guiding regions per patterned stripe. The fourth chapter looks at how guide stripe strength impacts and affects assembly kinetics, equilibrium structure, and process metrics such as line edge roughness (LER) and size of process window. It also introduces an analysis technique for evaluating assembly kinetics with an emphasis

on defect annihilation. The fifth chapter seeks to identify more thoroughly the root causes of LER in BCP line/space DSA by investigating a number of factors. The sixth and final full chapter describes initial success in the effort to extend the concepts of BCP DSA on patterned planar substrates to flexible or three-dimensional substrates (for roll-to-roll applications) by using functional layer-by-layer deposited films. Our final conclusion touches on the ideas of nucleation of self-assembled BCP structures and how they relate to kinetic pathways and timescales of assembly.

CHAPTER 1: INTRODUCTION

1.1 Technological Motivation

In recent years, nanoscale developments have come to dominate the forefront of many technologies. This explosion of nanotechnology has led to the development of nanoelectricalmechanical systems,[1] lab-on-a-chip biological devices,[2] energy storage media,[3] separations technology,[4-6] and drug delivery,[7-8] among other applications. The ability to design and manufacture at the nanoscopic level has opened up a hitherto unknown field of possibilities, enabling among other ideas the development of the internet of things (IoT).[9-10] Carbon nanotubes (CNT), nanoporous membranes, biomimetics, and nanoparticles are just a few of the materials with nanoscale dimensions that are now finding use in common consumer items ranging from cosmetics to sports gear, and the number of products is only growing.

One other field where nanoscale development has been strongly felt is in the field of electronics manufacturing. In 1965, Intel co-founder Gordon Moore made his now famous observation about the rapid increase in transistor density and hence computing power.[11] According to "Moore's Law," as it is commonly known, the number of transistors per given area doubles approximately every 18-24 months. This observation has become something of a self-fulfilling prophecy; it is used to project target roadmaps for technological advances and continued improvement in electronics manufacturing.[12] To date, the longevity of Moore's law has been extended repeatedly through the development of new technology in both manufacturing processes and device architecture. Photolithography, or the use of light to create patterns in a light-sensitive material known as a photoresist, has been used for several decades now as the manufacturing process of choice. Advances such as the shift from contact to proximity printing, the use of reticles and

steppers instead of projection masks, and improvements in resist chemistry have all contributed to the extension of Moore's law.

Concurrent with all the other improvements in patterning technology, industry has also tried to adopt patterning with shorter wavelength light, since the theoretical resolution limit is proportional to the wavelength of light used. Excimer lasers that produced 248 nm light were the most popular sources and are still in use today, though more advanced tools use 193 nm light. At smaller wavelengths, however, light is absorbed by air, necessitating the use of high vacuum in any tools that employ shorter wavelength light. Development of such an exposure tool (using 13.5 nm light, in the extreme ultraviolet or 'EUV' range) has been ongoing for many years but has suffered from numerous setbacks and delays. To continue to advance lithography, numerous other tricks have been employed including the use of immersion fluids, dual-tone resists, and double-patterning techniques. Currently, the theoretical limit to resolution for a pattern of equal lines and spaces using immersion lithography is just below 70 nm, with practical considerations revising that number upward. There are a handful of technologies that have been identified as likely candidates for further patterning advances, including spacer-defined double-patterning (SADP), nanoimprint lithography, extreme ultraviolet patterning (EUV), and litho-etch-litho-etch multiple patterning (LE^n).

1.2 Block Copolymers and Directed Self-Assembly

One additional technology that has attracted a growing degree of attention is the use of self-assembling materials, in particular block copolymers (BCP).[13] Block copolymers are polymer chains composed of two or more blocks of distinct chemistry joined by a covalent bond. By careful selection of the block chemistries, BCPs can be synthesized that have a moderate degree of unfavorable interaction between the blocks, leading to a repulsion between the blocks. When a

system of many of these molecules is assembled, the similar blocks of different polymers associate together, leading to phase-separation at the molecular length scale. By controlling the size of the polymer, the dimensions of each phase can be tuned. Diblock copolymers, or BCPs with exactly two distinct chemistries, separate to form phases in a range of morphologies, including dense arrays of spheres, cylinders, or lamellae with spaced at regular intervals, with the periodicity of the structures represented by L_0. The exact morphology formed is a function of the relative size of the two blocks as well as the degree of dissimilarity between the chemistries, quantified in the Flory-Huggins interaction parameter χ (chi). For this study, unless otherwise stated we restrict our discussion to assembly of roughly symmetric and therefore lamellae-forming block copolymers, where L_0 is defined as the period of the bulk lamellae.

Since BCP systems self-assemble at the molecular level into dense arrays of regular features,[14] they can be used to generate structures at length scales of 5-50 nm, or much smaller than the resolution limit for immersion lithography. This self-assembly process is thermodynamically driven: the system evolves to minimize its total free energy by striking a balance between the various enthalpic and entropic contributions. In order to control placement and orientation of these features, however, the bottom-up self-assembly process must be directed through some sort of external field or boundary condition. One example of this concept of directed self-assembly (DSA) is chemoepitaxy of block copolymer thin films, where the BCP system is assembled on a patterned substrate consisting of precisely defined regions of tunable chemistry.[15] By introducing these chemical boundary conditions, the system's free energy balance is changed. Some terms are modified and new ones are added, yet the overarching concept remains the same: the system – BCP film taken together with patterned substrate – seeks to assemble in a way that minimizes its overall free energy. It can therefore be seen that the final equilibrium structure of a BCP thin film

is a function of the pattern geometry and chemistry. Moreover, since the assembly mechanism of the system is also bottom-up in nature, the kinetic pathways along which the system evolves are dictated by its free energy landscape.

A great deal of work has gone into understanding the interplay between pattern parameters and the thermodynamics of assembly (both kinetic and equilibrium).[16] Extensive studies have given insight into many aspects of the system, and this thesis continues those efforts. We have specifically studied chemoepitaxial DSA with density multiplication, where the chemical pattern consists of alternating guide stripes preferential to one of the BCP chemistries and regions of background chemistry.[17-18] The distinguishing feature of such a chemical pattern is that the guide stripe pitch L_S is an integer multiple *n* of the natural periodicity of the block copolymer L_0. Consequently, when DSA on these sparse patterns is successful, the lamellae interpolate between the guide stripes at a resolution *n* times greater than that of the chemical pattern. For the majority of this work, the BCP lamellae L_0 = 28 nm, which can achieve 3x density multiplication on a pattern with pitch L_S = 84 nm. Through density multiplication, BCP DSA can be used as a resolution enhancement technique to access dimensions below the patterning limit of conventional lithography.

There are several challenges that must be overcome before full industrial implementation of BCP DSA is achieved. Generating optimized patterns with the proper geometry and chemistry requires application-specific development of materials and techniques,[19] but optimization of that development in turn requires a rigorous understanding on multiple levels of the science and technology underlying the overall process. Multiple methods for fabricating chemical patterns have been developed, but we will focus primarily on the use of the Liu-Nealey (LiNe) flow,[20] specifically in its implementation on 300 mm all-track tools in the R&D labs of imec (Leuven,

Belgium)[21-22] where much of this work was performed. Optimization of process technology is heavily invested in understanding the root cause of defectivity and line-edge roughness (LER) in BCP DSA, as current levels are above industry tolerance.[22-23] However, as mentioned briefly earlier, the thermodynamics of assembly – controlled by the chemical boundary conditions imposed by the chemical pattern – are what dictate not only the equilibrium and any metastable morphologies but also the minimum free energy pathways (MFEP) linking these states. Since many of the defects observed appear to be kinetically trapped states that heal over time, a thorough understanding of the fundamental thermodynamics at play, specifically in the context of the role played by the chemical pattern, is crucial to further progress on this front.

This, then, is the motivation for our current work: in trying to achieve the highest resolution possible with BCP structures, we find it necessary to explore and probe all the thermodynamic factors at play. We will first describe in detail the LiNe flow used to fabricate chemical patterns and note the characteristics of the patterns so generated. Next we will consider the free energy of a BCP film assembled on top of such a pattern in the context of chemical boundary conditions. Finally we will touch briefly on efforts to identify the root causes of defectivity in BCP DSA and show where our efforts fit into the massive undertaking of implementing this technology for next-generation nanolithography.

1.3 The Liu-Nealey (LiNe) Flow

For any chemoepitaxial DSA process, the most important step is generation of well-defined chemical patterns. As mentioned above, these patterns dictate the chemical boundary conditions of the system and therefore the equilibrium configuration of the overlying self-assembled BCP film. For DSA of line-space BCP arrays, the Liu-Nealey (LiNe) flow was developed and allowed

independent control of the relevant geometric and chemical parameters of the fabricated chemical patterns (Figure 1.1).

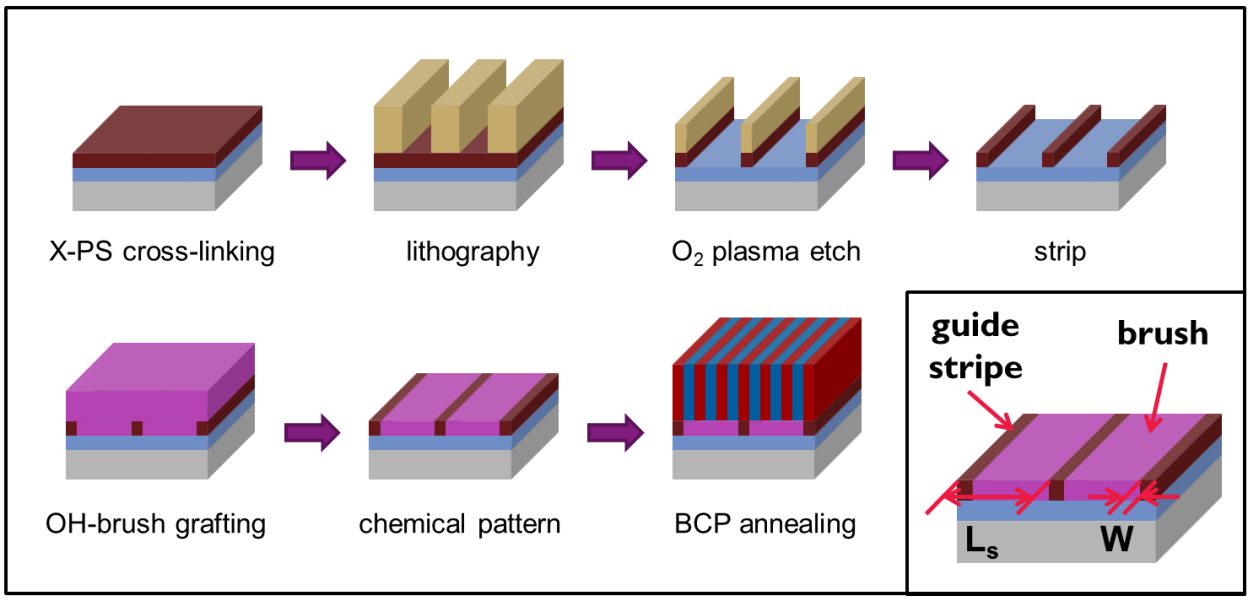

Figure 1.1: A schematic representation of the Liu-Nealey (LiNe) flow. A cross-linked polymer mat (in this case polystyrene) is patterned with photoresist and trim-etched to make a sparse pattern of lines, which are then backfilled with an end-grafted polymer brush. The resulting chemical pattern is then used to direct the self-assembly of a BCP thin film.

In this flow, the relevant geometric parameters are the spacing (L_S) and width (W) of the guide stripes and the chemistry of the guide stripe and brush regions. The chemistries are controlled directly by the material selection in the mat and brush grafting steps; the guide stripe pitch is dictated by the lithography step, and the guide stripe width is controlled by the initial lithographic and subsequent plasma trim etch step. Each of these parameters can be independently controlled, with the end result that the chemical pattern can be highly tuned and optimized. This flow was first developed at the laboratory benchtop level and later scaled up for use on full 300 mm wafer production tools, with appropriate changes to account for solvent compatibility.

The scale-up of this flow and subsequent studies have yielded additional insight into BCP thermodynamics and kinetics of assembly. The ability to integrate commercially rigorous process control into DSA production has allowed further optimization of the flow and also enabled high-

throughput metrology and review. At the same time, the fundamental physics remains the same as for the small-scale laboratory setup, and a proper understanding of the results from industry tools – which comprise the majority of this thesis – requires a careful analysis of the thermodynamics involved. We begin therefore by exploring simple cases and building up to the more complicated concepts explored in more depth in later chapters.

1.4 Thermodynamics of Thin-Film Block Copolymer Assembly on Chemical Patterns

1.4.1 Overview

Any discussion of thermodynamics should commence by recognizing the key concepts involved: free energy, kinetics, and equilibrium. A system tends towards states that minimize its free energy, which itself contains information about the enthalpy and entropy of the particular state. The system explores configuration space through fluctuations as it adopts various states, spending more time in those with lower free energy according to Boltzmann statistics. This move through different states and the rate at which such a move occurs comprise the kinetics of the system as it tends toward equilibrium, the state with the lowest free energy.

The free energy F_{total} of a thin film of BCP takes into account several different contributions (Figure 1.2): the conformational energy free energy of each block of copolymer, the interfacial energy between domains of blocks, the surface energy at the top surface of the film, and the interfacial energy component between the bottom surface and the blocks of the BCP with which it is in contact. With a chemical pattern, the equation is further complicated by the respective, relative interaction of the guiding and background regions of the pattern with the blocks of the BCP thin film.

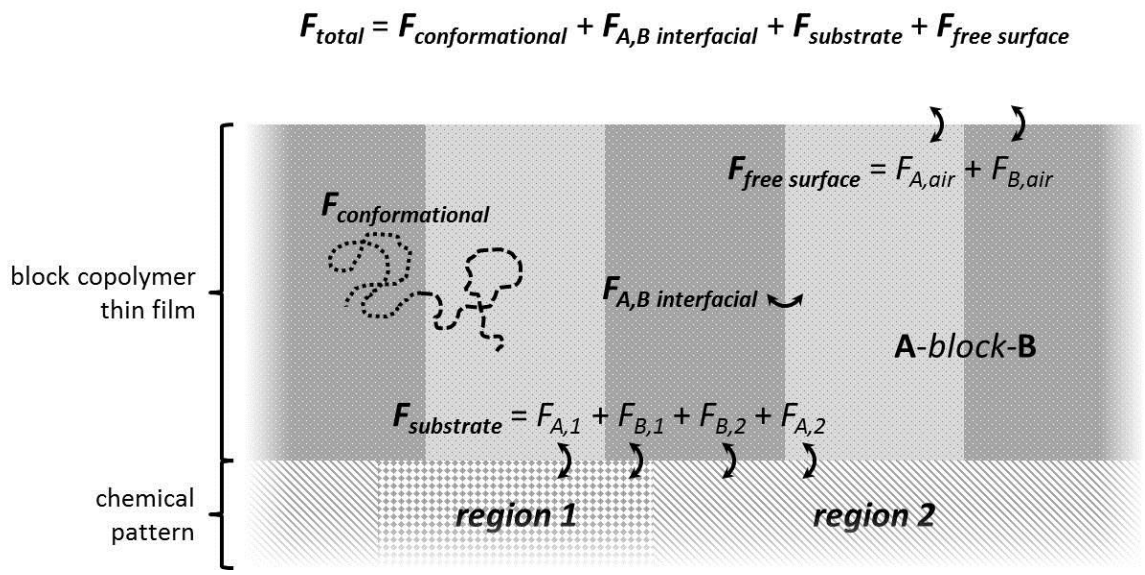

Figure 1.2: The components of the free energy equation for a block copolymer thin film on a chemically patterned surface. The terms of the form '$F_{i,j}$' denote the free energy of interaction between two phases. Conformational free energy is also sometimes referred to as the entropic term, as it captures the entropic nature of the individual polymer configuration.

To simplify this section, unless stated explicitly otherwise, we will initially limit our discussion to considering incompressible thin films of monodisperse, symmetric (having approximately equal block lengths and therefore lamellae-forming) diblock A-B copolymers with a free (exposed to air) surface. We will further simplify the discussion by assuming that the bulk block copolymer forms discrete A and B domains at equilibrium, and that the surface energies of the two domains are similar ($\gamma_A \approx \gamma_B$) at the annealing temperature. These assumptions are true for our example system of polystyrene-*block*-poly(methyl methacrylate) (PS-*b*-PMMA).

Consider a BCP thin film extending infinitely across an unpatterned surface that not preferential to either block of the BCP. The non-preferential nature of the substrate, coupled with our assumption in the preceding paragraph of equal surface energies of the two blocks, means that there is no enthalpic preference for any particular configuration, and instead entropy is the only contributing factor. The result is lamellae oriented perpendicularly to the substrate, similar to the lamellae in Figure 1.2. If the lamellae lack any long-range lateral order, at the free surface they

form “fingerprint” structures.[24] At equilibrium, our hypothetical film would consist of very large grains of lamellae with extremely long-range order. However, these grains would be randomly oriented and also randomly positioned on the substrate. Such an assembled film – with no positional or orientation control of the BCP domains – is not useful for applications where such control is necessary. The addition of a chemically patterned substrate, in which the guiding and background regions of the substrate are preferential to different blocks of the BCP, modifies the free energy of the system. When the film is in contact with a chemical pattern, there is an enthalpic gain to have similar chemistries in contact (and a corresponding penalty when dissimilar chemistries are adjacent), thereby directing the assembly to assume a specific geometry or pattern.

1.4.2 Chemical patterns

To further explore the effect of chemical patterns on the equilibration of a thin film of BCP, consider the BCP described above on an ideal chemical pattern (perfectly patterned with areas of surface chemistry exactly matching that of the respective BCP domains, and at the exact size and spacing of said domains ($L_S = L_0$)). A BCP film on top of such a chemical pattern would, at equilibrium, seek to minimize its free energy by minimizing the amount of dissimilar interactions (minimizing enthalpy) while maximizing entropy. The resulting equilibrium structure would consist of semi-infinite parallel lines of alternating composition, aligned perfectly with the regions of the underlying chemical pattern. The alignment of the BCP domains to the regions of the chemical pattern causes the block copolymer morphology to be registered to the chemical pattern. These lines would only be broken by occasional high (but finite) free energy defect structures in the registration and lateral order, such as the dislocations or disclinations shown in Figure 1.3. According to Boltzmann statistics, these defects would be present at equilibrium, but at vanishingly small numbers; current estimates put their equilibrium concentration at smaller than

one per 10^{100} m^2 of registered film.[25] (For comparison, the area of a disk the size of our galaxy is around 10^{40} m^2, so this concentration is so small as to be zero in any practical consideration; these structures are mentioned only to preserve the fidelity of this hypothetical system.)

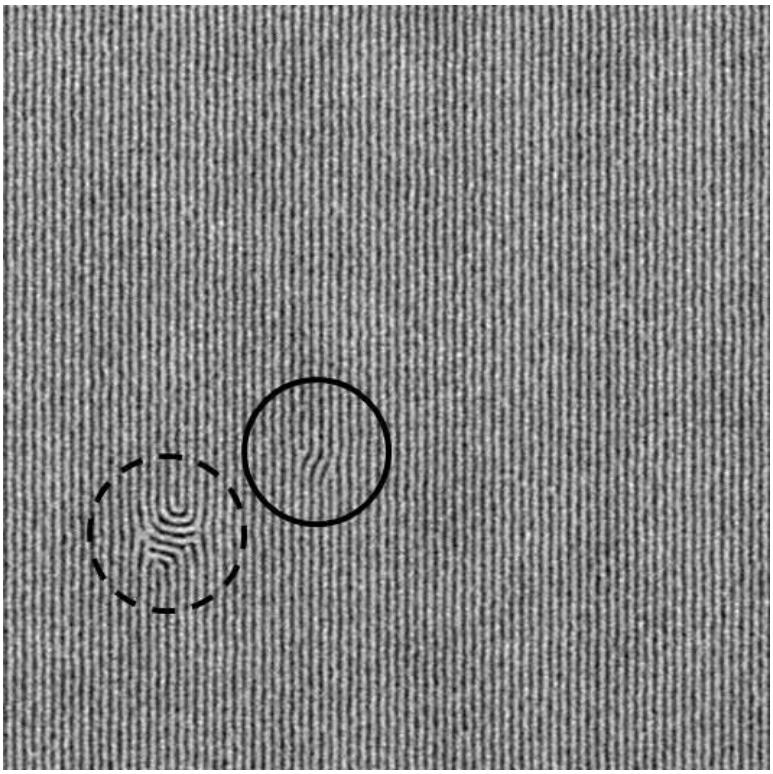

Figure 1.3: Top-down SEM of a large field of registered lamellae on a chemical pattern. The defect within the solid circle is a dislocation pair; that inside the dashed circle is a disclination cluster. Both defect types are present at effectively zero concentration at equilibrium.

Here we have touched briefly on a simple but powerful concept, central to the idea of bottom-up manufacturing: the free energy landscape that a self-assembling system explores can be modified to encourage that system to adopt a particular configuration. By introducing chemical boundary conditions, we create regions that have (for example) a lower enthalpy of interaction with one of the blocks, causing that block to preferentially wet that particular region. In more abstract thermodynamics terms, this has the effect of deepening certain free energy valleys or shifting or eliminating others, shaping the landscape to change its local and global minima as well as the pathways between them. The deeper the energy wells, the more time the system spends in

the corresponding configuration; the steeper the slopes of the energy pathways, the faster the system moves to the lower energy state. Conversely, moving away from the ideal chemical pattern described earlier modifies the free energy valleys. Shifting these valleys often corresponds to moving equilibrium towards frustrated non-bulk morphologies, while making the valleys shallower can cause a decrease in the degree of registration until the film becomes a randomly oriented fingerprint. There are many ways to modify that ideal pattern, changing either the geometric or chemical parameters. The figure of merit typically used to analyze the effect of this modification is the equilibrium (or quasi-equilibrium) degree of registration. Though the exact distinction between full vs. quasi-equilibrium structures can be challenging to discern for some systems, that distinction is not necessary in the scope of this discussion and we will for the sake of brevity refer to both collectively as simply "equilibrium."

1.4.3 Non-ideal chemical patterns

As mentioned above, an ideal chemical pattern will have $L_S = L_0$. If L_S is slightly larger or smaller than L_0, the system can choose to ignore the chemical pattern and relax to its unperturbed L_0, but then there is an enthalpic penalty as the BCP domains sit on dissimilar chemical pattern regions. Alternately, the individual chains can stretch or compress to fit the chemical pattern precisely, but that of course brings an entropic cost. Ultimately, a BCP film on such a substrate will choose the configuration that minimizes the overall free energy, accepting a degree of stretching/compressing but with increasing loss of registration as the chemical pattern moves further from the "ideal" geometry. Outside a certain range, registration is lost entirely and the film adopts a fingerprint (or otherwise unregistered) configuration; this range is about ±10% of the ideal L_S for lamellae on 1:1 chemical patterns. Similarly, changing the size (for example W in Figure 1)

of the chemical pattern regions relative to the BCP domains (rather than their spacing) can be tolerated but only up to a point.

The previous paragraph discusses changing the geometry of a chemical pattern, but it is also worthwhile to consider the effect of modifying the guiding chemistry. Intuitively, one would expect that the stronger the interaction between the guiding region and the domain of the BCP, the deeper the free energy well, and the better the registration of the BCP film to the chemical pattern at equilibrium. Conversely, we expect the geometric incommensurability tolerance to decrease with decreasing strength of that interfacial interaction; this effect has been demonstrated experimentally.[26]

1.4.4 Density multiplication (DSA on sparse chemical patterns)

The ability of BCPs to self-assemble on sparse chemical patterns, with $L_S = nL_0$ (n an integer > 1), with some domains interpolating between guiding regions on the substrate thereby achieve feature density multiplication and a corresponding resolution enhancement, increases the utility of DSA of BCPs for nanodevice fabrication. As the degree of density multiplication increases, however, fewer domains of the BCP film are directly guided by the chemical pattern, and the tolerance for the L_S/L_0 incommensurability decreases. Additionally, for sparse chemical patterns, there is a fundamental difference, compared to 1:1 DSA, in the enthalpic nature of the interaction between thin film and substrate. On 1:1 chemical patterns, each region is wet by only a single BCP domain. For density multiplication, however, multiple domains assemble above each background region. The more similar that region is to the one block, the more dissimilar it must necessarily be to the other, and therefore, even at optimal dimensions, these regions contribute an enthalpic penalty to the free energy equation. For a surface that exhibits wetting behavior that is a linear combination of the two blocks, the quantity f can be defined as the percent similarity of

the background region of the substrate to the 'A' rather than the 'B' block of the BCP (so $f = 1$ corresponds to a surface exactly like A, while a value of f approaching 0 means the surface is similar to B). An approximation of the normalized BCP-substrate interfacial free energy follows:

$$F_{substrate} = \frac{1}{2n}\left(F_{A,guide} + (n-1)\cdot(1-f)\cdot\gamma_{A,B} + n\cdot f\cdot\gamma_{A,B}\right),$$

where $F_{\mathrm{A,guide}}$ is the free energy of the A domain on the guided stripe, n is the degree of multiplication, and $\gamma_{\mathrm{A,B}}$ is the interfacial energy between the two blocks.[20] It is readily apparent that the free energy of the system is a function of how similar the non-guiding region is to the unguided domain. A more subtle observation is that at different density multiplication factors, the minimum free energy state can be found at differing degrees of similarity (values of f). In an experimental setup using random copolymer brushes in the background regions, this prediction translates into a different optimum brush composition for different density multiplication factors. The higher the density multiplication, the more non-preferential the brush composition should be to achieve the lowest free energy structure.

In addition to research that has focused on the behavior of DSA of BCPs at or near optimum conditions, a large body of work has also been devoted to far more complicated systems. The confinement effects in thin films can exacerbate conflicting terms in the overall free energy equation, leading to frustrated morphologies reflective of the strong, localized interplay between enthalpy and entropy in these systems. Unexpected, bizarre structures have been theoretically predicted and experimentally demonstrated in cases of strong chemical patterns at highly exaggerated geometries.[27] Areas of high interfacial curvature, normally not seen because of their strong free energy penalty, are possible under these non-standard conditions. The confinement

effects can be further complicated if a second chemically patterned substrate is introduced at the top surface of the BCP thin film.[28] Although the rigorous solution to the free energy minimization equation for each of these systems is too complicated to derive in detail, the fundamental concepts remain the same. The (quasi-) equilibrium structure adopted by the BCP thin film is a fragilely balanced compromise in the tug-of-war between the different free energy terms. In order to fully understand the thermodynamics at play in the very complicated systems described above, it is sometimes easier to treat exhaustively the thermodynamics of more elementary cases. Instead of analyzing the highly tortuous bicontinuous structures described in some reports, we can study the less curved yet still frustrated morphologies of programmed bends on more standard chemical patterns.[18, 29] Note that in these cases the "defect" structures are actually part of the chemical pattern, so a well-registered film would look as if it had jogs or other non-equilibrium morphologies. The formation and persistence of these features provides insight into BCP thermodynamics in general but also, more specifically, a parallel way of studying the same structures on ideal chemical patterns. Furthermore, these nonstandard structures are an avenue to realization of the complex shapes required to engineer functional nanoelectronic or other devices through block copolymer patterning.

1.5 Kinetics of Thin-film BCP Assembly on Chemical Patterns

1.5.1 Overview

In addition to understanding the equilibrium and quasi-equilibrium structures, it is critical to consider the time required or kinetic pathways taken to reach those structures. Investigating the kinetics of the DSA system not only improves our understanding of the physics involved but also helps to identify industry-compatible production steps, where process time is a key metric. We

will start this section on kinetics by describing the kinetic process undergone by a BCP thin film as it goes from disorder towards equilibrium.

One distinction that is important to make is the difference between the terms "ordered" and "disordered." From a BCP physics point of view, the a disordered block copolymer system is one that has not undergone the order-disorder transition (ODT) that results in microphase separation and the formation of distinct microdomains; a disordered BCP is a single phase and exhibits no scattering peaks. Once the film is brought through ODT – either through cooling or, in the case of spin-casting from solution, removal of solvent – the film immediately becomes ordered; that is, it undergoes spinodal decomposition and the domains microphase separate, though vitrification prevents their mobility and rearrangement. A newly ordered film initially has very poor long-range order, though it still exhibits a distinctive 1^{st}-order peak in scattering experiments.

As the film equilibrates, the individual chains move and explore configuration space, diffusing through and along the ever-growing phase-separated domain interfaces. In so doing, they adopt more energetically favorable states, and the film develops towards its equilibrium configuration. In free energy space, the system moves downhill along the steepest gradient possible, at a rate proportional to the slope along that gradient. This means that in the absence of stabilizing impurities, areas of higher interfacial curvature such as disclinations tend to disappear first due to the steep free energy penalty of these structures. Lower free-energy structures such as dislocations can persist longer but eventually move to the lowest energy state, found at equilibrium. When assembling on a chemical pattern, the polymer movement is of course also strongly influenced by the presence of the various substrate regions, which modifies the free energy landscape and can provide a location for seeding growth of the specific BCP domains.

1.5.2 Time to equilibration

The time scales for the formation of equilibrium structures of polymer systems often can be nontrivial, as can be expected for a process involving macromolecular diffusion, and in fact sometimes can last indefinitely as a particular state becomes trapped with no way for entangled polymers to disentangle and alter their configuration or position. These states correspond to free energy wells with either very steep sidewalls or very long pathways to lower free energy states. However, the timescales can be shortened and the trapped states avoided by judicial selection of processing materials and conditions. Since diffusivity exhibits an Arrhenius dependence on temperature, one simple way to shorten maturation times is simply by elevating the temperature.[30] This approach, known as thermal annealing, has been thoroughly explored and is the method of choice for many processes. The temperature for thermal annealing must be carefully chosen so as not to exceed ODT or cause chemical modification of the polymer system.

As mentioned above, the presence of a chemical pattern can strongly influence the kinetics of assembly by modifying the free energy landscape. Often this behavior is exhibited in the form of much slower assembly on a non-ideal chemical pattern. For values of L_S incommensurate with L_0, even when the equilibrium morphology consists of arrays free of registration defects, the assembly still takes much longer than when $L_S = L_0$.[31] Similarly, when comparing stronger to weaker interactions in different chemical patterns, the shallower free energy wells corresponding to the weaker chemical interactions led to slower assembly.[16] Sparse chemical patterns (used for density multiplication) are another example of weaker chemical patterns and exhibit similarly slower assembly kinetics when compared to the behavior of films on 1:1 patterns.[32]

1.5.3 Kinetic pathways and trapped states (defects)

One topic of particular interest is mapping out the exact mechanism for how the equilibrium structure is achieved, especially the elimination of the final trapped defect states often seen in line-space patterns. These dislocation pairs have been calculated through simulations to be very high energy states, as they are areas of high interfacial curvature and extra interfacial area, and yet they are observed frequently even after long, high-temperature maturation processes. Ultimately, their persistence is not due to their being equilibrium or quasi-equilibrium states, but rather the very long free energy path between these states and the equilibrium state. Since these dislocations always occur in pairs, they have to independently diffuse towards each other through the registered film until they finally annihilate upon encountering one another.[33] The diffusivity of these structures has been determined experimentally and found to have widely differing values depending on whether the diffusion is happening along or across the direction of the line-space pattern. One can understand the factors involved in the persistence of non-equilibrium states in terms of the rearrangement of the polymer chains. In order to move across the line-space array, many polymers have to simultaneously rearrange, temporarily creating a much larger interfacial area between the blocks. In contrast, moving along a domain interface only requires diffusion of the polymer chains along that interface without any additional enthalpic penalty.

Ultimately, the kinetics of block copolymer assembly are dictated by the accessible free energy pathways that are available as a system tries to move from one configuration to another. Even when the final state has a much lower free energy than the initial state, assembly can still be slowed indefinitely by the presence of pathway barriers. These barriers can be in the form of higher-energy states along the configuration space path between the initial and final states[34] or they can be simply

due to a deepening of the initial-state well through the presence of some sort of stabilizing nucleation material.

The topics of defect analysis and annihilation in BCP DSA are among the most pressing today, and a great deal of both experimental and simulation work is ongoing in elucidating the mechanisms at play under a wide variety of conditions.[23, 35-36] As with many other engineering problems, the solution to this challenge lies in deepening our understanding of the fundamental physics and thermodynamics of these systems. Especially in the case of these thermodynamically-driven processes, it is crucial to identify as fully as possible their nuanced complexity in order to fully analyze and ultimately control defectivity in the directed self-assembly process.

1.6 References

1. Li, M.; Tang, H. X.; Roukes, M. L., Ultra-sensitive NEMS-based cantilevers for sensing, scanned probe and very high-frequency applications. *Nature Nanotechnology* **2007,** *2* (2), 114-120.

2. Qin, D.; Xia, Y. N.; Whitesides, G. M., Soft lithography for micro- and nanoscale patterning. *Nature Protocols* **2010,** *5* (3), 491-502.

3. Stoller, M. D.; Park, S. J.; Zhu, Y. W.; An, J. H.; Ruoff, R. S., Graphene-Based Ultracapacitors. *Nano Letters* **2008,** *8* (10), 3498-3502.

4. Zhang, J.; Albelda, M. T.; Liu, Y.; Canary, J. W., Chiral nanotechnology. *Chirality* **2005,** *17* (7), 404-418.

5. Egas, D. A.; Wirth, M. J., Fundamentals of Protein Separations: 50 Years of Nanotechnology, and Growing. In *Annual Review of Analytical Chemistry*, **2008**, pp 833-855.

6. Wiesner, M. R., Responsible development of nanotechnologies for water and wastewater treatment. *Water Science and Technology* **2006,** *53* (3), 45-51.

7. Ferrari, M., Cancer nanotechnology: Opportunities and challenges. *Nature Reviews Cancer* **2005,** *5* (3), 161-171.

8. Peer, D.; Karp, J. M.; Hong, S.; FaroKhzad, O. C.; Margalit, R.; Langer, R., Nanocarriers as an emerging platform for cancer therapy. *Nature Nanotechnology* **2007,** *2* (12), 751-760.

9. Akyildiz, I. F.; Jornet, J. M., THE INTERNET OF NANO-THINGS. *Ieee Wireless Communications* **2010,** *17* (6), 58-63.

10. Wang, Z. L., Toward self-powered sensor networks. *Nano Today* **2010,** *5* (6), 512-514.

11. Moore, G. E., Cramming more components onto integrated circuits (Reprinted from Electronics, pg 114-117, April 19, 1965). *Proceedings of the Ieee* **1998,** *86* (1), 82-85.

12. Mollick, E., Establishing Moore's law. *Ieee Annals of the History of Computing* **2006,** *28* (3), 62-75.

13. Hamley, I. W., Ordering in thin films of block copolymers: Fundamentals to potential applications. *Progress in Polymer Science* **2009,** *34* (11), 1161-1210.

14. Segalman, R. A., Patterning with block copolymer thin films. *Materials Science & Engineering R-Reports* **2005,** *48* (6), 191-226.

15. Craig, G. S. W.; Nealey, P. F., Self-assembly of block copolymers on lithographically defined nanopatterned substrates. *Journal of Photopolymer Science and Technology* **2007,** *20* (4), 511-517.

16. Edwards, E. W.; Stoykovich, M. P.; Muller, M.; Solak, H. H.; De Pablo, J. J.; Nealey, P. F., Mechanism and kinetics of ordering in diblock copolymer thin films on chemically nanopatterned substrates. *Journal of Polymer Science Part B-Polymer Physics* **2005,** *43* (23), 3444-3459.

17. Ruiz, R.; Kang, H.; Detcheverry, F. A.; Dobisz, E.; Kercher, D. S.; Albrecht, T. R.; de Pablo, J. J.; Nealey, P. F., Density multiplication and improved lithography by directed block copolymer assembly. *Science* **2008,** *321* (5891), 936-939.

18. Liu, G.; Thomas, C. S.; Craig, G. S. W.; Nealey, P. F., Integration of Density Multiplication in the Formation of Device-Oriented Structures by Directed Assembly of Block Copolymer-Homopolymer Blends. *Advanced Functional Materials* **2010,** *20* (8), 1251-1257.

19. Liu, C.-C.; Han, E.; Onses, M. S.; Thode, C. J.; Ji, S.; Gopalan, P.; Nealey, P. F., Fabrication of Lithographically Defined Chemically Patterned Polymer Brushes and Mats. *Macromolecules* **2011,** *44* (7), 1876-1885.

20. Liu, C.-C.; Ramirez-Hernandez, A.; Han, E.; Craig, G. S. W.; Tada, Y.; Yoshida, H.; Kang, H.; Ji, S.; Gopalan, P.; de Pablo, J. J.; Nealey, P. F., Chemical Patterns for Directed Self-Assembly of Lamellae-Forming Block Copolymers with Density Multiplication of Features. *Macromolecules* **2013,** *46* (4), 1415-1424.

21. Gronheid, R.; Delgadillo, P. R.; Singh, A.; Younkin, T. R.; Sayan, S.; Chan, B. T.; Van Look, L.; Bekaert, J.; Pollentier, I.; Nealey, P. F., Readying Directed Self-Assembly for Patterning in Semi-Conductor Manufacturing. *Journal of Photopolymer Science and Technology* **2013,** *26* (6), 779-791.

22. Delgadillo, P. A. R.; Gronheid, R.; Thode, C. J.; Wu, H.; Cao, Y.; Neisser, M.; Somervell, M.; Nafus, K.; Nealey, P. F., Implementation of a chemo-epitaxy flow for directed self-assembly on 300-mm wafer processing equipment. *Journal of Micro-Nanolithography Mems and Moems* **2012,** *11* (3).

23. Pathangi, H.; Chan, B. T.; Bayana, H.; Vandenbroeck, N.; Van den Heuvel, D.; Van Look, L.; Rincon-Delgadillo, P.; Cao, Y.; Kim, J.; Lin, G.; Parnell, D.; Nafus, K.; Harukawa, R.; Chikashi, I.; Polli, M.; D'Urzo, L.; Gronheid, R.; Nealeyg, P., Defect mitigation and root cause studies in 14 nm half-pitch chemo-epitaxy directed self-assembly LiNe flow. *Journal of Micro-Nanolithography Mems and Moems* **2015,** *14* (3).

24. Park, S.-M.; Ravindran, P.; La, Y.-H.; Craig, G. S. W.; Ferrier, N. J.; Nealey, P. F., Combinatorial generation and replication-directed assembly of complex and varied geometries with thin films of diblock copolymers. *Langmuir* **2007,** *23* (17), 9037-9045.

25. Nagpal, U.; Mueller, M.; Nealey, P. F.; de Pablo, J. J., Free Energy of Defects in Ordered Assemblies of Block Copolymer Domains. *Acs Macro Letters* **2012,** *1* (3), 418-422.

26. Edwards, E. W.; Montague, M. F.; Solak, H. H.; Hawker, C. J.; Nealey, P. F., Precise control over molecular dimensions of block-copolymer domains using the interfacial energy of chemically nanopatterned substrates. *Advanced Materials* **2004,** *16* (15), 1315-+.

27. Detcheverry, F. A.; Liu, G.; Nealey, P. F.; de Pablo, J. J., Interpolation in the Directed Assembly of Block Copolymers on Nanopatterned Substrates: Simulation and Experiments. *Macromolecules* **2010,** *43* (7), 3446-3454.

28. Ramirez-Hernandez, A.; Liu, G.; Nealey, P. F.; de Pablo, J. J., Symmetric Diblock Copolymers Confined by Two Nanopatterned Surfaces. *Macromolecules* **2012,** *45* (5), 2588-2596.

29. Stoykovich, M. P.; Muller, M.; Kim, S. O.; Solak, H. H.; Edwards, E. W.; de Pablo, J. J.; Nealey, P. F., Directed assembly of block copolymer blends into nonregular device-oriented structures. *Science* **2005,** *308* (5727), 1442-1446.

30. Welander, A. M.; Kang, H.; Stuen, K. O.; Solak, H. H.; Mueller, M.; de Pablo, J. J.; Nealey, P. F., Rapid directed assembly of block copolymer films at elevated temperatures. *Macromolecules* **2008,** *41* (8), 2759-2761.

31. Delgadillo, P. A. R. Origin of Defects in Directed Self-Assembly of Diblock Copolymers using Feature Multiplication. KU Leuven, Leuven, Belgium, **2014**.

32. Liu, G.; Delcambre, S. P.; Stuen, K. O.; Craig, G. S. W.; De Pablo, J. J.; Nealey, P. F.; Nygard, K.; Satapathy, D. K.; Bunk, O.; Solak, H. H., Mechanism and dynamics of block copolymer directed assembly with density multiplication on chemically patterned surfaces. *Journal of Vacuum Science & Technology B* **2010,** *28* (6), C6B13-C6B19.

33. Tong, Q.; Sibener, S. J., Visualization of Individual Defect Mobility and Annihilation within Cylinder-Forming Diblock Copolymer Thin Films on Nanopatterned Substrates. *Macromolecules* **2013,** *46* (21), 8538-8544.

34. Li, W.; Nealey, P. F.; de Pablo, J. J.; Mueller, M., Defect Removal in the Course of Directed Self-Assembly is Facilitated in the Vicinity of the Order-Disorder Transition. *Physical Review Letters* **2014,** *113* (16).

35. Hur, S.-M.; Khaira, G. S.; Ramirez-Hernandez, A.; Mueller, M.; Nealey, P. F.; de Pablo, J. J., Simulation of Defect Reduction in Block Copolymer Thin Films by Solvent Annealing. *Acs Macro Letters* **2015,** *4* (1), 11-15.

36. Delgadillo, P. R.; Suri, M.; Durant, S.; Cross, A.; Nagaswami, V. R.; Van Den Heuvel, D.; Gronheid, R.; Nealey, P., Defect source analysis of directed self-assembly process. *Journal of Micro-Nanolithography Mems and Moems* **2013,** *12* (3).

CHAPTER 2: THE USE OF CROSSLINKED POLY(METHYL METHACRYLATE) AS A GUIDING MATERIAL IN BLOCK COPOLYMER DIRECTED SELF-ASSEMBLY

2.1 Abstract

Chemical patterns consisting of alternating stripes of crosslinked polymer mats and random copolymer brushes have been used for directing the assembly of lamellae-forming block copolymers (BCP). To date, most of the track-level process development for commercial insertion of this technology for advanced patterning has focused on the use of crosslinked polystyrene (X-PS) mats, but this chemistry is susceptible to process modifications and weakened guiding ability. Here we conducted parallel studies to investigate the use of crosslinked poly(methyl methacrylate) X-PMMA instead and succeeded in making patterns with stronger guiding capability. The increased strength of interaction between guide stripe and guided domain results in the formation of complex non-bulk morphologies, where the exact morphology observed is a function of the corresponding chemical patterns guide stripe pitch L_S and width W. Experimental results are supported by theoretically-informed molecular simulations that give additional insight into the three-dimensional nature of the structures formed. The higher etch rate of X-PMMA presents some challenges for high-fidelity pattern transfer, which can be addressed through optimization of the transfer etch process parameters or incorporation of etch-resistivity into the chemistry of the X-PMMA film.

2.2 Introduction

Block copolymer (BCP) directed self-assembly (DSA) is a promising technique for the extension of lithographic patterning capabilities beyond traditional resolution limits.[1-3] This technology employs the natural tendency of BCP thin films to phase-separate into dense arrays of

regularly spaced features to generate industry-relevant structures.[4-5] Precise placement and orientation control of the BCP domains can be achieved through various methods; one approach, known as chemoepitaxy, uses chemical patterns with distinct regions of controllable wetting behavior.[6] When a BCP film is assembled on such a pattern, the domains preferentially form over regions of matching geometry and chemistry. Fabricating precisely defined chemical patterns is therefore of paramount importance in proper implementation of BCP DSA.[7]

This engineering challenge has led to the development of several methods for generating patterns. Many utilize traditional lithography to make sparsely patterned templates and rely on the tendency of BCP domains to interpolate at regular intervals to enhance resolution, an approach known as density multiplication. One example of chemoepitaxy with density multiplication is the flow developed by Liu for DSA of lamellae-forming BCP thin films, where immersion lithography and plasma etch are used to create narrow lines of a crosslinked polymer mat and the interstitial regions are backfilled with a brush of different chemistry.[8] The resulting patterns of crosslinked polymer guiding stripes that preferentially wet one domain of the block copolymer and background regions that are weakly preferential for the other domain have been used to assemble BCP thin films at two, three, and four times the resolution of the initial lithographic patterning step.[9] The flow has been used extensively to study the BCP DSA both at the fundamental laboratory level and for industrial integration in an all-track 300 mm implementation at the imec nanotechnology research labs in Leuven, Belgium.[10-13]

This flow differed from other approaches to making similar chemical patterns in that it allowed for independent control of the four relevant parameters: the pitch or spacing of the guide stripes (L_S), the width of the guide stripes (W), the chemistry of the guide stripe (γ_s), and the chemistry of the background (γ_b). W and L_S are controlled through the patterning and trim etch steps, while the

respective chemistries are dictated by the materials chosen as the guide stripe and backfill. In the ideal implementation of this chemical pattern, L_S is an integer multiple of the natural BCP periodicity L_0, W is the width of one lamellar domain, γ_s exactly matches the surface chemistry of the guided domain, and γ_b is a weighted average of the surface chemistries of both domains and is designed to minimize the total interfacial energy with an assembled BCP film. This flow was first demonstrated with the use of polystyrene (PS) and poly(methyl methacrylate) (PMMA) chemistries and much of the subsequent work targeting industrial integration has focused on crosslinked polystyrene (X-PS) as the guiding material, with appropriate changes in materials and processing to meet commercial compatibility requirements.[13]

Although we have implied that the guide stripe chemistry γ_s is uniquely a function of the material chosen as the polymer mat, this is not, strictly speaking, entirely true. Modification of some guide stripe materials, including the specific example of X-PS, has been shown to occur during processing through exposure to solvents, heat, plasma treatment, and chemically reactive species.[14] All these modifications result in a change in γ_s so that it no longer exactly matches the guided chemistry, and the guiding interaction that serves as the directing force for DSA is weakened. Furthermore, for some materials such as X-PS, tight control over the three-dimensional profile of the guide stripe is a technical challenge.[15]

For these reasons, as well as to demonstrate expanded materials capability of all-track processing, we investigated the use of crosslinked poly(methyl methacrylate) (X-PMMA) as a guiding material. The guiding strength of X-PMMA is found to be significantly stronger than that of X-PS, leading to the formation of non-bulk structures in the assembled BCP film that are not seen on similarly processed chemical patterns with X-PS as the guiding material; these structures have been reported in previous studies to form on strongly preferential chemical patterns.[16-17]

However, the higher etch rate of PMMA, thought to be a possible advantage in achieving better control over the guide stripe profile, creates other problems with etch undercutting and domain collapse. In additional to presenting these results, herein we employ theoretically-informed molecular simulations to shed light on BCP thermodynamics, tying together and benefiting simultaneously the experimental and simulation communities.

2.3 Experimental

2.3.1 Materials

AZ Electronic Materials provided crosslinkable poly(methyl methacrylate) (X-PMMA) AZEMBLY^{TM} NLD-234, end grafting P(S-*r*-MMA) brush AZEMBLY^{TM} NLD-241 (styrene fraction 0.72), and lamellae-forming P(S-*b*-MMA) BCP AZEMBLY^{TM} PME-312 (L_0 = 28nm). ArF immersion photoresist AIM5484 was purchased from JSR Micro, organic solvent RER600 was purchased from Fujifilm, and Orgasolv STR 301 was purchased from BASF. All materials were used as received.

2.3.2 Process

300mm Si wafers, coated with an appropriate antireflective stack, were spin-coated with NLD-234 to a thickness of 8 nm and annealed at 250 °C for 2 min under a nitrogen environment on a TEL CLEAN TRACK ACT^{TM}12. AIM5484 processing was performed using vendor recommended settings on a SOKUDO DUO track and exposures performed on the accompanying ASML NXT:1950i scanner using quadrupole illumination (dipole40X, xy-polarization, NA = 1.35, σ_o = 0.98, σ_i = 0.86). The samples were plasma etched on a TEL Tactras™ to trim the resist structures and the underlying mat in order to define guiding stripes, and then the remaining resist was stripped with Orgasolv STR 301. Next, the wafers were spin-coated with NLD-241, annealed at 180°C for 2 minutes, and rinsed with RER600 to remove ungrafted material, leaving a pattern

of alternating X-PMMA guide stripes and backfill brush regions. PME-312 was spin-coated at a thickness of 35 nm and annealed at 250 °C for 5 minutes under nitrogen. The PMMA domains were partially removed with plasma etching on a TEL Tactras^{TM} for better SEM contrast. The resulting BCP assembly was scored using a rubric described below.

2.3.3 Large-area sample preparation

To probe the wetting behavior of the materials used, wafers were coated with X-PMMA as described above. Large (> 1 in^2) exposed and unexposed areas were patterned and developed, and the wafers were then processed with the same flow described above. After full processing, the unexposed regions are large areas of X-PMMA whereas the exposed regions are large areas of end-grafted backfill brush.

2.3.4 Characterization

A Hitachi CG4000 or CG5000 scanning electron microscope (SEM) was used to image and measure the samples at three stages in the process: after photoresist development, after trim-etch, and after PMMA domain removal. Measurement of line width of the photoresist structures after trim-etch, W, was performed by automated built in Hitachi software and user-verified with image-by-image inspection. Film thicknesses were determined with a KLA-Tencor Aleris^{TM} 8330 spectroscopic ellipsometer. Static water contact angle (WCA) measurements were obtained using a Dataphysics OCAH230L contact angle measurement system. A syringe dispensed 5μL drops of deionized water, which were measured after 0.3 s of stabilization; all WCA measurements were repeated five times to verify accuracy. For wetting behavior determination, BCP was coated and annealed as described above and imaged with a Hitachi CG5000 SEM.

2.3.5 Image classification

SEM images of final BCP assembly on line-space chemical patterns were inspected and assigned a classification based on the type of assembly in the field of view (FOV) of 2.25μm x 2.25μm. Those FOV showing defect-free DSA were classified as "perfect," those showing minor defects (such as single jogs or small areas of bridging) were classified as "minor," fields with large defect area or undirected assembly but still majority (over 50% of FOV) assembly were classified as "major," and fields showing randomly oriented perpendicular lamellae were classified as "fingerprint." Fields of view containing non-bulk behavior were not counted in any of the previous categories; they were instead classified by the presence of absence of 'zig-zag'-type structures, vertical lines, or inverted lamellae. When multiple non-bulk morphologies were present within a single FOV, that data point was included in all relevant data sets.

2.4 Results and Discussion

A series of chemical patterns was fabricated using the process illustrated schematically in Figure 2.1. A cross-linkable poly(methyl methacrylate) (X-PMMA) mat was deposited and crosslinked on a material stack selected for its anti-reflectivity properties. The X-PMMA mat was coated with resist, which was patterned using 193 nm immersion lithography to create line/space arrays of various width and pitch. The samples were then exposed to a plasma trim-etch, which isotropically shrinks the photoresist (PR) lines and removes the X-PMMA mat in the interstitial spaces. After trim etch, the remaining photoresist was stripped and the samples were coated with a film of an end-functional random poly(styrene-*random*-methyl methacrylate) (P(S-*r*-MMA)) copolymer brush (72% styrene) and thermally annealed. The thermal treatment causes the brushes to graft to the substrate between the X-PMMA lines; after annealing, any remaining ungrafted brush was rinsed away, leaving a sparse pattern of X-PMMA guide stripes alternating with regions

of backfill brush. A thin film of poly(styrene-*block*-methyl methacrylate) (P(S-*b*-MMA)) was assembled on the chemical pattern using thermal annealing. When the spacing of the chemically patterned lines (L_S) is at or near an integer multiple of the natural periodicity of the block copolymer (L_0), the domains can align with the guide stripes and interpolate between them in a manner known as density multiplication. The schematic in Figure 2.1 shows an example of the '3x' density multiplication used in this work; the final block copolymer (BCP) structure has a resolution three times that of the original lithographically defined template. The geometric and chemical parameters of the final pattern are directly and independently controlled through selection of materials and tuning of process variables. Specifically, the guide stripe pitch L_S is set by the pitch of the lithographic exposure, and the guide stripe width W is a function of both the initial PR line width (controlled through exposure dose) and the amount of line-shrink that occurs during the trim-etch step (a multi-variable function of etch process conditions). The chemistry of the guide stripe and backfill regions are controlled through the composition of the initial cross-linked mat and random copolymer brush.

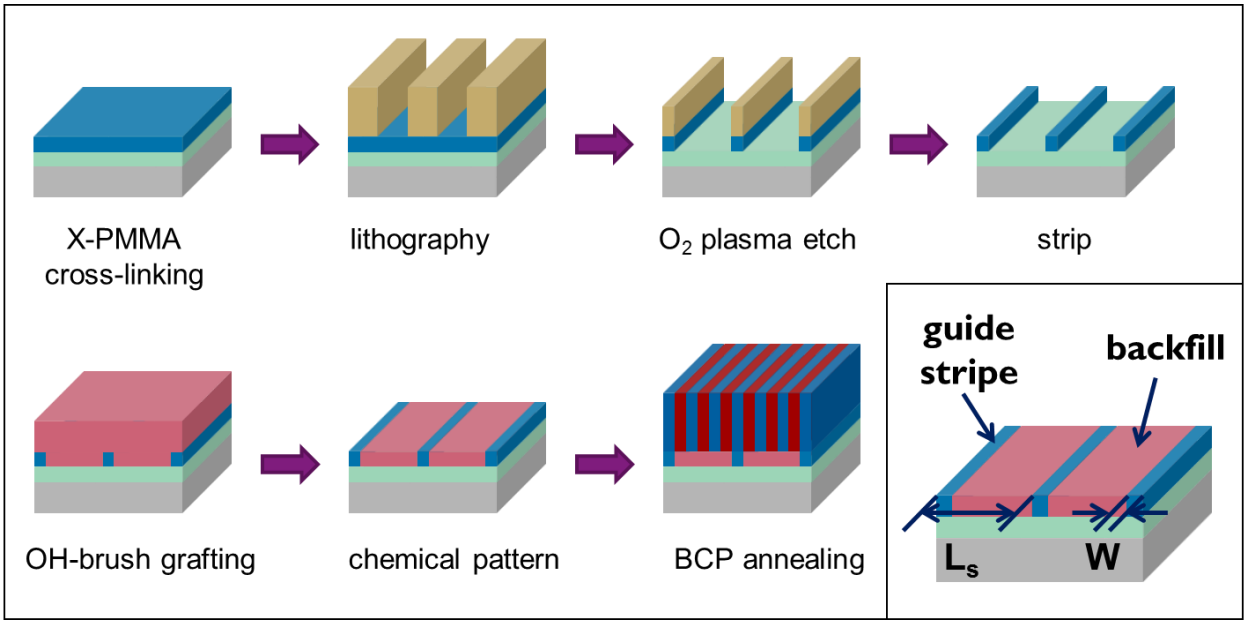

Figure 2.1: A schematic of the flow for generating chemical patterns for BCP DSA using an X-PMMA guide stripe. Inset: the component regions and geometric parameters of the chemical pattern.

2.4.1 Surface chemistry and energetics

Recent work has shown that under some process conditions, the chemistry of the guide stripe can be modified by certain process steps, such as trim-etch or backfill brush grafting, and that the final guide stripe chemistry may not match that of the as-deposited material.[14-15] It is therefore necessary to determine the wetting behavior of the guide stripe material after processing to properly evaluate and understand the self-assembly behavior on the chemical patterns, but direct measurement of nanoscale features is often impractical. Instead, we indirectly probed the guide stripe chemistry and measured the degree of modification during processing with the following method. We prepared large-area samples coated with X-PMMA and treated them with the full process flow: resist coating, plasma etch, strip, and brush grafting. The process-modified films were compared to unmodified films of as-cast X-PMMA using ellipsometry and static water contact angle (WCA) measurements (Figure 2.2). Ellipsometry results before and after each step show that the film thickness does not change significantly during processing, including during

brush grafting. The static water contact angle (WCA) of the modified X-PMMA (67.4°) is very close to that of the as-deposited material (63.2°), suggesting that the wetting behavior of the final guide stripes is not appreciably modified by processing.

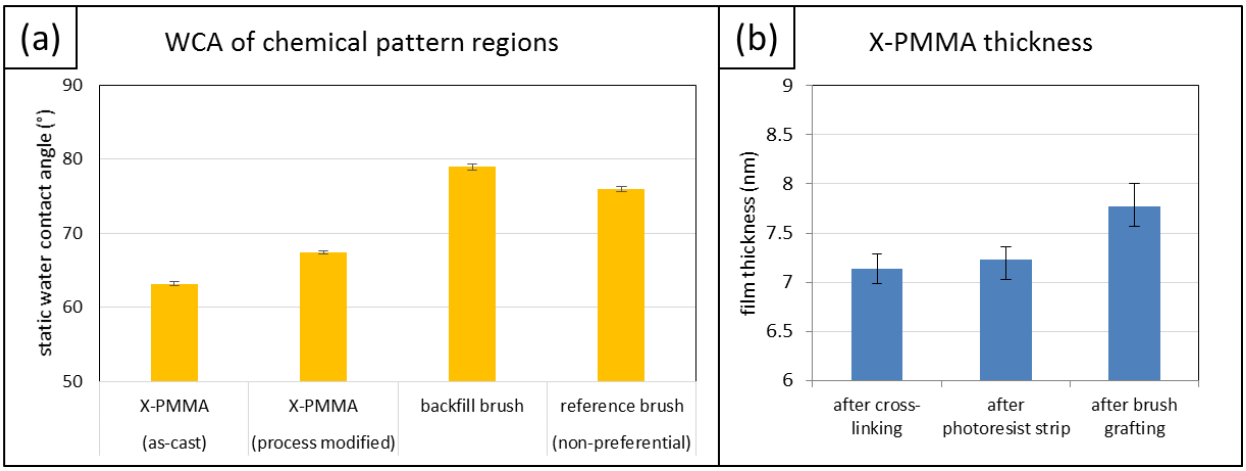

Figure 2.2: Characterization of the surfaces used in the chemical patterns. (a) Water contact angle measurements of the surfaces, showing that X-PMMA does not undergo significant modification during process and remains strongly PMMA-preferential. The backfill brush is similar to but slightly more PS-preferential than a non-preferential reference brush. (b) During processing, the film thickness does not change appreciably. Brush grafting adds ~0.6 nm of film thickness, likely the result of some reaction between X-PMMA and the brush, but this small amount does not substantially modify the mat's wetting behavior.

Water contact angle analysis is, however, an imperfect measurement technique for our systems. It is a macroscopic and therefore necessarily area-averaging technique, and the quantitative results are disproportionately influenced by roughness and indicative of the chemistry of only the very top of the surface under consideration. The much more complex macromolecular interactions driving BCP DSA are dependent on interfacial widths, interpenetration, configurational entropy, and other factors. Therefore, although WCA provides a quick, qualitative comparison along a single parameter axis, further information about the wetting behavior of a surface is obtained by assembling a lamellae-forming BCP on a sample. On a surface that is strongly preferential to one block of the copolymer, the domains align parallel to the surface to maximize the degree of preferential interaction between BCP and substrate.[18-19] For sufficiently non-preferential surfaces,

the polymer prefers to orient perpendicular to the substrate in a vertical fingerprint morphology that maximizes configurational entropy. The transition between parallel- and perpendicular-inducing surfaces is broad and is a function of several factors, including film thickness, relative surface energies of the BCP blocks, composition of the BCP film, and substrate topography; depending on the magnitude of and interplay between these factors, a range of surface chemistries can allow perpendicular assembly.[20] It is important to note that surfaces that support perpendicular assembly may have a preference – however slight – for one of the blocks of the BCP, but we can still describe these surfaces as sufficiently non-preferential in that they do not drive the polymer film to adopt the entropically-penalized parallel configuration. Similarly, depending on the surface energies of the respective phases of the BCP, a polymer film may adopt a parallel orientation even on non-preferential surfaces. For the PS-*b*-PMMA system considered here, however, that behavior is not observed; any surface that drives parallel orientation of the BCP is understood to be strongly preferential to one of the two domains. Therefore, to probe the wetting nature of the X-PMMA guide stripe, the representative large-area samples were coated with a film of lamellae-forming PS-*b*-PMMA and annealed. SEM images of the BCP film showed terraced 'hole/island' structures, indicative of the parallel lamellar orientation that forms on strongly preferentially-wetting surfaces.

These results, which all indicate that X-PMMA does not undergo significant modification during processing, are in contrast with previous work showing that cross-linkable polystyrene (X-PS) can undergo a change in wetting behavior during similar process conditions. However, the contrast is easily understood when considering the potential impact of each of the process steps. After PR coat, exposure, development, and strip, a small amount of the PR film may remain interdigitated within or adsorbed to the top of the cross-linked polymer mat. Photoresists in use

today are similar to PMMA in chemical structure, so a small PR residue on an X-PMMA mat would not affect the chemistry of the surface. Conversely, a PR residue on an X-PS mat could cause an appreciable change in its wetting nature. During the trim-etch step of the processing, the samples are treated with an oxygen-containing plasma. Even though the mats are covered in some areas by patterned PR lines, the high-energy plasma could still penetrate partially through the PR structures and modify the "protected" regions of the mat, which later become the guide stripes of the chemical pattern. As X-PMMA is already an oxygen-containing material, further oxidation does not cause it to become less PMMA-wetting. However, X-PS has been shown to undergo a marked change in wetting behavior during exposure to oxygen plasmas; indeed, oxidized X-PS has been used in past work as a PMMA-wetting material in chemical patterns.[6] Finally, during the backfill step, brush can graft not only to the interstitial spaces between the guide stripes but also, depending on their chemistry, to the guide stripes themselves, effectively resulting in a "masking" of their preferential, guiding nature. For reasons that are not fully understood, the brush used in this study grafted to the large area samples of X-PMMA to a very small degree (~0.6 nm), unlike in similar experiments with X-PS that showed a significant (~2.0 nm) layer of brush grafted to the guide stripes. Cumulatively, the modifications of the X-PS layer during processing are enough to substantially weaken its preferential interaction, such that a BCP assembled on this substrate adopts the vertical fingerprint configuration indicative of non-preferential (or at best weakly-preferential) surfaces. By contrast, a lamellae-forming BCP assembled on the X-PMMA film forms terraced 'hole/island' structures, revealing the strongly-preferential nature of that substrate. This greater strength of interaction between guide stripe chemistry and guided domain distinguishes this study from previous work with process-modified X-PS and frames the remaining discussion of our results.

Lamellae-forming block copolymer films were assembled by thermal annealing on a series of chemical patterns with a range of guide stripe widths (W) and pitches (L_S). The pitch of the chemical patterns is dictated by the initial pitch of the lithographic pre-pattern, but the guide stripe width is a function of both the PR structures after patterning as well as the duration of the isotropic trim etch used to shrink the lines. In our study, we used a fixed etch time for all samples, and the final guide stripe width W was therefore varied solely through the exposure step; for the positive-tone resist in this study, a higher dose corresponds to narrower resist lines after patterning and therefore narrow guide stripes after trim etch. Note that since the X-PMMA guide stripes cannot be sharply imaged or precisely measured using top-down SEM, their width is defined to be that of the more easily measured overlying PR structures remaining after trim-etch, even though a PR line may reside on top of a slightly narrow or slightly wider X-PMMA structure, depending on the quality of the trim etch process. Although the measured values of W therefore cannot be guaranteed to be quantitatively identical to the width of the actual X-PMMA stripe, this approach still allows for both qualitative and quantitative relative comparison of guide stripes and is thus the convention that has been adopted in both past work and our current study.

2.4.2 Morphologies observed

After assembly, the block copolymer films on the different chemical patterns were briefly treated with a mild plasma etch to partially remove one domain for enhanced imaging contrast and characterized using top-down SEM analysis. A wide variety of morphologies were observed in these block copolymer films, including both bulk lamellae ('hole/island', unregistered fingerprint, and registered lamellae) and non-bulk (zig-zags, short horizontal lines, 'pea-pod' vertical lines, and 'inverted wetting') structures. The particular morphology observed on a given chemical

pattern is a function of its guide stripe width and pitch, as shown in Figure 2.3. Although we will discuss each of the morphologies in turn, a few key points should be mentioned first.

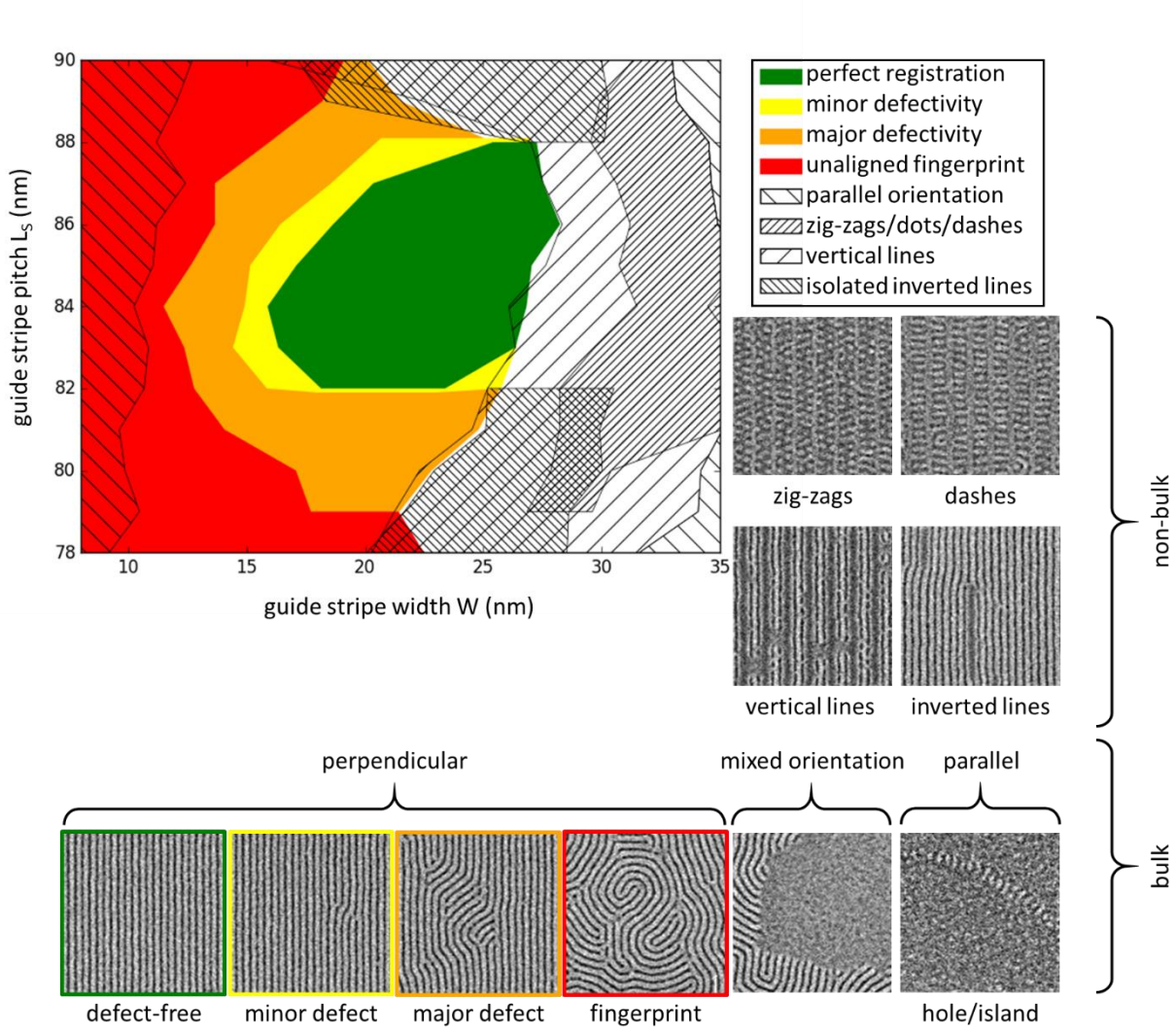

Figure 2.3: Morphologies observed as a function of guide stripe width (W) and pitch (L_S). Sample SEM images of each morphology are included for reference.

First of all, some of the morphologies observed correspond to the bulk behavior of this lamellae-forming BCP, namely, they are themselves lamellae. These lamellae can orient parallel or perpendicular to the substrate and orient randomly or align with the chemical patterns, giving rise to different top-down imaging results, but still belong to fundamentally the same category of structure. Other structures, however, adopt configurations not seen in the bulk, due to strong

interactions between the BCP domains and the underlying substrate. Past work has shown that when averaged through the volume of the film on a per-chain basis, these interactions can be equal to or stronger than the intra- and intermolecular forces that drive the bulk self-assembly process.[17] The equilibrium structure of a film assembled on a chemical pattern is a function of all the forces at play, and therefore reflects the balance between the polymer's natural self-assembly characteristics and the energetic boundary conditions imposed by the chemical pattern regions. If the chemical pattern geometry does not match the bulk BCP dimensions, the equilibrium structure can often be a frustrated, highly tortuous morphology. Note that to form these non-bulk structures, the interactions between film and chemically-patterned substrate must be sufficiently strong to overcome the natural tendency of the BCP to assemble into regularly spaced lamellae.

A second point that should be made is that on many of the chemical patterns, multiple morphologies were observed within a single SEM field of view (2.25 μm x 2.25 μm). In these samples, represented by the overlapping areas in Figure 2.3, quantitative analysis to determine the fraction of the sample covered by each morphology was not performed; they were instead evaluated using the simple binary metric of whether or not a particular structure was observed in the single SEM image. Therefore, the boundaries of each region should be interpreted as indicative of experimental observation and qualitative trends rather than any quantitatively-defined or sharply-delineated transition. Furthermore, the simultaneous presence of multiple morphologies on a single sample itself deserves comment. Since the chemical patterns exhibit variation in line width and edge definition, it could be argued that the observation of mixed morphologies is simply the effect of random experimental variation and non-uniformity in the fabrication of the substrate. However, as we show in a later section, a more thorough analysis of the results combined with

theoretically-informed simulations suggests that different morphologies can have similar free energies and therefore be competing quasi-equilibrium states.

As a final point before discussing the different morphologies in turn, it bears repeating that although the chemical pattern directs the assembly of the final BCP structure, sometimes in ways that do not match the spacing, curvature, or morphological behavior of the bulk material, these structures should not be thought of as bulk morphologies *perturbed* by the substrate. Instead, we must consider that the substrate and BCP film together constitute a new type of system that should be evaluated in a fundamentally different way. The equilibrium morphology is one that minimizes the free energy of the entire system, which includes both the bulk BCP intra- and intermolecular forces as well as the interactions with the patterned surface. With the introduction of chemical boundary conditions from the chemical pattern, the BCP/substrate system takes on a fundamentally different character.[16]

Registered lamellae

The simplest morphology to discuss is the registered lamellae structure observed in Figure 2.4, where each X-PMMA guide stripe is preferentially wet by the single PMMA domain that overlies it; the remaining BCP domains interpolate between guide stripes across the backfill, oriented perpendicular to the substrate. The geometric parameters of the patterns that support this morphology are the best match to the bulk dimensions of the BCP film: the width of the guide stripe W is roughly that of a single domain, and the spacing of the guide stripes L_S is an integer multiple of the BCP periodicity L_0. Alignment of the BCP to the pattern is driven by the strong attraction between the guide stripe and guided PMMA domain, resulting in an enthalpic gain and thus lower free energy state when perfect registration is achieved. The remaining, interpolated BCP domains are in contact with the backfill, the composition of which is selected to minimize

the overall interfacial energy in a manner developed by Liu. The optimum composition is a function of both the guide stripe chemistry and the degree of density multiplication, but is typically weakly preferential for the non-guided chemistry. In this study, since styrene is the non-guided block, the backfill has a 0.72 styrene fraction and is weakly preferential for PS.

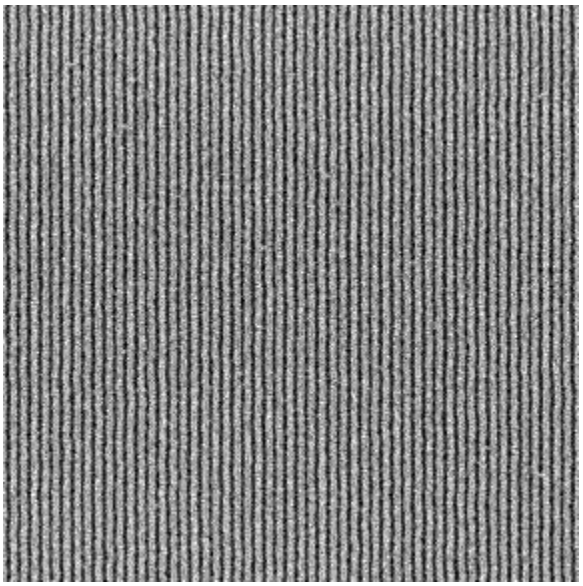

Figure 2.4: Defect-free registered assembly, fully aligned with chemical pattern.

Even on patterns with slightly mismatched dimensions, either in guide stripe width or pitch, the BCP domains still assemble with this morphology; W can vary by up to almost 25% and L_S up to about 3% and pattern registration is still achieved within the short five minute anneal used here. Registration occurs on slightly mismatched patterns because it is still the lowest free-energy state: the entropic penalty of the domains stretching, compressing, or otherwise being distorted is outweighed by the strong enthalpic benefit of the guide stripe / guided domain interaction. The distortion can be tolerated up to a certain point, based on this balance between the entropic and enthalpic contributions to the system free energy. This analysis was developed by Edwards and has been used in more recent work to investigate BCP assembly on chemical patterns with different guide stripe and backfill brush composition.

Registered lamellae with misalignment defects

When the mismatch between the pattern dimensions and the bulk geometry is more pronounced, we observe various levels of misalignment, as shown in Figure 2.5. These samples are represented by the yellow and orange regions in Figure 2.3, with yellow representing samples where a single dislocation or minor (<1% of the image) defectivity and orange representing those samples with significant defectivity but still majority registration. In these samples, the enthalpic benefit of alignment is the same as described for perfectly commensurate patterns, but the entropic penalty is higher, resulting in a lower thermodynamic drive towards registration. However, based on experimental studies of assembly kinetics and parallel theoretically-informed simulations, we believe that even on these patterns the equilibrium structure is defect-free registration. Therefore, at infinite anneal times, the defects would annihilate and the system would achieve perfect registration.

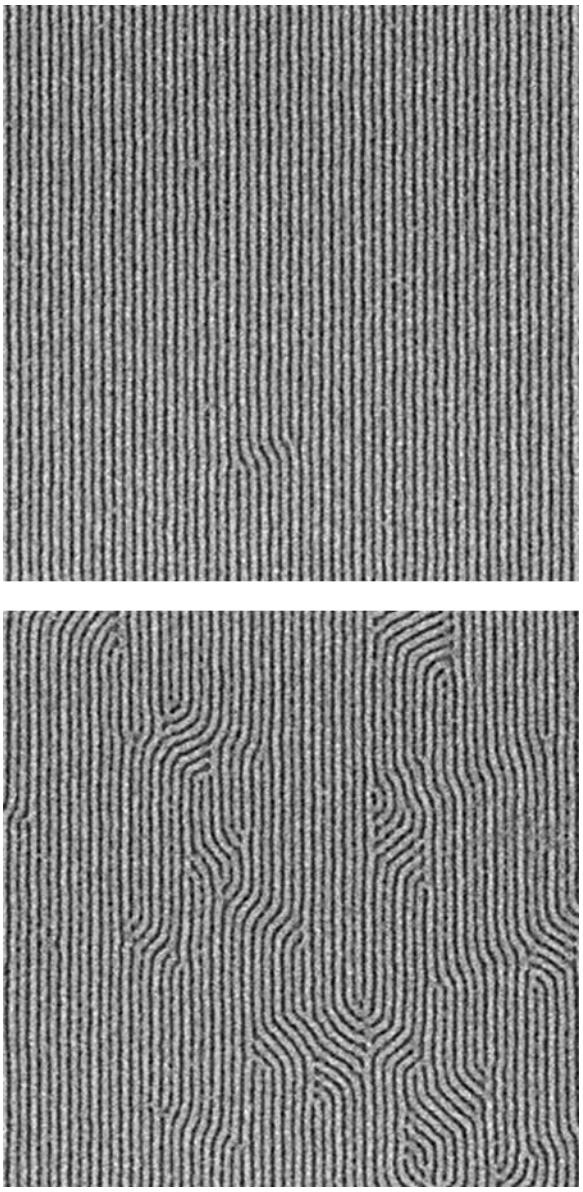

Figure 2.5: Different degrees of misalignment or registration defects in a majority-aligned BCP film. The top image is an example of the "minor defect" classification, whereas the bottom image is close to the maximum defectivity that is still at least 50% aligned and is therefore considered a "major defect" image. This assembly behavior is observed on substrates with moderately mismatched geometry, where the final equilibrium structure (i.e. at infinite time) is perfectly registered lamellae.

The explanation for why the BCP structures observed here do not match the predicted equilibrium morphology comes from consideration of kinetic minimum free energy pathways (MFEP) coupled with the still poorly understood nucleation mechanism that governs assembly dynamics as the film initially orders. Recent theoretical work has yielded considerable insight into

the annihilation mechanism for registration defects at long anneal times. This work predicts that surmountable but nontrivial barriers exist in the MFEP of the annihilation process, where the height of the barrier depends on the specific geometric and chemical system parameters. This prediction suggests that on certain chemical patterns, registration defects can persist over long time scales even at elevated temperatures; this effect would naturally be more pronounced on mismatched patterns, where the thermodynamic driving force for assembly is lessened. Nucleation is also believed to play a major role in how many of these energetic barriers through which the system must evolve to reach the equilibrium state. When the BCP film is initially spin-cast on the chemical pattern, it is in solution and disordered. As the solvent evaporates off, the film crosses the order-disorder transition (ODT) and phase separates into nanoscale domains. However, if the spin-casting temperature is below the BCP T_g (which is the case in our system), the polymer is vitrified and the individual chains have effectively no mobility. When the film is thermally annealed, the domains quickly become more sharply defined and then more slowly evolve to explore configuration space, seeking the equilibrium structure. Depending on where this initial nucleation – the initial phase separation and domain orientation – falls in multidimensional configuration space, the system may experience a different kinetic pathway to the defect-free equilibrium structure. It is therefore believed that the initial state of the system as well as the nature of the MFEP contribute to the timescale of defect persistence; the chemistry and geometry of the chemical pattern are intimately tied into that understanding.

Unaligned fingerprint

For certain chemical patterns, the mismatch between the pattern geometry and the bulk BCP dimensions is too severe to support registered assembly. In these cases, the BCP film orients with the domains perpendicular to the substrate but with no further alignment control. Top-down SEM

images of these samples reveal the characteristic ‘fingerprint’ structure shown in Figure 2.6; these samples are represented by the red region of Figure 2.3. Note that the fingerprint morphology is observed chiefly on chemical patterns with narrower guide stripes ($W < 12$ nm) or substantially mismatched guide stripe pitch (L_S more than 4% different from $3L_0$). In the first case, the guide stripes are small enough that the substrate acts as an effectively homogeneous, relatively non-preferential surface. As described earlier, such a surface supports the preferred lamellar configuration of randomly-oriented fingerprint. In the second case, the degree of incommensurability between L_S and $3L_0$ cannot be accommodated by stretching or compressing of the BCP domains without a large entropic penalty. Therefore, the domains relax to their natural spacing and assemble randomly without any regard for the alignment of the underlying chemical pattern. In contrast with the systems described in the preceding paragraphs, these mismatched patterns do not support registered assembly even at equilibrium: the fingerprint morphology persists indefinitely.

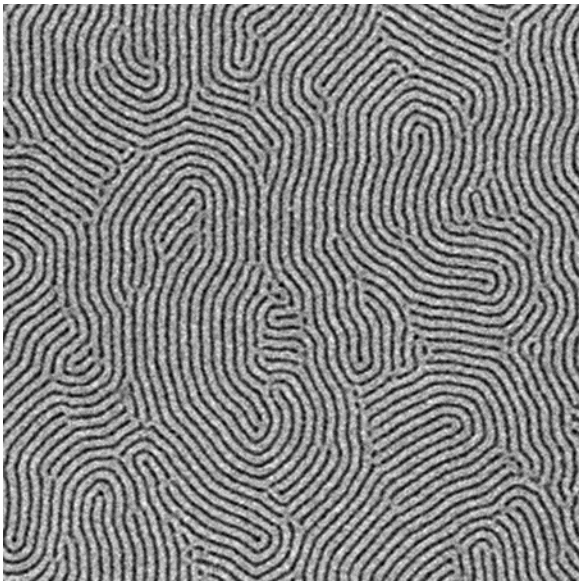

Figure 2.6: Randomly aligned fingerprint. This assembly is observed on substrates with significant mismatch between chemical pattern geometry and bulk BCP dimensions. On these substrates, there is no tendency towards aligned structures.

Parallel wetting

On some samples, namely those with very wide or very narrow guide stripes (around W > 35 nm or W < 10 nm, respectively), parallel wetting is observed, as shown in Figure 2.7 and represented with  in Figure 2.3. When the guide stripes are very wide, their strong preferential interaction with the PMMA domains of the BCP overwhelm the weak preference of the backfill for the PS block. The effect is that the substrate behaves as a homogeneous, PMMA-preferential surface. A film of P(S-*b*-MMA) assembled on this substrate orients with domains parallel to the substrate with PMMA as the bottom wetting layer and forms terraced hole/island structures at the top of the film. It should be noted that for these very wide guide stripes, the measured width W (as determined by top-down SEM of the post-trim PR lines) may be an underestimate of the actual effective width. The low exposure doses used to generate these wide lines also can underexpose the spaces between them, leaving PR bridges that increase the area of the final substrate covered by X-PMMA (please see supplemental information for image of PR lines). The difficulty in quantitatively measuring wide guide stripes is why we do not show values for W > 35 nm in the plot in Figure 2.3, though hole/island assembly is observed on these wider guide stripe samples. Parallel wetting behavior is also observed in the regime of very narrow guide stripes, where the PR lines are so narrow that the X-PMMA underneath is almost completely removed. Indeed, due to potential undercutting effects during the trim etch process (which will be discussed later in this paper), the measured width of these narrow resist lines may actually underestimate the width of the guide stripe (image in supplemental information). In these cases, the substrates are covered entirely by the weakly PS-preferential backfill brush. It has previously been shown that on weakly preferential substrates, and depending on parameters including film thickness, BCP surface energy, and anneal temperature, parallel and perpendicular assembly occurs simultaneously. That

behavior is also observed here, where a mixture of perpendicular fingerprint and parallel wetting structures is present on substrates effectively consisting of only backfill brush. It should be noted that the hole/island formation on very wide guide stripes is indicative of a strongly PMMA-preferential surface, whereas the mixed orientation present on vanishingly narrow guide stripes suggests only weak preferentiality.

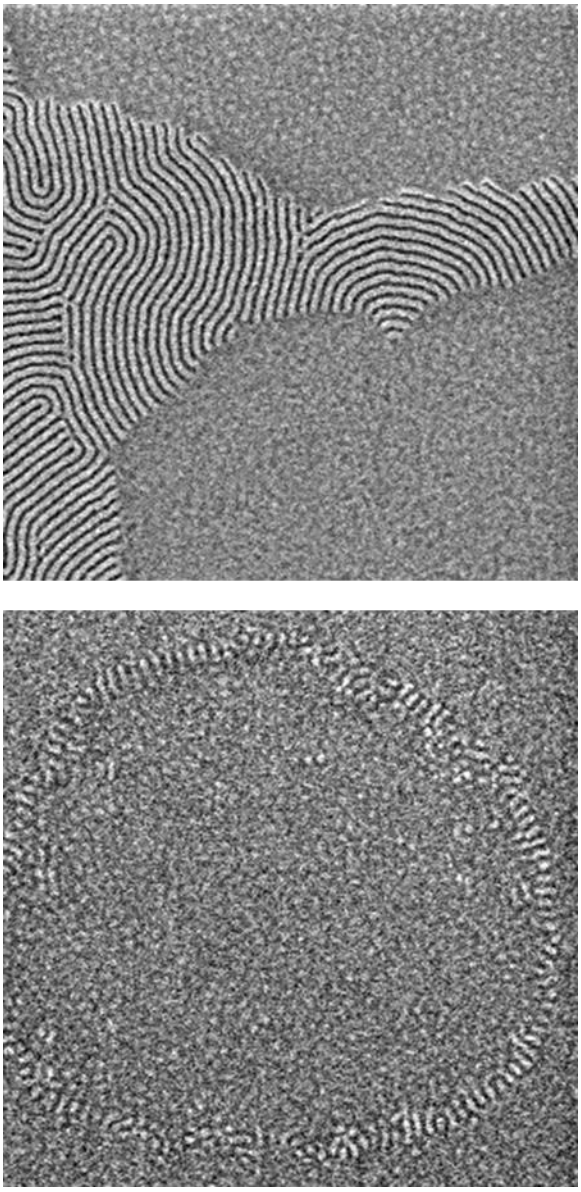

Figure 2.7: Parallel wetting behavior on preferential substrates. The bottom image shows characteristic behavior of "true" hole/island, where the entire film is oriented with domains parallel to the substrate and terracing occurs because of volume confinement effects, and is indicative of a strongly preferential substrate. The top image shows mixed orientation, where domains are parallel to the substrate in some places and perpendicular to it in others.

Non-bulk: zig-zag and short cross-lines

The structures described in previous paragraphs are all variations of bulk lamellae, either parallel or perpendicular to the substrate, but non-bulk morphologies are also observed on some

chemical patterns. The most interesting of these structures are the ‘zig-zags’ and ‘horizontal lines’ shown in Figure 2.8 and indicated by the  hash in Figure 2.3. These structures form on wide guide stripes ($W > L_0$) at all investigated values of L_S. Of all the morphologies, these are the most difficult to visualize with experimental techniques, so we turn to theoretically informed simulations to gain insight into their behavior. As can be seen in Figure 2.8b, these structures are complex, bicontinuous, and three-dimensional, with a high degree of through-film non-uniformity. They form in areas where the guide stripes are too wide to accommodate a single BCP domain in a perpendicular orientation. The strong interactions between X-PMMA guide stripe and guided PMMA domain cause a local wetting layer to form, but the PS-preferential nature of the backfill prevents the wetting layer to extend through the entire film as it does in a parallel wetting configuration. Constraints on single chain dimensions mean that every part of the PMMA wetting layer must be within one chain length of an adjacent PS domain. Furthermore, the symmetry of the diblocks means that each of the phases must occupy the same overall volume fraction. Taken together with the local wetting layer formed by the strong guiding interactions, these constraints produce the complex non-bulk morphologies observed.

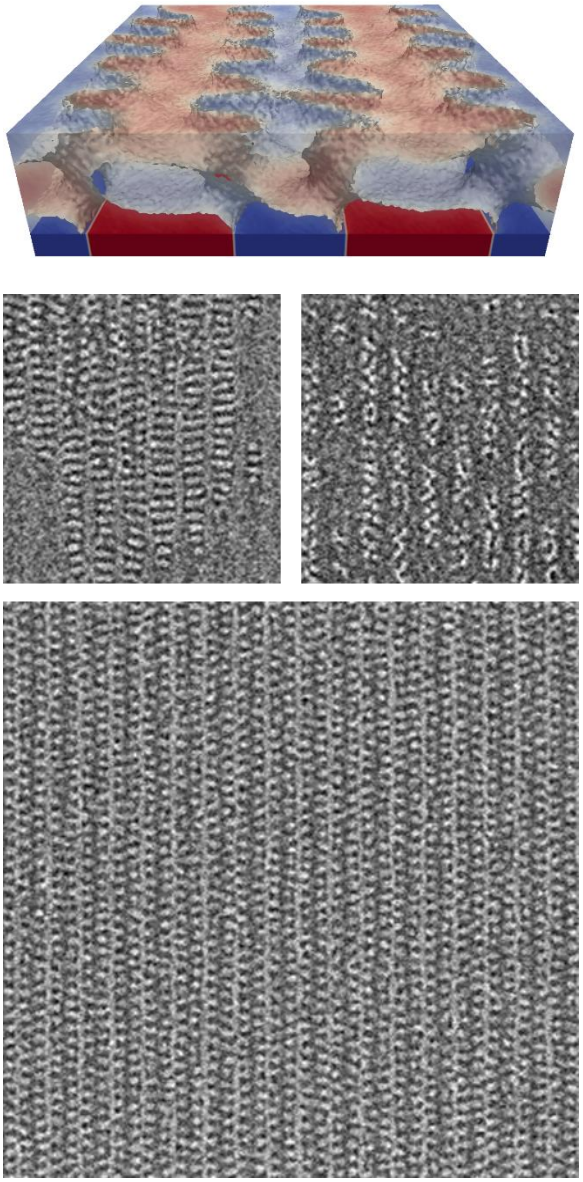

Figure 2.8: Complex non-bulk structures. Zig-zags are shown in the large image at the bottom, while the top left and right are horizontal PMMA dashes and polystyrene dots, respectively. The structures form on wide guide stripes and are all variations on the same non-bulk structure. Dots and dashes are more rarely seen and are usually found in locations on the sample believed to have non-uniform BCP film thickness. The PS (lighter) zig-zag is centered over the backfill and the PMMA (darker) zig-zag is centered over the guide stripe.

There are several variations in this class of non-bulk structures: zig-zags, PS or PMMA dashes, PS or PMMA dots, and other configurations. Past work has identified many of these structures and classified them as distinct, but the results examined in this study suggest that they are fundamentally quite similar. Each is the result of a local wetting layer forming over a wide guide

stripe coupled with the constraints described in the preceding paragraph. Often, two or more of these variants appear in the same SEM field of view, with no delineated transition between them. This observation is likely an effect of experimental nonuniformity, where the exact structure formed is a function of the local film thickness, guide stripe width, surface roughness, or other similar parameters.

Non-bulk: vertical lines, or through-film 'U's

On chemical patterns with even wider guide stripes ($W \sim 1.5L_0$), we observe the peapod-like "vertical line" structures shown in Figure 2.9 and indicated by  in Figure 2.3. In these structures, a single PS domain (bright region in the SEM images) sandwiched between two PMMA domains (dark in the SEM) overlies each guide stripe; the inverse behavior (one PMMA domain between two PS domains) occurs over the backfill. This assembly behavior is qualitatively similar to the previously reported "$1.5L_0$ assembly" of perpendicular lamellae, though in our system the strongly preferential nature of the guide stripe forms a wetting layer; the PS domain centered over the guide stripe is therefore a floating structure and a cross-section of these structures would show a PMMA 'U'-shape over the guide stripe and a PS 'U' over the backfill. In images of these samples, the PS domains over the backfill do not appear as bright as the single PS domain over the guide stripe, possibly due to narrowing of the former domains near the surface of the film due to volume-filling constraints. Furthermore, in these images, the PS and PMMA domains often bridge across each other to improve connectivity, giving rise to the "peapod-like" structures seen in Figure 2.9. This bridging effect is likely exacerbated by the short plasma etch used to remove PMMA and increase imaging contrast: as the PMMA separating the PS domains is etched away, minor structural collapse can occur as the PS domains seek to minimize their overall surface area. It should be noted that this morphology was always observed in the same FOV as the zig-zag

structures described previously (represented by the overlapping hashed regions in Figure 2.3), though in increasing proportion at larger values of W. Supporting results from simulations performed in parallel with the experiments suggest that the two structures have similar free energies especially on wider guide stripes, making them competing equilibrium states. Experimental observations further suggest that slight nonuniformity in film thickness may influence the formation of one morphology over the other.

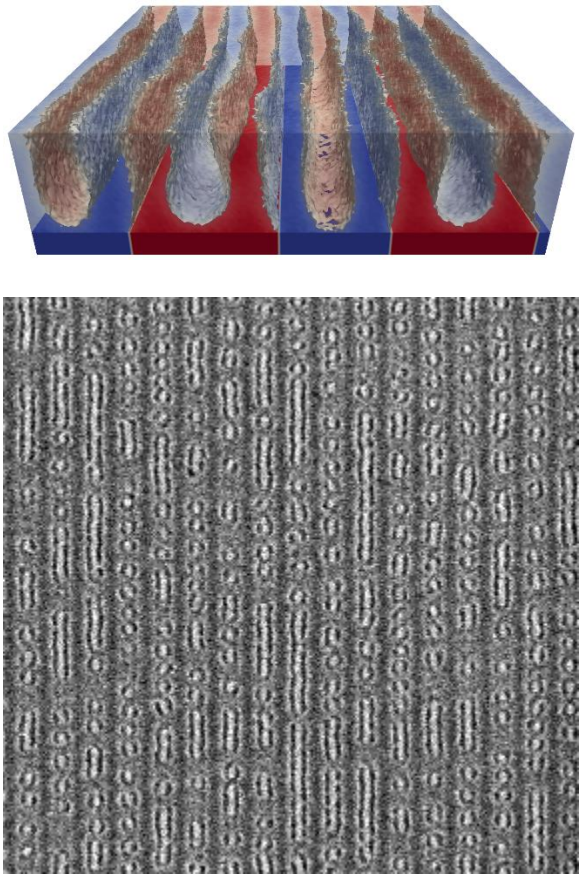

Figure 2.9: Vertical-line non-bulk structures. These structures form on wide guide stripes and have a through-film U-shaped morphology, as can be seen in the simulation results. Each X-PMMA guiding stripe has two PMMA domains above it, separated by a 'floating' PS domain; the opposite occurs over the backfill.

As mentioned above, this morphology forms over guide stripes roughly $1.5L_0$ in width, corresponding to roughly equal width of guide stripe and backfill regions. In a system where there is equal strength of interaction between these regions and their respective preferred blocks (i.e.

when the backfill is strongly preferential or the guide stripe is strongly preferential), there ceases to be a distinction between guided vs. unguided chemistries. At such a point, the chemical pattern is geometrically and chemically symmetric across the two regions, and the BCP morphologies above each region would be exact inverses of each other. In our system, the backfill is only weakly preferential for PS, but the morphology observed is still quite similar to the hypothetical "symmetric inverse" structure described here.

Non-bulk: isolated inverted lines

Finally, on some patterns, we observe a structure described as "isolated inverted lines," shown in Figure 2.10 and denoted by  in Figure 2.3. This morphology is a variant of the previous "vertical line" morphology, but with some distinguishing features that deserves a separate discussion. These morphologies are found on patterns with larger W but, for reasons not fully understood, only at incommensurate L_S, in both compression and extension. Taken together with the vertical line morphology, these structures are found in a band that arcs around the window of perfect assembly. In fact, in contrast with the vertical lines, which are only found on patterns with very large W and almost always alongside zig-zag nonbulk structures, these isolated lines often appear in otherwise defect-free FOV. This observation leads to our hypothesis that these structures represent an effort by the BCP film to relieve some of the stretching or compression in the domain dimensions by adding or removing an extra domain. The inverted lines always manifest as floating PMMA structures centered over the backfill. Since in registered assembly there is a PS domain centered over the backfill, PS domain splitting occurs at the ends of the isolated lines to accommodate the mismatch in domain placement.

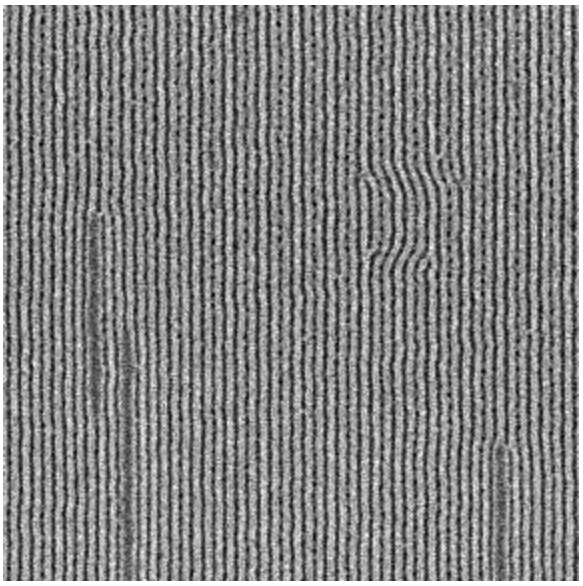

Figure 2.10: Isolated inverted-line structures. The dark lines are areas of removed PMMA and always form over the center of the backfill region. In the majority of the FOV, a PS domain is centered over backfill region; where these two regions meet (at the end of the isolated line structures) we observe PS domain splitting to preserve domain connectivity.

2.4.3 Undercutting and PS domain collapse

To improve imaging contrast of the final assembled BCP structures, they are exposed to a brief plasma etch that selectively removes the PMMA domains. This technique has been used successfully in the past for X-PS guided BCP films, but caused some problems in the X-PMMA guided work. When subjected to a 20-second etch, the PMMA domains on both X-PS and X-PMMA guided structures are fully removed and also removes some material at the bottom of the trenches formed where PMMA originally was located. When the guiding lines are X-PS, all three PMMA domains are over the backfill region and therefore the bottom of each trench is etched uniformly. In our work, however, one PMMA domain is centered over the X-PMMA guide stripe and the other two are located above the polystyrene-rich backfill brush. Since the etch is designed to remove PMMA, the X-PMMA guide stripe is also consumed by the etch process but the backfill brush is left relatively untouched. When the guide stripe is wider than a single PMMA domain, its removal undercuts the adjacent PS domains causing them to collapse as can be seen in the cross-

sectional profile of the BCP film after PMMA removal. The wider the guide stripe, the more pronounced this collapse, as shown in the series of top-down SEM images in Figure 2.11. To remedy this issue, we tested the use of shorter etch times to only partially remove the PMMA domains; a 10-second etch was selected for subsequent processing, as it produced the best imaging contrast without causing collapse of the PS structures. For future applications where complete removal of the PMMA domain is necessary for pattern transfer, undercut and collapse can be avoided either by optimizing the etch to be far more directional. Alternately, and perhaps more easily, etch resistance can be added to the X-PMMA mat by incorporating certain highly etch-resistant chemistries directly into the crosslinked matrix.

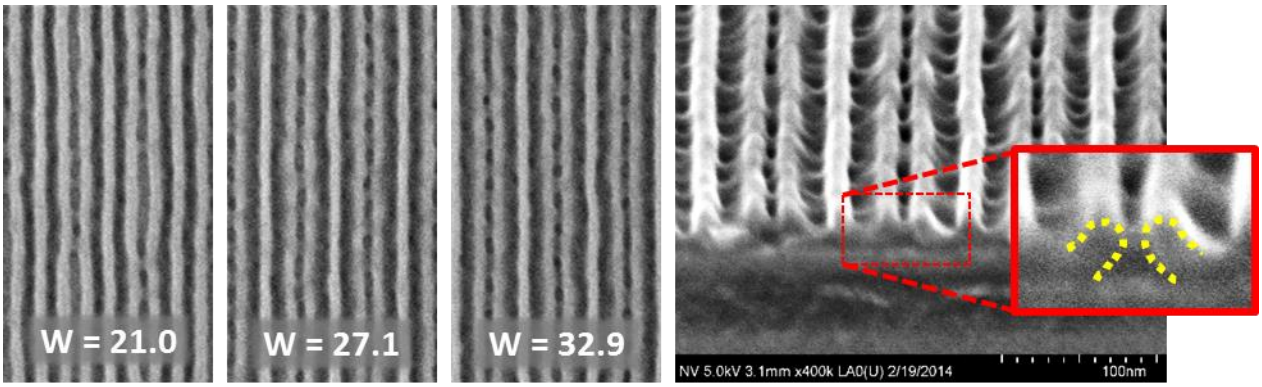

Figure 2.11: (Left) Top-down SEM images of collapse of PS lines after PMMA removal due to undercutting, confirmed by (right) cross-sectional SEM analysis. When the PMMA domains are fully removed, the guide stripe also etches. The wider the guide stripe, the more pronounced the undercut and subsequent collapse.

2.5 Summary and Conclusions

In summary, we have fabricated chemical patterns with guide stripes of X-PMMA; the strong guiding interactions of these stripes lead to complex nonbulk morphologies that are not otherwise observed on weaker guiding stripes. The strength of interaction and forced local wetting layers provides for possible use in transition regions of chemical patterns. At the edge of a pattern, it is sometimes advantageous to induce adjacent parallel and perpendicular orientation of lamellar

domains. This type of structure is heavily enthalpically penalized due to the increased interfacial area between the dissimilar chemistries but the penalty can be overcome by using strongly preferential patterns. We propose that for future work, such strongly wetting guide stripes be used for in-line edge definition. To overcome the challenge of etch undercut and pattern collapse, we recommend incorporation of higher etch resistance side groups into the X-PMMA matrix, taking care that in so doing the wetting behavior of the guide stripes is not modified or weakened.

2.6 References

1. Kim, H. C.; Hinsberg, W. D., Surface patterns from block copolymer self-assembly. *Journal of Vacuum Science & Technology A* **2008,** *26* (6), 1369-1382.

2. Ruiz, R.; Kang, H.; Detcheverry, F. A.; Dobisz, E.; Kercher, D. S.; Albrecht, T. R.; de Pablo, J. J.; Nealey, P. F., Density multiplication and improved lithography by directed block copolymer assembly. *Science* **2008,** *321* (5891), 936-939.

3. Detcheverry, F. A.; Papakonstantopoulos, Y.; Daoulas, K. C.; Stoykovich, M. P.; Nealey, P. F.; Mueller, M.; de Pablo, J. J., Driven self assembly of block copolymer nanocomposites on nanopatterned substrates for lithographic applications. *Abstracts of Papers of the American Chemical Society* **2007,** *233*.

4. Stoykovich, M. P.; Muller, M.; Kim, S. O.; Solak, H. H.; Edwards, E. W.; de Pablo, J. J.; Nealey, P. F., Directed assembly of block copolymer blends into nonregular device-oriented structures. *Science* **2005,** *308* (5727), 1442-1446.

5. Stoykovich, M. P.; Kang, H.; Daoulas, K. C.; Liu, G.; Liu, C.-C.; de Pablo, J. J.; Mueller, M.; Nealey, P. F., Directed self-assembly of block copolymers for nanolithography: Fabrication of isolated features and essential integrated circuit geometries. *Acs Nano* **2007,** *1* (3), 168-175.

6. Edwards, E. W.; Mueller, M.; Stoykovich, M. P.; Solak, H. H.; de Pablo, J. J.; Nealey, P. F., Dimensions and shapes of block copolymer domains assembled on lithographically defined chemically patterned substrates. *Macromolecules* **2007,** *40* (1), 90-96.

7. Liu, C.-C.; Han, E.; Onses, M. S.; Thode, C. J.; Ji, S.; Gopalan, P.; Nealey, P. F., Fabrication of Lithographically Defined Chemically Patterned Polymer Brushes and Mats. *Macromolecules* **2011,** *44* (7), 1876-1885.

8. Liu, C.-C.; Ramirez-Hernandez, A.; Han, E.; Craig, G. S. W.; Tada, Y.; Yoshida, H.; Kang, H.; Ji, S.; Gopalan, P.; de Pablo, J. J.; Nealey, P. F., Chemical Patterns for Directed Self-Assembly of Lamellae-Forming Block Copolymers with Density Multiplication of Features. *Macromolecules* **2013,** *46* (4), 1415-1424.

9. Liu, C.-C.; Nealey, P. F.; Raub, A. K.; Hakeem, P. J.; Brueck, S. R. J.; Han, E.; Gopalan, P., Integration of block copolymer directed assembly with 193 immersion lithography. *Journal of Vacuum Science & Technology B* **2010,** *28* (6), C6B30-C6B34.

10. Liu, C.-C.; Thode, C. J.; Delgadillo, P. A. R.; Craig, G. S. W.; Nealey, P. F.; Gronheid, R., Towards an all-track 300 mm process for directed self-assembly. *Journal of Vacuum Science & Technology B* **2011,** *29* (6).

11. Delgadillo, P. A. R.; Gronheid, R.; Thode, C. J.; Wu, H.; Cao, Y.; Neisser, M.; Somervell, M.; Nafus, K.; Nealey, P. F., Implementation of a chemo-epitaxy flow for directed self-assembly on 300-mm wafer processing equipment. *Journal of Micro-Nanolithography Mems and Moems* **2012,** *11* (3).

12. Gronheid, R.; Delgadillo, P. R.; Singh, A.; Younkin, T. R.; Sayan, S.; Chan, B. T.; Van Look, L.; Bekaert, J.; Pollentier, I.; Nealey, P. F., Readying Directed Self-Assembly for Patterning in Semi-Conductor Manufacturing. *Journal of Photopolymer Science and Technology* **2013,** *26* (6), 779-791.

13. Rincon-Delgadillo, P.; Craig, G.; Gronheid, R.; Nealey, P. F., Scale-up of a Chemo-Epitaxy Flow for Feature Multiplication Using Directed Self- Assembly of Block-Copolymers. *Journal of Photopolymer Science and Technology* **2013,** *26* (6), 831-839.

14. Williamson, L. L., Guanyang; Cao, Yi; Gronheid, Roel; Nealey, Paul F., Tuning the strength of chemical patterns for directed self-assembly of block copolymers. In *SPIE Advanced Lithography*, San Jose, CA, **2014**.

15. Seidel, R. W., Lance; Her, YoungJun; Kim, Jihoon; Lin, Guanyang; Nealey, Paul; Gronheid, Roel, The role of guide stripe chemisty in block copolymer directed self assembly. In *SPIE Advanced Lithography*, San Jose, CA, **2015**.

16. Liu, G.; Detcheverry, F.; Ramirez-Hernandez, A.; Yoshida, H.; Tada, Y.; de Pablo, J. J.; Nealey, P. F., Nonbulk Complex Structures in Thin Films of Symmetric Block Copolymers on Chemically Nanopatterned Surfaces. *Macromolecules* **2012,** *45* (9), 3986-3992.

17. Detcheverry, F. A.; Liu, G.; Nealey, P. F.; de Pablo, J. J., Interpolation in the Directed Assembly of Block Copolymers on Nanopatterned Substrates: Simulation and Experiments. *Macromolecules* **2010,** *43* (7), 3446-3454.

18. Fasolka, M. J.; Mayes, A. M., Block copolymer thin films: Physics and applications. *Annual Review of Materials Research* **2001,** *31*, 323-355.

19. Suh, H. S.; Kang, H.; Liu, C.-C.; Nealey, P. F.; Char, K., Orientation of Block Copolymer Resists on Interlayer Dielectrics with Tunable Surface Energy. *Macromolecules* **2010,** *43* (1), 461-466.

20. Suh, H. S.; Kang, H.; Nealey, P. F.; Char, K., Thickness Dependence of Neutral Parameter Windows for Perpendicularly Oriented Block Copolymer Thin Films. *Macromolecules* **2010,** *43* (10), 4744-4751.

CHAPTER 3: THREE-TONE CHEMICAL PATTERNS FOR BLOCK COPOLYMER DIRECTED SELF-ASSEMBLY

3.1 Abstract

Chemical patterns for directed self-assembly (DSA) of lamellae-forming block copolymers (BCP) with density multiplication can be fabricated by patterning resist on a cross-linked polystyrene layer, etching to create guide stripes, and depositing end-grafted brushes in between the stripes as background. To date, two-tone chemical patterns have been targeted with the guide stripes preferentially wet by one block of the copolymer and the background chemistry weakly preferentially wet by the other block. In the course of fabricating chemical patterns in an all-track process using 300 mm wafers, it was discovered that the etching process followed by brush grafting could produce a three-tone pattern. In its best form, the three-tone pattern consists of guide stripes preferentially wet by one block of the copolymer, each flanked by two additional stripes that wet the other block of the copolymer, with a third chemistry as the background. We characterized the three regions of the chemical patterns with a combination of SEM, glancing-incidence small-angle x-ray scattering (GISAXS), and assessment of BCP wetting behavior. Three-tone patterns guide three times as many BCP domains as two-tone patterns and thus have the potential to provide a larger driving force for the system to assemble into the desired architecture with fewer defects in shorter time and over a larger process window.

3.2 Introduction

Devising strategies to multiply the density of features derived from 193 nm immersion lithography templates dominates current research and development of semiconductor patterning.[1] One approach uses block copolymers (BCP) that self-assemble into periodic arrays of nanoscale

features.[2] Precise placement and orientation of these nanoscale features can be obtained through directed self-assembly (DSA).[3] In chemoeptiaxial DSA of lamellae-forming block copolymers in line/space arrays, the BCP film is assembled on lithographically defined templates which serve as chemical patterns consisting of guide stripes and background regions and direct the registration of assembled BCP domains.[4-8] The perfection of registration and control of through-film morphology depends on key parameters of the chemical pattern: the width and periodicity of the guide stripes and the chemistry of the guide stripes and background regions.[9-11] Optimally, the guide stripes are the width of one lamellar domain, the pattern chemistries are selected to minimize the interfacial energy between the BCP and the chemical pattern, and the guide stripe periodicity, L_S, is an integer multiple of the natural period of the block copolymer, L_0. In this way chemoepitaxial DSA with density multiplication enables sub-resolution extension of lithographic patterning.

Liu et al. developed a method to fabricate chemical patterns with independent control over each of the key pattern attributes described above.[12] In this process, as applied towards directing the assembly of poly(styrene-*block*-methyl methacrylate) (PS-*b*-PMMA), a crosslinked polystyrene (X-PS) mat is deposited on an inorganic substrate, and photoresist is patterned on top of the mat. The resulting structures are treated with a plasma trim etch that laterally shrinks the photoresist lines and removes X-PS in the spaces between them. The remaining photoresist is stripped and the spaces are backfilled by grafting an end-functional random copolymer brush P(S-*r*-MMA) of tunable composition, resulting in a two-tone pattern of sparse X-PS guide stripes and background brush regions. The composition of the brush is chosen to minimize the interfacial energy with the overlying BCP domains and is a function of the degree of density multiplication. The pitch and width of the photoresist features after lithographic patterning combined with the trim etch process therefore control the geometry of the pattern, and materials chosen for the mat

and brush determine its chemistry. These 'two-tone' surface patterns have been used extensively to understand the fundamental science behind directed assembly in the laboratory. More recently, the full process has been implemented as the 'LiNe' flow for all-track processing using 193 nm immersion lithography at imec with appropriate changes to materials and processing for 300 mm tool compatibility.[13]

In the course of investigating the impact of process conditions in this flow using high-volume manufacturing tools, we discovered a method to fabricate 'three-tone' rather than 'two-tone' chemical patterns. The three-tone patterns consist of PS-wetting guide stripes, each flanked by broad PMMA-wetting sidewalls, with polymer brushes of a third chemistry in the background spaces. Three-tone chemical patterns present a potential advantage over two-tone patterns because they guide three times as many BCP domains towards the desired domain architecture. Past work has shown that a higher fraction of guided domains results in faster annealing kinetics,[14] suggesting that this type of pattern may better enable DSA to meet requirements for high-volume manufacturing. We characterized the geometry of the three-tone patterns using grazing-incidence small-angle X-ray scattering (GISAXS) and the chemistry of the regions of the pattern with various techniques. Finally, we discuss the implications for improvement of DSA using the three-tone chemical patterns.

3.3 Experimental

3.3.1 Materials

Crosslinking polystyrene (X-PS) (AZEMBLY^{TM} NLD-128), P(S-*r*-MMA) brush (AZEMBLY^{TM} NLD-127, 51% PS), P(S-*b*-MMA) BCP with L_0 = 28 nm (AZEMBLY^{TM} PME-312) and a P(S-*b*-MMA) BCP formulation (L_0 = 28.5 nm) engineered to form microbridges were provided by Merck Performance Materials. ArF photoresist AIM5484 was purchased from

JSR Micro. Orgasolv STR 301 was purchased from BASF. Organic solvent RER600 was purchased from Fujifilm.

3.3.2 Chemical pattern fabrication and BCP assembly

The chemical patterns were fabricated on a 300 mm process line devoted to DSA at the imec nanoelectronics R&D lab in Belgium.[13] A 13 nm silicon nitride (SiN) film was deposited on 300 mm Si wafers as an inorganic antireflective coating. The wafers were coated with an 8 nm spincast film of X-PS, then annealed at 315 °C for 5 min in a nitrogen environment using a TEL CLEAN TRACK ACT^{TM}12 track. The wafers were coated with AIM5484 (95 nm) using a SOKUDO DUO track, exposed on an ASML 1950 immersion scanner (optimum dose = 11 mJ, optimum focus = -0.02 μm, NA = 1.35, dipole illumination, σ_o = 0.98, σ_i = 0.86, blade angle = 40°) and developed to create 84 nm pitch line-space patterns of various line widths. The samples were etched with an oxygen-containing plasma, which simultaneously isotropically etched the photoresist and removed unprotected X-PS. The remaining resist was stripped with Orgasolv STR 301, leaving isolated X-PS stripes on the nitride. The pattern was coated with backfill brush AZEMBLY^{TM} NLD-127 (50 nm), then annealed for 5 min at 250 °C to graft the brush to the nitride surface. The remaining ungrafted brush was removed through rinsing with RER600, leaving a chemical pattern of alternating X-PS stripes and backfill brush regions. BCP was spin-coated at a thickness of 35 nm and annealed at 250 °C with nitrogen purge for various times. The PMMA domains were removed with plasma etching on a TEL Tactras^{TM} for better SEM contrast.

3.3.3 Unpatterned surface (designed to emulate regions of chemical pattern) preparation

For areas representative of the guide stripe top and backfill region, wafers were coated with X-PS according the process described above. Large (> 1 in^2) exposed and unexposed areas were patterned and developed, and then the wafers were processed according to the remainder of the

treatment above. The unexposed regions (protected by photoresist during the trim etch process) were therefore large areas of unmodified X-PS, whereas the exposed regions were large areas of grafted backfill brush.

To create a large area surface of similar chemistry to that of the sidewall, the following procedure was implemented. X-PS was coated, then lightly crosslinked at 250 °C for 1 minute. This coating procedure was repeated five times, for a total thickness of 32 nm, and then the whole stack was thoroughly crosslinked using the standard bake of 5 minutes at 315 °C. Alternating exposed and unexposed areas were patterned and developed as described above, and the wafers were trim etched. The trim etch process, however, only removed ~12 nm of the thick X-PS film, leaving ~20 nm of plasma-modified polystyrene in the exposed areas. The treatment then proceeded in the standard manner, with photoresist strip and brush grafting.

3.3.4 Characterization

Grazing incidence small angle x-ray scattering (GISAXS) was performed at Sector 8-ID-E of the Advanced Photon Source at Argonne National Laboratory. The measurements were taken under vacuum with an incident x-ray beam of 7.35 keV. The 5 mm x 7.5 mm block of 84 nm pitch pattern was aligned so that the X-PS stripes were parallel to the x-ray beam. The incidence angle was set at 0.2° a Pilatus CCD detector placed 2.17 m from the sample. The 2D GISAXS spectra are the sum of 30 one-second exposures collected.

Scanning electron microscope (SEM) imaging was performed with a Hitachi CG5000 after trim etch and after PMMA domain removal. The line width of the photoresist structures after trim etch, W, was measured by automated built-in Hitachi software and user verified with image-by-image inspection. Film thicknesses were determined with a KLA Tencor Aleris^{TM} 8330 spectroscopic ellipsometer. Static water contact angle measurements were obtained using a

Dataphysics OCAH230L contact angle measurement system. A syringe dispensed 5 μL drops of deionized water, which were measured after 0.3 s of stabilization. In addition, BCP was coated and annealed as described above, then imaged with a Hitachi CG5000 SEM.

3.4 Results and Discussion

The process to generate chemical patterns for the directed self-assembly (DSA) of block copolymers (BCP) is shown schematically in Figure 3.1a. Photoresist is patterned on top of a crosslinked polystyrene (X-PS) mat using 193 nm immersion lithography, and then the photoresist lines are trim etched and stripped to leave a pattern of X-PS stripes at 84 nm pitch. An end-functional P(S-*r*-MMA) (51% PS) brush is coated on the pattern. The samples are annealed to allow the brush to graft to the spaces between the stripes. After excess brush is rinsed off, a BCP film is deposited on the chemical pattern and assembled by thermal annealing. The period of the guide stripes (L_S) is an integer multiple of the BCP natural periodicity (L_0); the BCP domains interpolate between the guiding stripes of the chemical pattern to form arrays of regular structures at a higher density than the original chemical pattern. Figure 3.1a illustrates an example of 3x density multiplication of features.

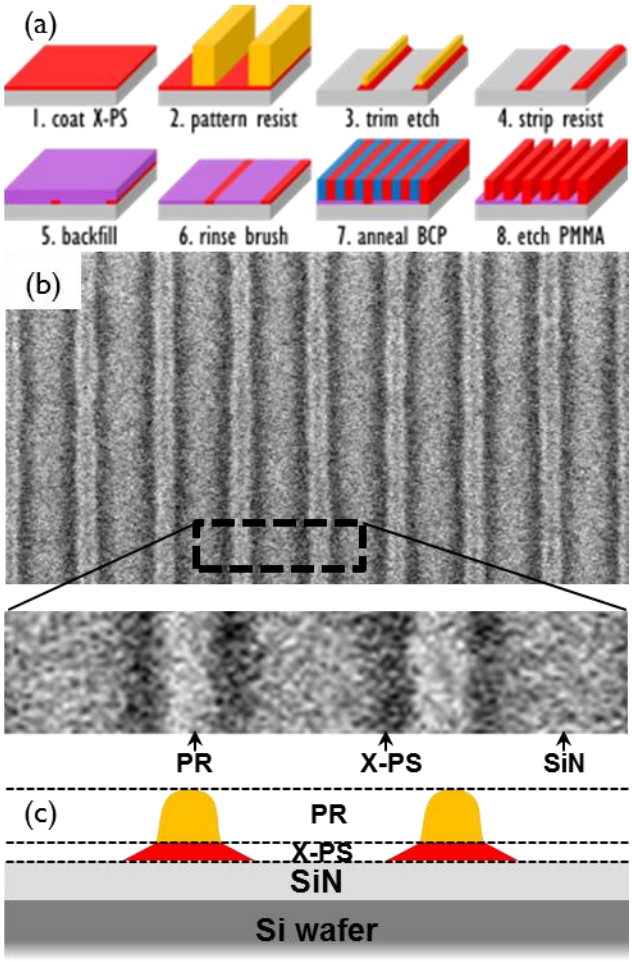

Figure 3.1: (a) Schematic representation of processing steps, including chemical pattern fabrication and BCP DSA. (b) Top-down SEM images show the X-PS stripe and resist after trim etch. (c) The cross-sectional schematic of the expected X-PS structure.

In order to better understand the guiding nature of the X-PS stripes in the chemical patterns, it is imperative to carefully consider the effects of the processing steps used in generating these patterns. In particular, the trim etch process (step 3) has a significant impact on both the geometry and chemistry of these structures. During the trim etch process as implemented in the current process flow at imec, the patterned photoresist lines and the X-PS mat underneath them are exposed to an oxygen-containing plasma environment. This plasma treatment isotropically etches the photoresist structures and the unprotected X-PS mat; the etch rate of the photoresist, however,

is higher than that of the X-PS. As the photoresist lines shrink, additional X-PS is revealed and etched. When the etch is complete, the three regions indicated in the top-down SEM images of Figure 3.1b are observed. The brightest regions are the remaining photoresist lines; the guide stripe width, W, is defined as the width of these lines. Since the etch is isotropic rather than directional, the X-PS underneath is not a perfect vertical projection of the resist structures but can be seen as dark regions flanking each resist line. Finally, the bare SiN wafer can be seen as a lighter region between the periodic resist/X-PS lines. In these samples, the X-PS adjacent to the unremoved resist has been plasma treated for a short time and is therefore only partially removed, whereas the X-PS exposed to the plasma from the beginning undergoes a longer etch time and is completely removed. This gradient of exposure time yields the trapezoidal structures represented schematically in Figure 3.1c.

We have been describing the tapered sidewalls of the trapezoidal structures as X-PS, but a careful consideration of the plasma etching process suggests that the surface of the partially etched X-PS has different properties. During the trim etch process, the X-PS is exposed to an oxygen-containing plasma that modifies and eventually removes it. The portions of the X-PS mat etched but not completely removed therefore undergo some degree of oxidation.[10] The wetting behavior of this "sidewall" chemistry is thus different both from the protected X-PS (the top of the trapezoidal guide stripe) and from the background regions backfilled with the non-preferential brush later in the process (step 5 in Figure 3.1a). Herein we explain how we characterized more fully the trapezoidal cross-section of the X-PS stripes as well as the wetting nature of each of the three surfaces (guide stripe top, plasma-modified sidewall, and backfill brush) present in these chemical patterns.

3.4.1 GISAXS Characterization

We characterized the shape of the X-PS stripes after trim etch and before backfill by grazing incidence small angle x-ray scattering (GISAXS) and SEM analysis as shown in Figure 3.2. SEM provides real-space imaging of discrete locations on the substrate, while GISAXS gives average information about the 3D structure across large areas. GISAXS patterns were obtained from X-PS structures of various widths, which were controlled by tuning the exposure dose during the patterning process (step 2, Figure 3.1a). The remaining resist after trim etch was stripped (step 4) prior to the GISAXS experiment. In our GISAXS configuration, q_x is along the beam direction and parallel to the guide stripes, q_y is orthogonal to the guide stripes in the sample plane, and q_z is the sample normal.

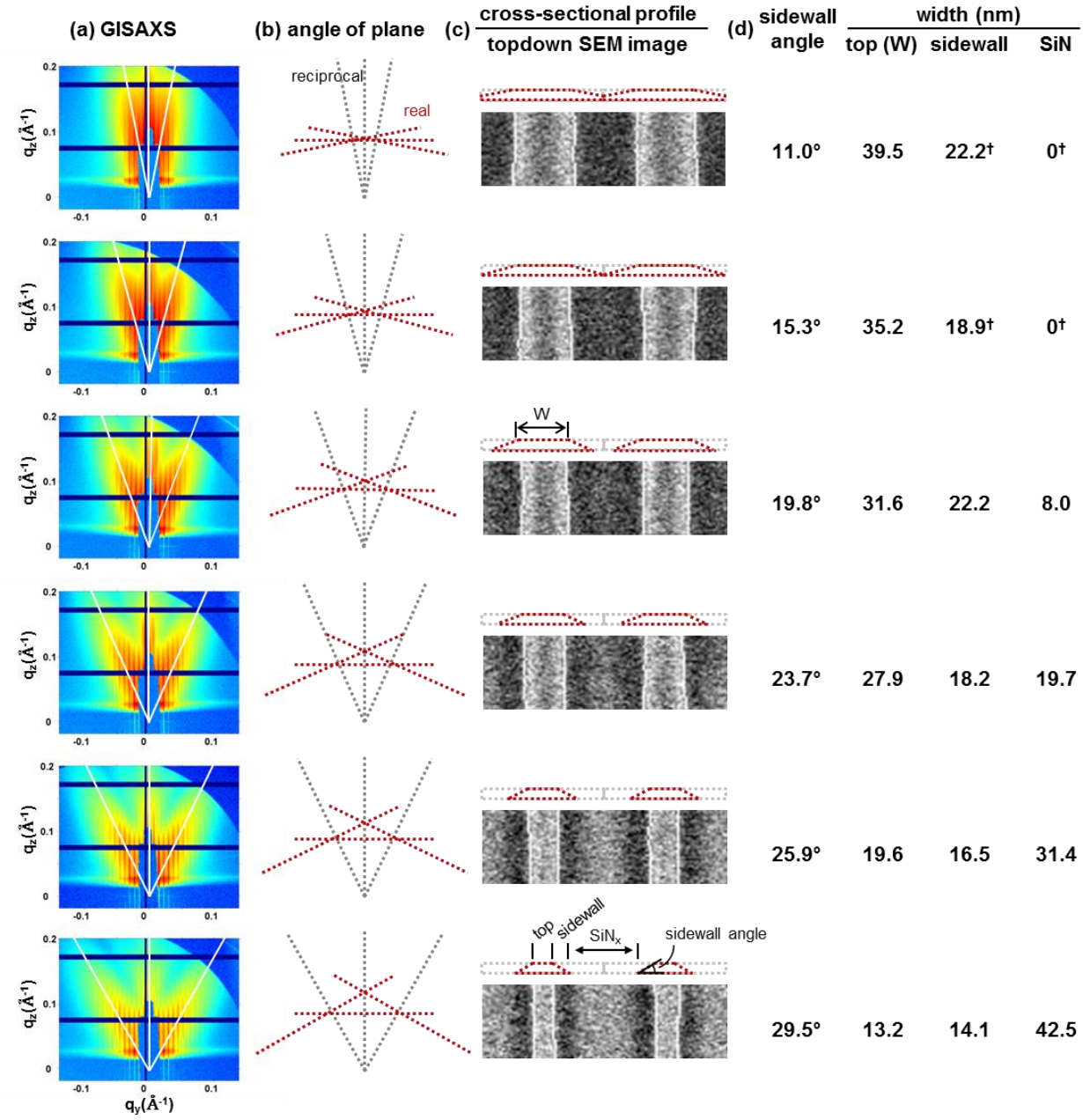

Figure 3.2: Characterization of the X-PS stripe geometry for a series of guide stripe widths W. GISAXS spectra in (a) were used to determine the slope of the sidewall, converted from reciprocal space to real space in (b). SEM images (c) were used to measure W after trim and confirm the presence of broad sidewalls on the X-PS structures. Stripe dimensions are summarized in (d). For the largest two guide stripe widths, the sidewalls merge and no SiN is visible, so the dimensions marked with † are based on gap width.

GISAXS patterns show the periodic sharp Bragg rods along the q_z direction for all samples. The pitch of the Bragg rods, 0.0075 $Å^{-1}$ in q_y, corresponds to an 83.8 nm pitch of the X-PS stripe,

consistent with the pitch defined by lithography as 84 nm. These periodic Bragg rods are convoluted with the diffuse scattering in the background of the GISAXS patterns. The diffuse scattering is of highest intensity along three directions extending out from the origin of the detector in directions indicated by the white lines in Figure 3.2a, which correspond to three planes in real space normal to those directions in reciprocal space, as shown in Figure 3.2b. Thus, we estimate the sidewall angle from the angle of the diffuse scattering. The differences in the diffuse scattering patterns in Figure 3.2a indicate the varying shape of the X-PS stripes illustrated in Figure 3.2c. The sidewall angle increases from 11.0^{o} to 29.5^{o} as W decreases from 39.5 nm to 13.2 nm, and can be attributed to the trim etch process. During the trim etch, a larger space between resist lines allows better access of the plasma to interact with the X-PS mat, resulting in a higher etch rate. Additionally, line-of-sight restrictions lead to higher etch rates near the center of the space compared to along the edge of the resist. These nonuniformity effects in the etch rate contribute to the difference in sidewall angle. Furthermore, upon breakthrough of the X-PS (when the underlying SiN stack is exposed), the added local loading density of the plasma species increases the lateral etching of the X-PS footing, further increasing the sidewall angle.

The overall dimensions of the X-PS stripes can be estimated from the sidewall angles, resist widths (W), and thickness of X-PS (8 nm). The calculated sidewall width shown in Figure 3.2 is in agreement with the width of the darker region corresponding to the sidewall in top-down SEM images. The combination of GISAXS and SEM measurements give quantitative geometrical information about the trapezoidal X-PS structure. The widths of the three regions (unetched top of guide stripe, partially etched sidewall, and SiN) are listed in Figure 3.2d; for the widest guide stripes, the sidewalls merge and no SiN is uncovered.

3.4.2 Wetting behavior characterization

In addition to characterizing the geometry of the X-PS stripes, we analyzed the wetting behavior of each region of the chemical pattern by mimicking the processing environment on large-area surfaces. The chemical patterns consist of three regions: the top of the X-PS guide stripe protected by photoresist, the sidewall of the X-PS stripe exposed to the trim etch, and the backfill region where X-PS was completely removed by the trim etch. In order to determine the wetting behavior of each of the three regions of the chemical pattern, large areas of X-PS and backfill brush were generated and processed through all pattern fabrication steps. In order to imitate the sidewall surface, a 32 nm thick X-PS film was prepared and subjected to the standard trim etch process. The trim etch process removes only 12 nm of the film, leaving a 20 nm thick oxygen-modified X-PS film, as illustrated in Figure 3.3a. After brush backfill to simulate the full processing conditions, the water contact angle of each surface was measured.

The composition of the backfill brush (AZEMBLY^{TM} NLD-127, 51% PS) has been independently optimized to minimize the interfacial energy between the interpolated domains and the background regions for 3x BCP DSA.[11] The surface coated with this brush (saturation thickness 7 nm) was measured to have a water contact angle (WCA) of 76.0°, roughly halfway between the contact angles for PS (88.4°) and PMMA (63.2°). Surfaces with contact angles greater than the brush (more hydrophobic) are therefore expected to be more PS wetting; conversely, those with lower contact angles (more hydrophilic) are expected to be more PMMA wetting than the brush. The wetting behavior of the final guide stripe top is not necessarily equivalent to that of the as-deposited material. In particular, treatment with solvents, resist, plasma, and other processing can modify the chemical nature of the stripes.[15] The WCA of the process-treated X-PS mimicking the protected guide stripe top was measured to be 83.7°, which is higher than the brush but lower than

the as-deposited value of 88.4° due to chemical modification during processing suggesting a weakly PS-preferential surface. One of these modifications happens in the backfill step of the process; the brush not only grafts to a thickness of 7 nm in the bare wafer regions of the pattern but also grafts 1-2 nm on top of the X-PS. This thin additional layer partially screens the wetting nature of the underlying X-PS. In comparison, the WCA on the simulated sidewall was measured to be 73.3° after backfill processing, which is significantly increased from the WCA measured prior to backfill (53.2°) but still less than that of the brush grafted to the substrate (76.0). The backfill treatment adds ~4 nm to the simulated sidewall, accounting for the change in contact angle during this process step. Since the water contact angle on this surface is still lower than that of the backfill, the polar nature of the oxidized sidewall is expected to make it slightly preferentially wet by the PMMA domain of the BCP.

Water contact angle measurements are an indirect probe of surface energetics, however, and do not probe the full complexity of macromolecular surfaces. Therefore, to further demonstrate the wetting behavior of these surfaces, two lamellae-forming BCP thin films were annealed on large-area surfaces representing the background, guide stripe top, and sidewall, respectively and their orientation on these substrates recorded; the results are shown in Figure 3.3c and d. Preferentially wetting surfaces direct lamellae to orient parallel to the substrate, leading to terraced holes or islands, whereas sufficiently non-preferentially wetting surfaces allow the lamellae to adopt a perpendicular 'fingerprint' orientation.[16] Past work has shown that for end-grafted brushes, compositions ranging from 45% to 57% PS can support this perpendicular assembly.[17] Since our brush is in the middle of this window (51% PS), both BCP films form fingerprint on the “backfill” (left column, Figure 3.3c and d). These films exhibited differing wetting behavior on the other two surfaces. The first film, consisting of a symmetric BCP, showed PS-preferential wetting on the

"guide stripe" but non-preferential wetting on the "sidewall." By contrast, the second film, consisting of a slightly PS-rich BCP, exhibited non-preferential wetting on the "guide stripe" but PMMA-preferential wetting on the "sidewall." The shift in wetting behavior can be understood by considering that a non-preferential surface for a slightly PS-rich BCP would be itself slightly PS-rich and therefore slightly PS-preferential for a symmetric BCP. These results indicate that the X-PS protected by the resist and the plasma-modified X-PS are only weakly preferential for PS and PMMA, respectively.

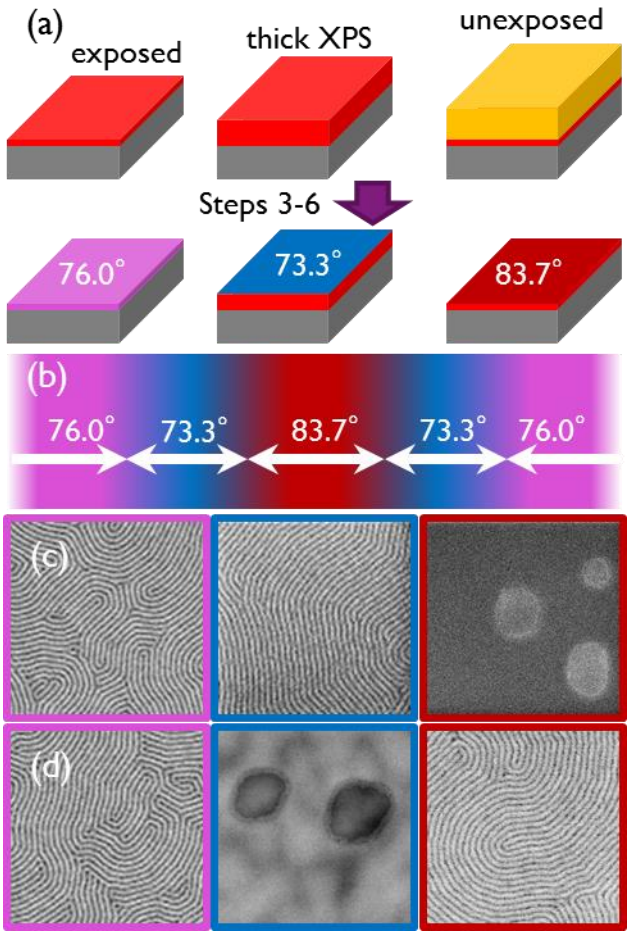

Figure 3.3: Unpatterned surfaces were processed with the steps described in Figure 3.1 to emulate the regions of the chemical pattern. The sidewall surface is simulated by etching partway through a thick coat of X-PS. Water contact angle measurements in (a) are associated with different regions of the chemical pattern, schematically illustrated from the top-down perspective in (b). Two BCP's were assembled on each surface in (c-d); the left, middle and right columns correspond to backfill, sidewall, and top surfaces, respectively. A symmetric BCP in (c) has PS-preferential wetting on the top of the guide stripe while a PS-rich lamellae-forming BCP in (d) has PMMA-preferential wetting on the sidewall. All other combinations resulted in perpendicular lamellae, indicative of non-preferential wetting.

3.4.3 BCP assembly behavior

BCP assembly on the chemical pattern is also consistent with the three-tone description. This investigation focused on the use of 84 nm pitch chemical patterns and 28 nm L_0 block copolymer, for 3x density multiplication. When assembling the BCP on a series of chemical patterns with different guide stripe widths, three ranges of guide stripe widths give ordered arrays.

Representative images for each range of assembly are shown in Figure 3.4. Previous efforts in chemoepitaxial DSA have focused on using guide stripes roughly the width of one BCP domain, or half of the lamellar period.[12, 18] This regime of well-registered assembly is referred to as the "0.5L_0 window" and can be observed in Figure 3.4(c). In this mode of registration, a PS domain (red) is centered over the guide stripe. The guide stripe is flanked by PMMA-wetting sidewalls with backfill brush in the interstitial space, resulting in a three-tone chemical pattern. A certain degree of incommensurability in the guide stripe width can be tolerated and still give good registration, but for guide stripes too narrow or too wide, the registration breaks down, as shown in Figure 3.4(b) and (d). Previous work has demonstrated the formation of complex non-bulk architectures on sufficiently wide guide stripes (W~L_0). These metastable morphologies form due to very strong interactions with the guide stripe that dominate the polymer's natural tendency to adopt the lamellar configuration.[12, 13] Conversely, for a weakly guiding system where this substrate interaction is insufficient to overcome that tendency, one would expect the formation of undirected fingerprint. As discussed in the previous paragraph, our system is only weakly guiding in that all three regions of the pattern are within or near the range of non-preferential wetting conditions, leading to the fingerprint morphology observed in Figure 3.4(d).

For certain wider guide stripes, where the stripe is roughly the width of three BCP domains, well-registered assembly is again observed as shown in Figure 3.4(e). This region of parameter space, known as the "1.5L_0 window," was also explored experimentally and through simulations by Liu et al.[11] In this mode of registration, two PS domains separated by a PMMA domain lie over the guide stripe top. As shown in the first rows of Figure 3.2, the sidewalls of our widest guide stripes merge, leaving no area of SiN where the backfill brush grafts. Since these patterns only

consist of protected X-PS guide stripes and plasma-modified X-PS sidewalls, they are two-tone in nature.

In our system, a third mode of registration is also observed when the X-PS stripes are over-etched, to the point of leaving only the PMMA-wetting residual sidewall behind. As illustrated in Figure 3.4a, these patterns also have a two-tone nature because they consist only of plasma-modified sidewall and backfill brush grafted to SiN. They are similar in design to the traditional $0.5L_0$ window in that only a single BCP domain is guided. In both this mode (denoted by the "residual assembly" window) and in the $1.5L_0$ mode, a PMMA domain is centered over the X-PS structure. Therefore, as the guide stripe width goes from vanishingly narrow to roughly $0.5L_0$ to $1.5L_0$, the registered assembly over the guide stripe transitions from PMMA-centered to PS-centered and then back to PMMA-centered. The fundamental change in centering mode is evidenced by the breakdown in registration at guide stripe widths in the transition between windows of good assembly. The presence of a PMMA-preferential sidewall leads to a new assembly window, adds three-tone wetting in the standard $0.5L_0$ window, and composes the background for the $1.5L_0$ window.

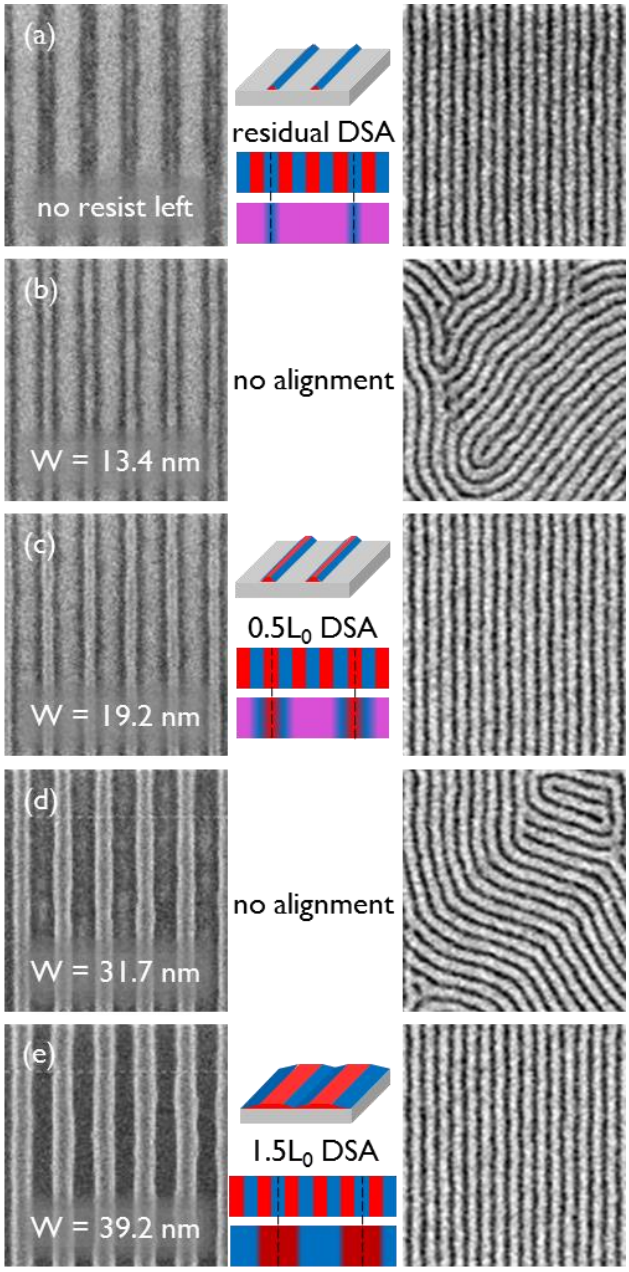

Figure 3.4: SEM images after trim etch and PMMA etch as W increases from (a) to (e). Three separate ranges (a), (c), and (e) lead to ordered arrays of BCP separated by ranges (b) and (d) corresponding to no pattern registration.

The evidence for the three-tone chemical pattern is further supplemented by experimental results when assembling a PS-rich BCP system that naturally forms PS microbridges, where PS domains connect through the PMMA domains, similar to a perforated lamellae morphology.[19-20] As seen in Figure 3.5a, assembly of a PS-rich BCP on an unpatterned surface of 51% PS brush

results in dense microbridges in all PMMA domains. When assembly takes place on a patterned surface, the microbridges still form over the background region. However, microbridge formation is suppressed over the PMMA-wetting sidewalls due to an enthalpically penalizing interaction between these surfaces and the PS microbridge structures. In the residual DSA regime (Figure 3.5b), every third PMMA domain is over a plasma-modified sidewall rather than the background and microbridges are confined to the other two-thirds of the PMMA domains. In the $0.5L_0$ window (Figure 3.5c), a PS domain is over the guide stripe and two of the three PMMA domains assemble over the sidewall on either side. The third PMMA domain forms over the backfill region, and is therefore where microbridges are observed. For guide stripes in the $1.5L_0$ window (Figure 3.5d), adjacent sidewalls merge and no backfill brush region is present so microbridge formation is suppressed. In all cases, microbridge formation is observed primarily over the brush.

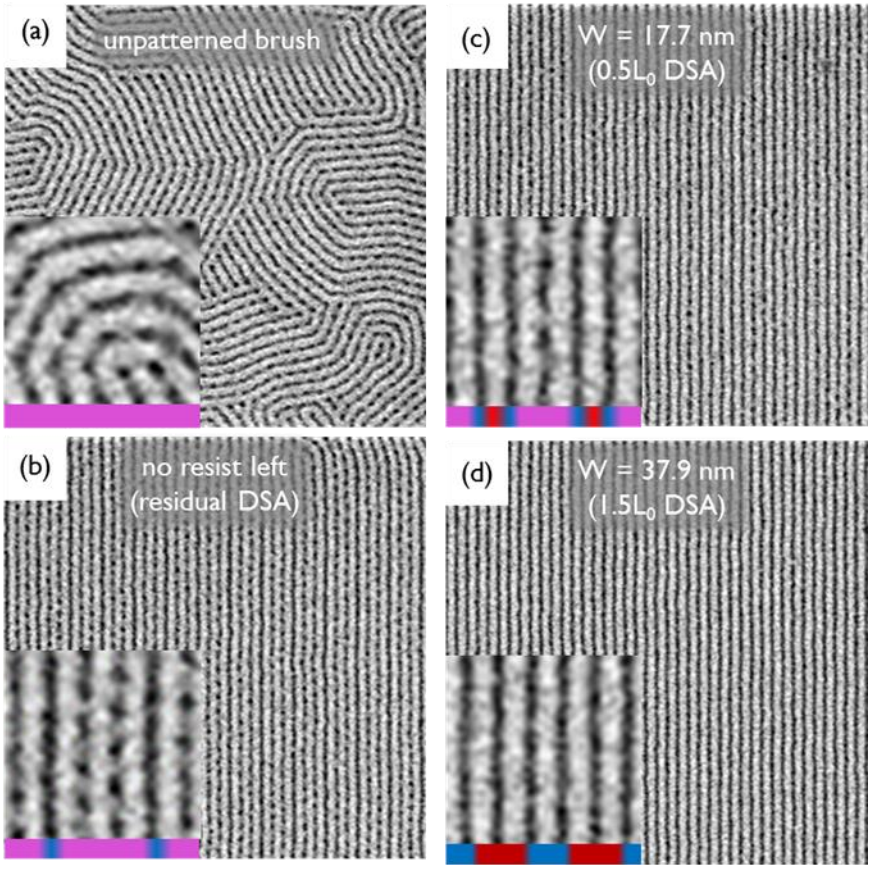

Figure 3.5: A BCP formulation that exhibits dense PS microbridges on (a) unpatterned brush, (b) overetched X-PS stripe, (c) guide stripe ~0.5 L0, (d) guide stripe ~1.5L0. In all cases, PS microbridges form over backfill brush rather than over plasma-treated X-PS sidewall.

The ideal substrate for chemoepitaxial DSA of through-film lamellar BCP with vertical sidewalls is the two-dimensional projection of the line-space array at its natural periodicity. This one-to-one pattern, however, does not provide any resolution enhancement for lithographic purposes. For applications requiring density multiplication, the target pattern consists of a sparse set of guide stripes of width $W = 0.5L_0$ matched in chemistry to one domain of the BCP while the background minimizes the interfacial energy with the remaining domains. In this case, the thermodynamic equilibrium structure is well-registered perpendicular lamellae, but the kinetics of assembly have been shown to be significantly slower, with long-term persistence of misalignment defects.[14] Since three-tone patterns decouple the guiding nature of guide stripe, sidewall, and

backfill, they can even more closely resemble the two-dimensional projection of the desired BCP morphology. Specifically, in a traditional two-tone pattern with density multiplication, only one domain per guide stripe is directly guided by its matching chemistry. Our three-tone patterns match the chemistry of three domains per patterned stripe: the domain over the guide stripe as well as the two adjacent domains over the sidewalls. In a fully optimized three-tone pattern, the geometry and chemistry of both guide stripe and sidewall would perfectly match those of their respectively guided BCP domains.

Furthermore, since DSA is a thermodynamically driven process, the free energy landscape dictates not only the equilibrium states but also the minimum free energy pathways along which the system evolves to the final assembled structure. Past work has indicated that for some systems, high-energy registration defects may correspond to local energy minima, and that these states may therefore be kinetically trapped.[21-22] For the system to bypass those states and reach the global energy minimum and equilibrium morphology, it is necessary to reduce or eliminate local energy minima. In chemoepitaxy, the free energy landscape is a function of the boundary conditions imposed by the chemical pattern. Therefore, adding detail through the use of three-tone patterns can provide an avenue to modifying the system's free energy space, potentially resulting in fewer defects for a given annealing condition.

In a recently published report, prepared concurrently with our study, Cushen et al. describe a process comparable to our flow, as outlined in Figure 3.1a. They used e-beam lithography and plasma etch to pattern stripes in an 8 nm thick X-PS, which is non-preferential to their BCP poly(trimethylsilylstyrene-*block*-*p*-methoxystyrene) (PTMSS-*b*-PMOST).[8] The sidewalls of the X-PS stripes are oxidized during etching, altering their chemistry and making them preferential to the PMOST block. A short, non-preferential PS brush was used to backfill the pattern, leaving 5

nm of sidewall unblocked to serve as a guiding surface. Since the patterned stripe is thicker than the backfill, topography also assists in guiding the BCP domains. They assembled the BCP through thermal annealing with a non-preferential top coat. In this manner, they succeeded in making a 'double-patterned' substrate that combines graphoepitaxy with chemoepitaxy to guide two domains per lithographically defined line. These patterns are similar to the ones used in our work in that they both use a plasma treatment that modifies the sidewall, causing it to be preferentially wetting for one of the domains, and are made using the same general process flow. However, their work is different in that their patterned stripe is non-preferential and therefore does not guide assembly; their patterns are two-tone since both the patterned stripe and backfill are the same non-preferential chemistry.

3.5 Conclusions

We have identified a method to make a new style of chemical pattern and characterized the geometry and wetting behavior of its components. Certain processing conditions result in chemical patterns with three regions of distinct wetting behavior: PS-preferential guide stripes, PMMA-wetting sidewalls, and non-preferential background. Certain BCP DSA behavior that cannot be explained by a two-tone description of the chemical pattern provides evidence of three-tone patterns. For chemoepitaxial density multiplication, a three-tone chemical pattern directs assembly with three times the number of guided domains and therefore is an avenue for increased control of the assembly behavior. The creation of three-tone patterns described here pertains strictly to the exact materials, tools, and processing conditions of the DSA line at imec. Future improvement of chemical pattern processing should account for and optimize the properties of the sidewall to achieve the highest quality of DSA for these three-tone patterns.

Whereas our discussion has focused on the creation and optimization of three-tone chemical patterns, the concept of innovation in processing to create patterns for DSA is more broadly applicable. Past work has focused on novel material development as the primary driver for enhanced performance, but here we have demonstrated how creative development in processing could play a key role. Knowledge of fundamental science behind DSA will enable continued innovation in materials and processing.

3.6 References

1. ITRS *Lithography*; **2013**.

2. Bates, F. S.; Fredrickson, G. H., Block copolymers - Designer soft materials. *Physics Today* **1999,** *52* (2), 32-38.

3. Ruiz, R.; Kang, H.; Detcheverry, F. A.; Dobisz, E.; Kercher, D. S.; Albrecht, T. R.; de Pablo, J. J.; Nealey, P. F., Density multiplication and improved lithography by directed block copolymer assembly. *Science* **2008,** *321* (5891), 936-939.

4. Kim, S. O.; Solak, H. H.; Stoykovich, M. P.; Ferrier, N. J.; de Pablo, J. J.; Nealey, P. F., Epitaxial self-assembly of block copolymers on lithographically defined nanopatterned substrates. *Nature* **2003,** *424* (6947), 411-414.

5. Cheng, J. Y.; Sanders, D. P.; Truong, H. D.; Harrer, S.; Friz, A.; Holmes, S.; Colburn, M.; Hinsberg, W. D., Simple and Versatile Methods To Integrate Directed Self-Assembly with Optical Lithography Using a Polarity-Switched Photoresist. *Acs Nano* **2010,** *4* (8), 4815-4823.

6. Bencher, C.; Finders, J.; Englard, I.; Cohen, Y.; Sagiv, A.; Ben-Yishai, M.; Mangan, S.; Dai, H.; Ngai, C.; Dotan, K.; Knops, R.; Mouraille, O.; Mos, E.; Kremer, A., Toward 22 nm: fast and effective intrafield monitoring and optimization of process windows and critical dimension uniformity. *Journal of Micro-Nanolithography Mems and Moems* **2011,** *10* (4).

7. Kim, J.; Yin, J.; Cao, Y.; Her, Y.; Petermann, C.; Wu, H.; Shan, J.; Tsutsumi, T.; Lin, G., Toward high-performance quality meeting IC device manufacturing requirements with AZ SMART DSA process. *Proc. SPIE Advanced Lithography* **2015,** *9423*, 94230R.

8. Cushen, J.; Wan, L.; Blachut, G.; Maher, M. J.; Albrecht, T. R.; Ellison, C. J.; Willson, C. G.; Ruiz, R., Double-Patterned Sidewall Directed Self-Assembly and Pattern Transfer of Sub-10 nm PTMSS-b-PMOST. *ACS Applied Materials & Interfaces* **2015,** *7* (24), 13476-13483.

9. Edwards, E. W.; Montague, M. F.; Solak, H. H.; Hawker, C. J.; Nealey, P. F., Precise control over molecular dimensions of block-copolymer domains using the interfacial energy of chemically nanopatterned substrates. *Advanced Materials* **2004,** *16* (15), 1315-+.

10. Edwards, E. W.; Mueller, M.; Stoykovich, M. P.; Solak, H. H.; de Pablo, J. J.; Nealey, P. F., Dimensions and shapes of block copolymer domains assembled on lithographically defined chemically patterned substrates. *Macromolecules* **2007,** *40* (1), 90-96.

11. Liu, C.-C.; Ramirez-Hernandez, A.; Han, E.; Craig, G. S. W.; Tada, Y.; Yoshida, H.; Kang, H.; Ji, S.; Gopalan, P.; de Pablo, J. J.; Nealey, P. F., Chemical Patterns for Directed Self-Assembly of Lamellae-Forming Block Copolymers with Density Multiplication of Features. *Macromolecules* **2013,** *46* (4), 1415-1424.

12. Liu, C.-C.; Han, E.; Onses, M. S.; Thode, C. J.; Ji, S.; Gopalan, P.; Nealey, P. F., Fabrication of Lithographically Defined Chemically Patterned Polymer Brushes and Mats. *Macromolecules* **2011,** *44* (7), 1876-1885.

13. Delgadillo, P. A. R.; Gronheid, R.; Thode, C. J.; Wu, H.; Cao, Y.; Neisser, M.; Somervell, M.; Nafus, K.; Nealey, P. F., Implementation of a chemo-epitaxy flow for directed self-assembly on 300-mm wafer processing equipment. *Journal of Micro-Nanolithography Mems and Moems* **2012,** *11* (3).

14. Liu, G.; Delcambre, S. P.; Stuen, K. O.; Craig, G. S. W.; De Pablo, J. J.; Nealey, P. F.; Nygard, K.; Satapathy, D. K.; Bunk, O.; Solak, H. H., Mechanism and dynamics of block copolymer directed assembly with density multiplication on chemically patterned surfaces. *Journal of Vacuum Science & Technology B* **2010,** *28* (6), C6B13-C6B19.

15. Williamson, L.; Lin, G.; Cao, Y.; Gronheid, R.; Nealey, P., Tuning the strength of chemical patterns for directed self-assembly of block copolymers. *SPIE Advanced Lithography* **2014,** *9049*, 9049-1B.

16. Fasolka, M. J.; Mayes, A. M., Block copolymer thin films: Physics and applications. *Ann. Rev. Mater. Res.* **2001,** *31*, 323-355.

17. Han, E.; Stuen, K. O.; La, Y.-H.; Nealey, P. F.; Gopalan, P., Effect of Composition of Substrate-Modifying Random Copolymers on the Orientation of Symmetric and Asymmetric Diblock Copolymer Domains. *Macromolecules* **2008,** *41* (23), 9090-9097.

18. Detcheverry, F. A.; Liu, G.; Nealey, P. F.; de Pablo, J. J., Interpolation in the Directed Assembly of Block Copolymers on Nanopatterned Substrates: Simulation and Experiments. *Macromolecules* **2010,** *43* (7), 3446-3454.

19. Khandpur, A. K.; Forster, S.; Bates, F. S.; Hamley, I. W.; Ryan, A. J.; Bras, W.; Almdal, K.; Mortensen, K., Polyisoprene-polystyrene diblock copolymer phase diagram near the order-disorder transition. *Macromolecules* **1995,** *28* (26), 8796-8806.

20. Perego, M.; Ferrarese Lupi, F.; Ceresoli, M.; Giammaria, T. J.; Seguini, G.; Enrico, E.; Boarino, L.; Antonioli, D.; Gianotti, V.; Sparnacci, K.; Laus, M., Ordering dynamics in symmetric

PS-b-PMMA diblock copolymer thin films during rapid thermal processing. *Journal of Materials Chemistry C* **2014,** *2* (32), 6655-6664.

21. Mueller, M.; de Pablo, J. J., Computational Approaches for the Dynamics of Structure Formation in Self-Assembling Polymeric Materials. *Annual Review of Materials Research, Vol 43* **2013,** *43*, 1-34.

22. Li, W.; Nealey, P. F.; de Pablo, J. J.; Mueller, M., Defect Removal in the Course of Directed Self-Assembly is Facilitated in the Vicinity of the Order-Disorder Transition. *Physical Review Letters* **2014,** *113* (16), 8301-8301.

CHAPTER 4: THE IMPACT OF GUIDE STRIPE STRENGTH ON BLOCK COPOLYMER ASSEMBLY: EQUILIBRIUM AND KINETICS

4.1 Abstract

Directed self-assembly (DSA) of lamellae-forming block copolymer (BCP) thin films can be achieved with chemical patterns consisting of alternating guide stripes and background regions, and the geometry and chemistry of the chemical patterns are important parameters in this type of chemoepitaxial DSA. Here the influence of the strength of interaction between the guide stripes and the guided BCP domains on the quality and mechanism of assembly in the BCP film was investigated. This affinity is a function of the chemistry of the guide stripe, which was controlled using two methods. In the first approach, four different polystyrene-rich materials were used to create guide stripes of varying chemistry. In the second approach, cross-linked polystyrene stripes were exposed to a dose array of UV radiation, tunably altering their chemistry and preferential affinity for the guided BCP chemistry. The kinetics of block copolymer assembly on the resulting chemical patterns were evaluated by assessing the DSA quality through a range of guide stripe widths and pitches. The range of incommensurability tolerance increased through both guide stripe width and pitch for stronger guide stripes and longer anneal time. However, when the degree of partial alignment is considered for a given guide stripe strength, the ultimate thermodynamic commensurability tolerance can be extrapolated from the kinetics study and is independent of anneal time. The DSA performance was also evaluated based on line edge roughness, which increased as the guide stripe became less preferential.

4.2 Introduction

Block copolymer directed self-assembly (BCP DSA) is a promising resolution enhancement technique for dense arrays of features, where naturally forming microdomains are aligned through a thermodynamically driven process.[1] In chemoepitaxial DSA, a BCP film is assembled on a substrate composed of chemically distinct regions that are designed to interact with the BCP domains to induce long-range order.[2-3] A lithographic template can be used to define a chemical pattern of sparse guide stripes and relatively non-preferential background regions, where one of the BCP phases preferentially wets the guide stripes and the remaining domains assemble over the background region. The best surfaces to use in a chemical pattern minimize the interfacial energy between the pattern and the BCP in the aligned state. Since the backfill region is designed to be in contact with both domains, the optimum backfill can be achieved by selecting the proper backfill material that minimizes the interfacial energy with the BCP domains that it contacts, as described by Liu et al.[4] The optimum guide stripe chemistry only needs to minimize the interfacial energy with the guided domain and therefore should theoretically be identical to the chemistry of the guided BCP domain, similar to the design of chemical patterns with no resolution enhancement. The total interfacial energy between the BCP and chemical pattern is minimized when the BCP is perfectly registered, which is the driving force for chemoepitaxial DSA. The aligned system gains an enthalpic benefit compared to randomly oriented vertical lamellae, but that alignment imparts an entropic penalty due to restricting the BCP domains. The equilibrium structure favors aligned domains when the enthalpic benefit exceeds the entropic penalty for alignment. This balance between enthalpy and entropy was developed by Edwards et al. for the case where the resolution of the chemical pattern is matched to that of the assembled BCP.[5]

In this study, poly(styrene-*block*-methyl methacrylate) (PS-*b*-PMMA) BCP was assembled on chemical patterns that were generated from a series of PS-rich cross-linkable random copolymer P(S-*r*-MMA) guide stripe materials. Higher polystyrene content is associated with more preferential wetting of the PS block, leading to larger geometric commensurability tolerance (guide stripe width and pitch) for assembly at a given annealing condition. This trend was more noticeable at short annealing time when the DSA is partially aligned on slightly incommensurate patterns; at longer anneal times, the geometric commensurability converges on the same thermodynamic tolerance for all guide stripe compositions. Furthermore, the line edge roughness (LER) of the DSA pattern is reduced by using a strongly preferential guide stripe composition.

4.3 Experimental

4.3.1 Materials

A series of cross-linkable P(S-*r*-MMA) guide stripe materials (AZEMBLY^{TM} NLD-300, NLD-301, NLD-302, and NLD-128), P(S-*r*-MMA) brush (AZEMBLY^{TM} NLD-127), and P(S-*b*-MMA) BCP (AZEMBLY^{TM} PME-312) were provided by Merck Performance Materials. ArF photoresist AIM5484 was purchased from JSR Micro. Orgasolv® STR 301 was purchased from BASF. RER600 was purchased from Fujifilm.

4.3.2 DSA process

Sample processing was performed on imec's 300 mm process line in Belgium as described previously.[6] A 13 nm film of silicon nitride was deposited on 300 mm Si wafers for reflectivity control. An 8 nm film of cross-linkable guide stripe material was spincast, then annealed at 315°C for 5 min in a nitrogen environment using a TEL ACT12 track. AIM5484 was spincast (95 nm) using a SOKUDO DUO track, exposed on an ASML 1950 immersion scanner (optimum dose = 13 mJ, optimum focus = -0.02 μm, NA = 1.35, dipole illumination $\sigma_o = 0.87$ $\sigma_o = 0.76$, blade angle

= 40°), then developed using manufacturer recommended settings. The resist and X-PS were trim etched in either a Lam or TEL plasma etch chamber. The remaining resist was stripped with Orgasolv in a TEL ACT12 track. The pattern was backfilled by coating 50 nm of AZEMBLY^{TM} NLD-127, then annealing for 5 min at 250°C, resulting in 7 nm of brush grafted to the bare regions of underlying substrate. The wafer was rinsed with RER600 to remove ungrafted brush and dried with a 100°C, 1 min bake. BCP was spincoated onto a chemical pattern at 1500 RPM, soft baked at 100°C for 1 min to remove solvent, and then annealed at 250°C for 1, 5, or 240 min. PMMA was etched on the TEL TACTRAS plasma etch chamber for enhanced imaging contrast.

4.3.3 Characterization

Scanning electron microscope (SEM) imaging was performed with a Hitachi CG5000 after trim etch and after PMMA domain removal. The line width (W) of the photoresist structures after trim etch was measured by automated built-in Hitachi software. Static water contact angle measurements were obtained using a Dataphysics OCAH230L contact angle measurement system. A syringe dispensed 5 μL drops of deionized water, which were measured after 0.3 s of stabilization. Line edge roughness was measured using LERDEMO version 2014b software on rectangular scan (0.45μm x 2.25μm) SEM images taken with a Hitachi CG5000.

4.4 Results and Discussion

Chemical patterns were generated using a series of poly(styrene-*random*-polymethyl metacrylate) P(S-*r*-MMA) guide stripe materials (GSM) at step 1 of Figure 4.1 in order to align the lamellae-forming block copolymer (BCP). This layer is fabricated into guide stripes by patterning photoresist with immersion lithography, and then trimming the photoresist lines with plasma etching. The remaining resist is stripped and a random copolymer brush is grafted to the uncovered substrate between the guide stripes. A BCP film is coated and annealed on the resulting

chemical pattern and the PMMA domain is selectively removed with plasma etching, resulting in a line-space array with 3x pitch reduction compared to the initial patterned resist.

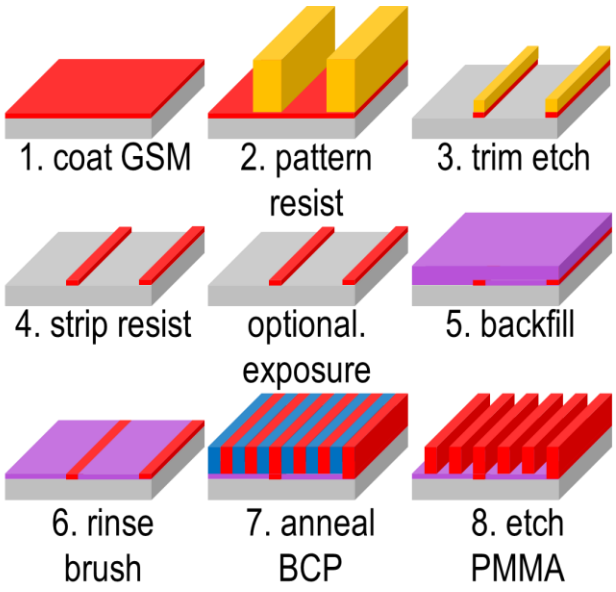

Figure 4.1: Schematic of process flow for fabricating the chemical patterns and assembling BCP.

The wetting behavior for all guide stripe materials was determined on a large-area unexposed surface as a function of composition after processing. The GSM differ in composition from 80-100% PS, but all of them were modified to be less PS-preferential than the as-cast material by the chemical pattern fabrication process, specifically by the trim etch and backfill steps.[7] The water contact angle of the GSM in the final chemical pattern ranges from 83.7° to 79.4° as the PS content decreases as seen in Figure 4.2. Lower water contact angles indicate a more polar and thus less PS-preferential surface, both from GSM composition and process modification.[8] All of these surfaces are more hydrophobic than the backfill brush (contact angle of 76.0°) indicating that the guide stripes are always more PS-preferential than the background region. Note that WCA probes the very top surface, whereas polymers can form a thicker interpenetrated interface; in the context of this study, the brush grafted to the GSM may over-represent the modification. However, BCP

annealed on each of the simulated guide stripe surfaces assembles as vertical fingerprint lamellae, indicating that none of the surfaces are strongly selective to the PS block.

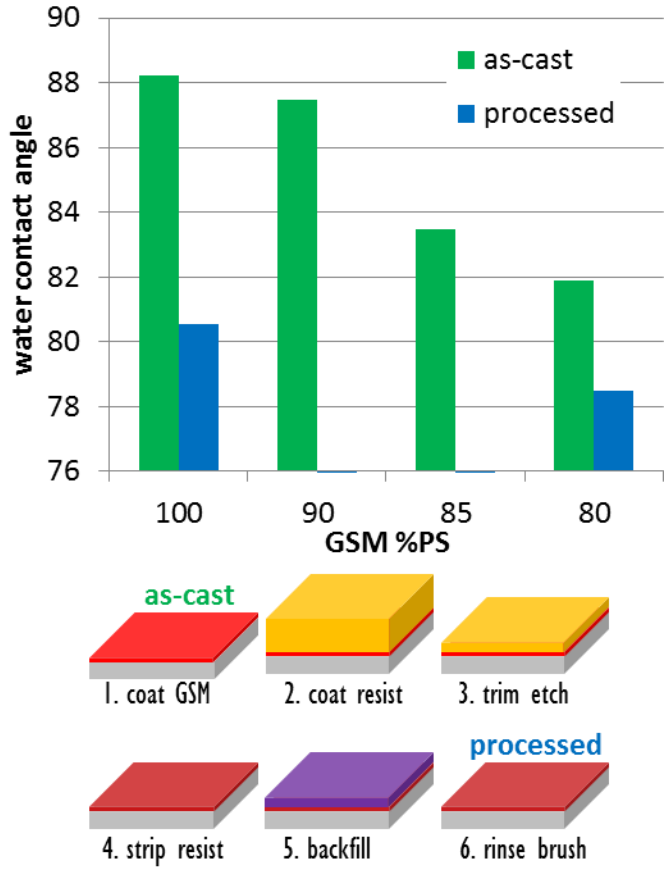

Figure 4.2: Water contact angle of each GSM before and after processing to simulate the guide stripe surface. Lower water contact angles correspond to less PS-preferential surfaces.

BCP films were assembled on patterns with a series of pattern fields with a range of guide stripe pitches and widths generated from each of the four GSM. The range of conditions that are well-aligned was assessed after the BCP was annealed for 1 min at 250 °C by inspecting a single SEM image with 2.75 x 2.75 μm field of view for each field, then assigning it as defect-free (green) or containing misalignment (red) in Figure 4.3. The data are fit with an axis-aligned ellipse by balancing the number of good and bad fields that are on the wrong side of the ellipse boundary. The dimensions of the ellipses quantify the geometric commensurability window for a given wafer

as a metric to evaluate the DSA performance through different guide stripes. Note that the pitch of the guide stripes, L_S, is normalized by the natural periodicity of the BCP (L_0 = 28 nm). Also, the width of the guide stripes, W, has been normalized to the lamellar period imposed by the pattern, $L_S/3$, which can be different from L_0. This normalization minimizes the covariance of the commensurability ellipses that would otherwise be present without proper normalization, meaning that all L_S have the same optimal normalized W. The major and minor axes of the commensurability ellipse correspond to the maximum guide stripe width and pitch commensurability tolerances, respectively. Both geometric parameters impose an entropic penalty for DSA and are therefore correlated from sample to sample.

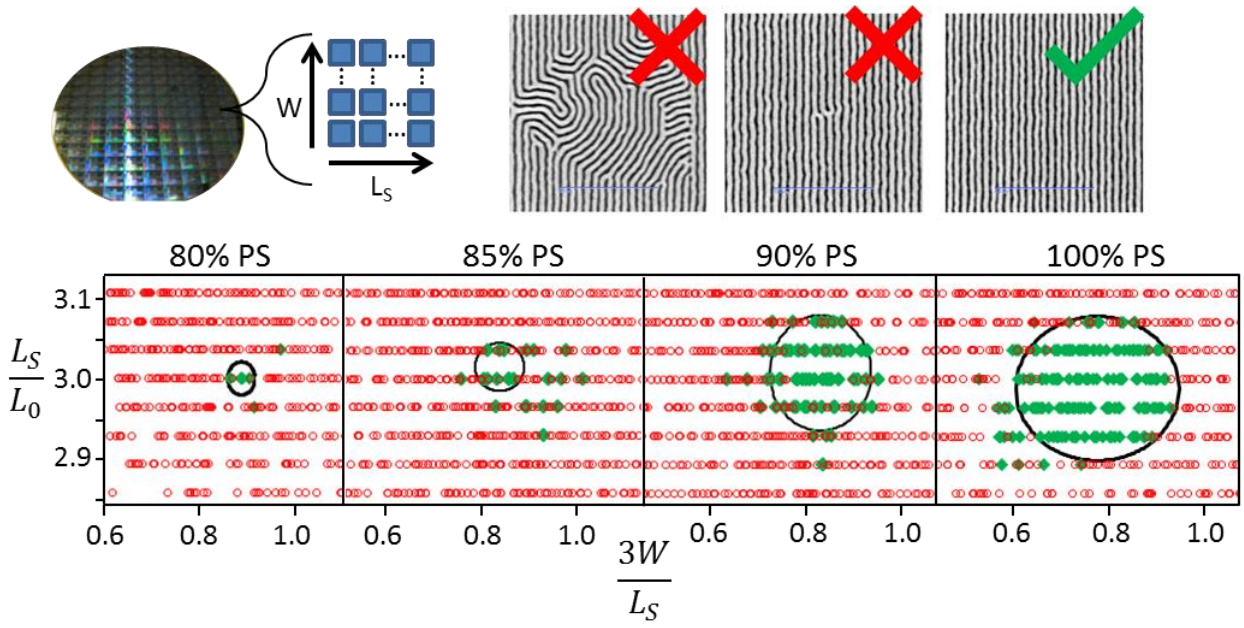

	80%PS	85%PS	90%PS	100%PS
trim	0.028	0.051	0.11	0.17
pitch	0.021	0.030	0.072	0.090

Figure 4.3: Geometric commensurability is assessed for different guide stripe compositions after 1 min of anneal. Fields with perfect registration in the representative field of view are marked green. An axis-aligned ellipse is fit to the data to describe the range of guide stripe width and pitch commensurability. The range of commensurability in width and pitch are the major and minor axes of the ellipse.

A more detailed analysis of these SEM images measures the degree of alignment after DSA, leading to more information at the edge of the commensurability window. A custom image analysis algorithm vertically smears the image in-line with the pattern stripes so that misaligned regions are blurred and thus detected. An example of the misalignment identified in this manner is shaded red in Figure 4.4a. As the chemical pattern is increasingly non-optimal, the area fraction of misalignment linearly increases. At a certain threshold, the BCP is randomly aligned and saturates at a value of ~0.8 for an unguided system for this analysis because some regions will statistically be in the direction of interest. The fraction of misalignment is plotted through guide stripe width

in Figure 4.4b. To avoid congestion in the figure, only two series of misalignment measurements are plotted. A linear regression is plotted through the misalignment fraction for narrow guide stripe widths and the slope of the regression is plotted for all four GSM at two pitches in Figure 4c. GSM with higher PS content have a sharper transition between perfect registration and no alignment.

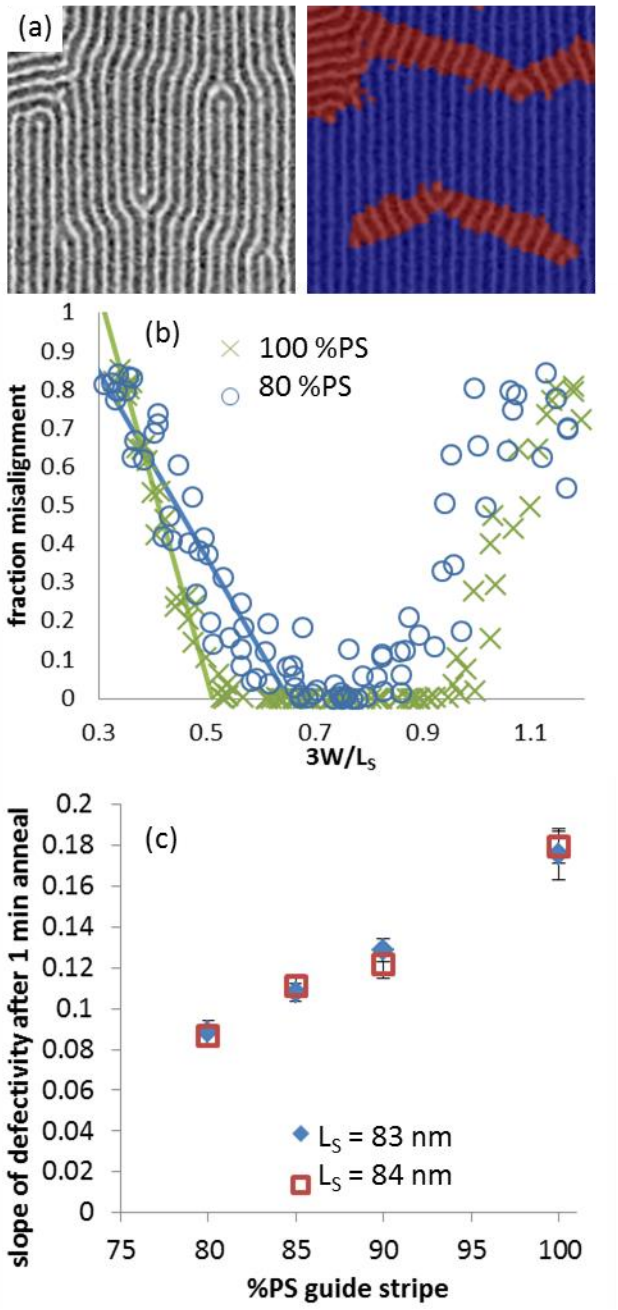

Figure 4.4: (a) Sample image with 20% fraction misalignment marking the aligned BCP in blue and misaligned BCP in red. (b) The fraction of misalignment through guide stripe width at optimum pitch. (c) The gradient in the misalignment area for the series of GSM. A steeper transition to the ordered regime is observed for a more preferential guide stripe (higher %PS).

Additional annealing of the BCP on chemical patterns increased the commensurability window. Notably, the pitch and guide stripe width tolerance increases dramatically from 1 min to

5 min of annealing, and the commensurability tolerances for different GSM converge. Annealing for 4 hr has little effect on the commensurability tolerance, suggesting that it approaches a maximum range. Further evidence for the presence of a maximum geometric tolerance for a given system is illustrated by the area fraction of misalignment plotted through the guide stripe width at constant pitch in Figure 4.5b. The gradient in misalignment fraction is steeper at longer anneal time, but the boundaries of the process window (identified by the guide stripe width that leads to completely random orientation) are unchanged. These boundaries define the maximum commensurability window independent of anneal time and is identifiable after a 1 min anneal. The steeper gradient in misalignment area is due to the commensurability ellipse approaching this maximum range. Previous work has demonstrated that ultimate defect density at the best pattern geometry continues to improve with long anneal times, which is beyond the sensitivity of this analysis.[9]

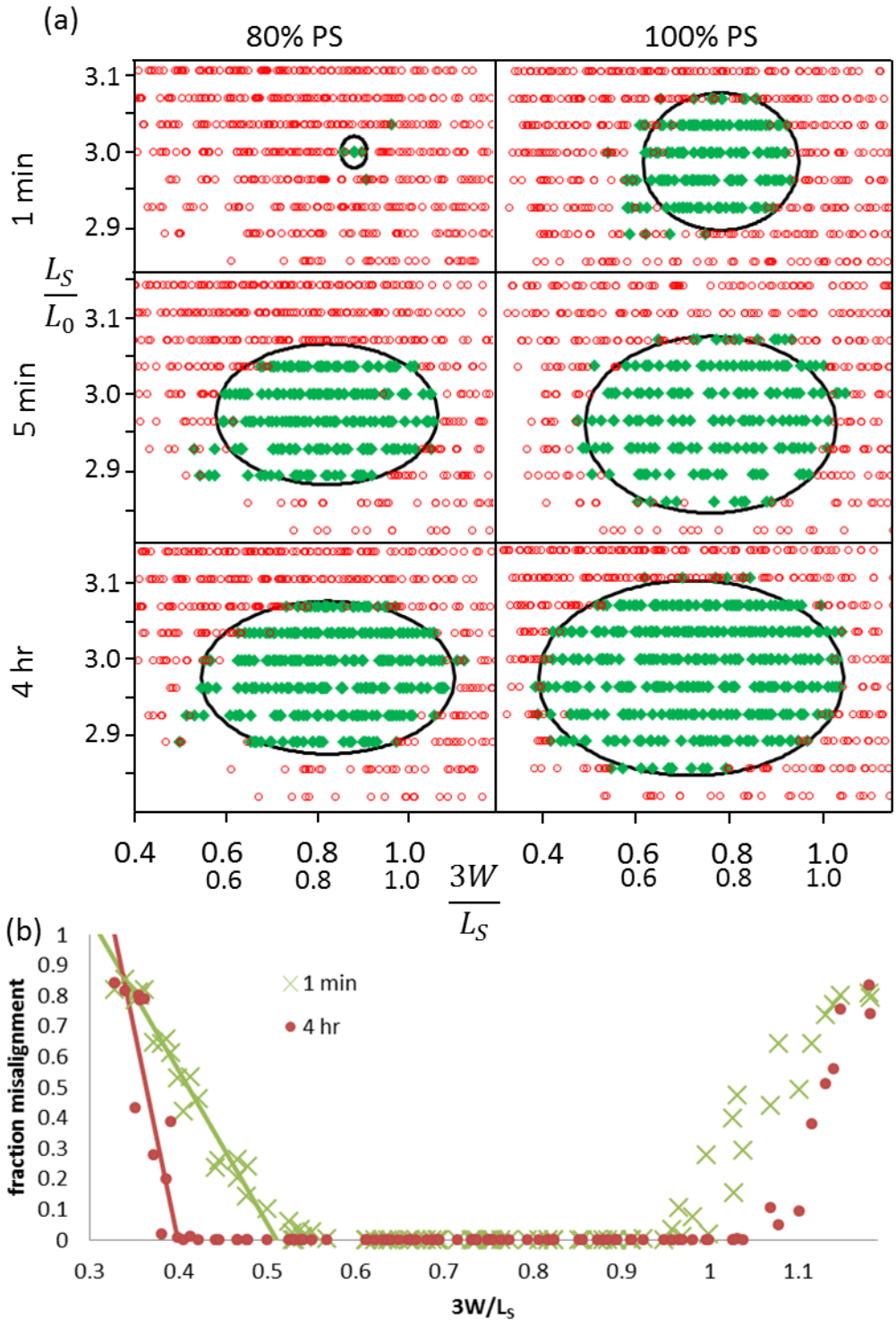

Figure 4.5: (a) Geometric commensurability after 1, 5 min and 4 hr BCP anneal. (b) Fraction of misalignment for 100% PS GSM after 1 min and 4 hr BCP anneal. Additional annealing increases the number of defect-free fields, but does not alter the maximum commensurability tolerance.

In addition to misalignment defects, line edge roughness (LER) is also sensitive to the free energy balance of the DSA system. The LER of the BCP domains was measured in the field of optimal pattern dimensions after PMMA removal. As the guide stripe wetting selectivity decreases, the LER increases as demonstrated in Figure 4.6. The trend in LER demonstrates that a stronger thermodynamic interaction between the guide stripe and guided domain corresponds to tighter control over the placement of the BCP domains and therefore lower LER.

Line edge roughness is associated with the tendency of the polymer domain to introduce spontaneous curvature. Entropically, the polymer would prefer to assemble with spontaneous curvature, as found in an unguided system. This tendency to induce curvature generates local variation in the line placement for a guided system. The higher the enthalpic driving force, the more that the entropic effects can be overcome, resulting in lower LER.

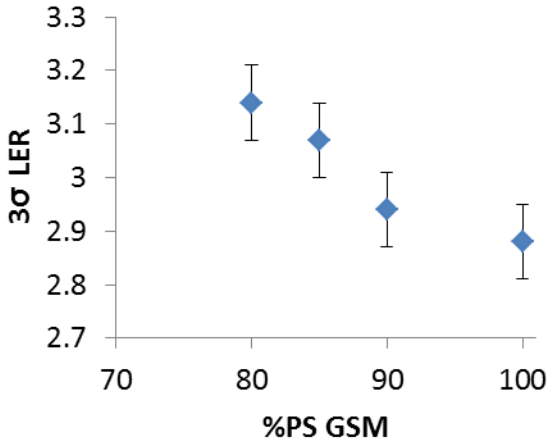

Figure 4.6: Line edge roughness comparing DSA performance on the series of GSM.

All non-idealities in the DSA system are sources of penalties in the driving force for achieving pattern registration. The primary parameters for chemical pattern design are the guide stripe and backfill materials, and the pitch and width of the guide stripes. The chemistry of the chemical

pattern regions determines the interfacial energy between the pattern surfaces and the BCP domains. The interfacial energies dictate the enthalpic benefit for the BCP to epitaxially align to the guide stripes. In contrast, the geometric incommensurability exacerbates the entropic penalty when polymer chains are required to adopt conformations deviating from the unguided polymer behavior, which can slow or prevent pattern registration.

The system is most sensitive to differences in driving force for DSA at short anneal times, so identifying the system parameters with the strongest driving force is most straight-forward at short annealing times. The driving force for assembly is independent of anneal time, and a pattern that gives better assembly at short anneal times is expected to always have the best defectivity for a given BCP anneal. For a given anneal time, a larger commensurability tolerance indicates that the chemical pattern provides a higher enthalpic gain for DSA, as it is able to overcome a larger entropic penalty. The simple SEM image analysis approach to identify the degree of registration is only sensitive to partially aligned systems, but the registration at a short anneal time could be correlated with vanishing defect density for an equivalent system given a longer anneal.

Recent characterization of the chemical patterns made through the same process line as described in this work demonstrates that the system has additional complexity that contributes to the DSA. The guide stripes fabricated on this process line have broad sidewalls after trim etch and the sidewalls become PMMA-prefential due to plasma treatment. The resulting pattern has three regimes where both the resist-protected GSM and plasma-modified GSM contribute as guiding surfaces. When PMMA is added to the GSM, the etch characteristics and wetting behavior of the final surface in the chemical pattern may be different from that of the pure PS-containing GSM. However, dark footing regions were still observed for all GSM and the plasma modification is likely very similar in all cases.

4.5 Conclusions

This work demonstrates the importance of the preferential wetting nature of the guide stripe in a chemical pattern for BCP DSA. Any reduction in the guide stripe wetting selectivity should be minimized in order to achieve the best DSA performance, both through defectivity and LER metrics. A stronger guide stripe contributes a larger enthalpic gain for alignment, increasing the pitch commensurability and decreasing line edge roughness. It is not clear whether a guide stripe can be more selective in wetting of one block than a guide stripe of matching polymer chemistry. However, any modification that reduces the wetting selectivity decreases the driving force for DSA. Such a modification impedes defect annihilation and contributes to line edge roughness in the assembled domains.

4.6 References

1. Bates, C. M.; Maher, M. J.; Janes, D. W.; Ellison, C. J.; Willson, C. G., Block Copolymer Lithography. *Macromolecules* **2014,** *47* (1), 2-12.

2. Cheng, J. Y.; Rettner, C. T.; Sanders, D. P.; Kim, H. C.; Hinsberg, W. D., Dense self-assembly on sparse chemical patterns: Rectifying and multiplying lithographic patterns using block copolymers. *Advanced Materials* **2008,** *20* (16), 3155-3158.

3. Craig, G. S. W.; Nealey, P. F., Self-assembly of block copolymers on lithographically defined nanopatterned substrates. *Journal of Photopolymer Science and Technology* **2007,** *20* (4), 511-517.

4. Liu, C.-C.; Ramirez-Hernandez, A.; Han, E.; Craig, G. S. W.; Tada, Y.; Yoshida, H.; Kang, H.; Ji, S.; Gopalan, P.; de Pablo, J. J.; Nealey, P. F., Chemical Patterns for Directed Self-Assembly of Lamellae-Forming Block Copolymers with Density Multiplication of Features. *Macromolecules* **2013,** *46* (4), 1415-1424.

5. Edwards, E. W.; Montague, M. F.; Solak, H. H.; Hawker, C. J.; Nealey, P. F., Precise control over molecular dimensions of block-copolymer domains using the interfacial energy of chemically nanopatterned substrates. *Advanced Materials* **2004,** *16* (15), 1315-+.

6. Liu, C.-C.; Thode, C. J.; Delgadillo, P. A. R.; Craig, G. S. W.; Nealey, P. F.; Gronheid, R., Towards an all-track 300 mm process for directed self-assembly. *Journal of Vacuum Science & Technology B* **2011,** *29* (6).

7. Williamson, L. L., Guanyang; Cao, Yi; Gronheid, Roel; Nealey, Paul Tuning the strength of chemical patterns for directed self-assembly of block copolymers. *SPIE Advanced Lithography* **2014,** *9049*, 9049-1B.

8. Han, E.; Stuen, K. O.; La, Y.-H.; Nealey, P. F.; Gopalan, P., Effect of Composition of Substrate-Modifying Random Copolymers on the Orientation of Symmetric and Asymmetric Diblock Copolymer Domains. *Macromolecules* **2008,** *41* (23), 9090-9097.

9. Delgadillo, P. A. R.; Harukawa, R.; Parnell, D.; Lee, Y.-T.; Chan, B. T.; Lin, G.; Cao, Y.; Nagaswami, V. R.; Somervell, M. H.; Nafus, K.; Gronheid, R.; Nealey, P. F., Kinetics of defect annihilation in directed self-assembly of block copolymers using chemically nanopatterned surfaces. *SPIE Advanced Lithography* **2014,** *9049*, 9049-19.

CHAPTER 5: ROOT SOURCES OF LINE EDGE ROUGHNESS IN DIRECTED SELF-ASSEMBLY OF LAMELLAR BLOCK COPOLYMERS

5.1 Abstract

The sources of line-edge roughness (LER) in block copolymer (BCP) films prepared via chemoepitaxial directed self-assembly (DSA) were investigated and evaluated. A systematic approach was used to identify possible root causes of LER and then experimentally determine trends and relative magnitude of influence of the respective process variables. The possible sources were group broadly into two categories: those factors present in the BCP film itself and those coming from the chemical pattern. Qualitative trends were used to identify several key influences on BCP LER, most notably the chemistry (χ) and polydispersity of the BCP film and the guiding strength of the chemical pattern. Targeted development of designer materials will exploit this new insight into LER in BCP DSA to lower roughness and improve overlay performance.

5.2 Introduction

Block copolymer (BCP) directed self-assembly (DSA) as a technique to extend the capability for nanoscale patterning beyond the limit of traditional lithography has been demonstrated at the laboratory scale[1] and is now being evaluated at the industrial scale on full 300 mm production tools.[2-4] In chemoepitaxial DSA, a BCP film is assembled on a pattern consisting of well-defined regions of controllable geometry and chemistry.[5] Although resolution enhancement to sub 10 nm half-pitch has been demonstrated with this technique,[6] defect levels and placement accuracy remain outside industry tolerance.[7] Significant effort focused on reducing defectivity, with an emphasis on identifying and understanding the root causes of various defect modes, has yielded

impressive results.[8-9] To date, however, no comparable study has been undertaken to comprehensively address the issue of placement accuracy.

In BCP DSA, placement accuracy is closely linked to roughness, another common industry performance metric. Line roughness is often expressed as having three components: line width roughness (LWR), line placement roughness (LER), and line edge roughness (LPR). LWR refers simply to the nonuniformity of line width, LER describes the variation of a given structure's edge, and LPR quantitatively captures how much a line's center deviates from its target position. These three measures of roughness are highly interdependent, and it can be mathematically demonstrated that LPR + LWR = LER. For BCP DSA, where each line is a BCP domain, the line width is primarily a function of the polymer size. When the polymer size distribution is very narrow, LWR can be suppressed so that LER effectively becomes a measure of LPR and therefore of placement accuracy.

For commercial applications, rigid placement control and tight error budget motivate many exploratory studies to report LER as a figure of merit for quantitative evaluation. However, the approach is often limited to the scope of the individual study, without discussion of the "why" behind the number reported. Herein we attempt to discuss more thoroughly the root causes of LER in BCP DSA, with a focus on using our understanding of polymer thermodynamics to explain qualitative trends. We identify several experimental process parameters that strongly influence LER performance and discuss how future work can seek to mitigate the placement error in this technique.

5.3 Experimental

5.3.1 Materials

Crosslinking polystyrene (X-PS) (AZEMBLY^{TM} NLD-128), P(S-*r*-MMA) brush (AZEMBLY^{TM} NLD-127, 51% PS), P(S-*b*-MMA) BCP with L_0 = 28 nm (AZEMBLY^{TM} PME-312), and specialized brushes and BCP formulations were provided by Merck Performance Materials. ArF photoresist AIM5484 was purchased from JSR Micro. Orgasolv STR 301 was purchased from BASF. Organic solvent RER600 was purchased from Fujifilm. All materials were used as received.

5.3.2 DSA process

The chemical patterns were fabricated on a 300 mm process line devoted to DSA at the imec nanoelectronics R&D lab in Belgium. In the baseline process, a 13 nm silicon nitride (SiN) film was deposited on 300 mm Si wafers as an inorganic antireflective coating. The wafers were coated with an 8 nm spincast film of X-PS, then annealed at 315 °C for 5 min in a nitrogen environment using a TEL CLEAN TRACK ACT^{TM}12 track. The wafers were coated with AIM5484 (95 nm) using a SOKUDO DUO track, exposed on an ASML 1950 immersion scanner (optimum dose = 11 mJ, optimum focus = -0.02 μm, NA = 1.35, dipole illumination, σ_o = 0.98, σ_i = 0.86, blade angle = 40°) and developed to create 84 nm pitch line-space patterns of various line widths. The samples were etched with an oxygen-containing plasma, which simultaneously isotropically etched the photoresist and removed unprotected X-PS. The remaining resist was stripped with Orgasolv STR 301, leaving isolated X-PS stripes on the nitride. The pattern was coated with backfill brush AZEMBLY^{TM} NLD-127 (50 nm), then annealed for 5 min at 250 °C to graft the brush to the nitride surface. The remaining ungrafted brush was removed through rinsing with RER600, leaving a chemical pattern of alternating X-PS stripes and backfill brush regions. BCP

was spin-coated at a thickness of 35 nm and annealed at 250 °C with nitrogen purge for various times. The PMMA domains were removed and the resulting patterns were transferred into the underlying hardmask with plasma etching on a TEL Tactras^{TM}. For some experiments, steps were modified or suppressed as necessary, described in the results section below.

5.3.3 Characterization

Scanning electron microscope (SEM) imaging was performed with a Hitachi CG5000 after trim etch, after PMMA domain removal, and after pattern transfer. The line width (W) of the photoresist structures after trim etch and the edge profiles of the BCP and silicon structures were measured by automated built-in Hitachi software. Line edge roughness was measured using LERDEMO version 2014b software on rectangular scan (0.45μm x 2.25μm) SEM images taken with a Hitachi CG5000.

5.4 Results and Discussion

5.4.1 Methodology

The process flow used to fabricate line-space arrays from lamellae-forming block copolymers (BCP) is an example of chemoepitaxial directed self-assembly (DSA) and is shown in Figure 5.1 below. This flow, known as the Liu-Nealey (LiNe) flow,[2, 10] employs lithographic patterning and a lateral trim etch to generate patterns of cross-linked polystyrene (X-PS) which are backfilled with an endgrafted brush of complimentary and relatively non-preferential chemistry. The resulting chemical patterns are used to direct the assembly of a poly(styrene-*block*-methyl methacrylate) (PS-*b*-PMMA) thin film into a regular array of PS and PMMA lines. Selective removal of the PMMA domains leaves a pattern of PS lines, which can then be transferred into a functional material layer below.

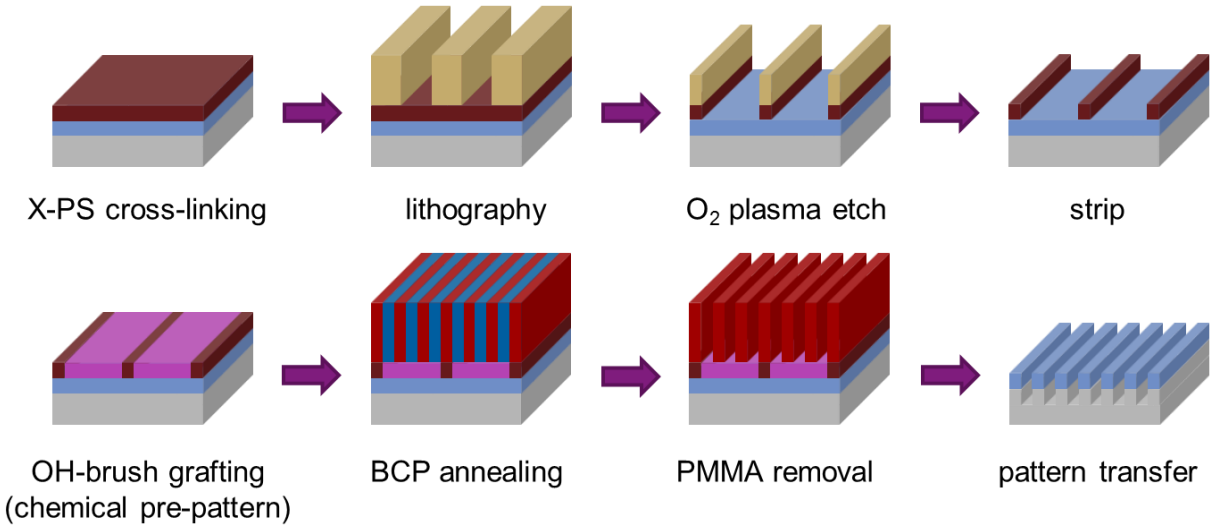

Figure 5.1: A schematic of the Liu-Nealey ('LiNe') chemoepitaxial DSA flow used to assemble ordered line-space arrays of BCP domains. LER can be measured in the BCP directly (after PMMA removal) or in the active silicon layer (after pattern transfer).

When investigating line-edge roughness (LER) in these samples, we can therefore measure after PMMA removal but before pattern transfer, or after transfer into the silicon substrate. The former measurements capture the LER without the compounding effects of pattern transfer and therefore more closely represent the roughness of the BCP structures themselves. However, since the measurements are taken from top-down SEM images, they do not probe the full complexity of LER through the depth of the BCP structures. Furthermore, the motivation for this study is the mitigation of roughness in the final active layer, so measurement of the lines after pattern transfer more closely reflects this ultimate goal. Therefore, whenever possible, measurements were obtained both before and after pattern transfer; in all cases, there is a good qualitative match between the "before" and "after" data trends. For some experimental conditions it was not possible to obtain measurements before pattern transfer. In these cases only the final silicon structure was measured, but the data trends are expected to reflect the behavior of LER in the BCP structure as well. After transfer into silicon, it was sometimes possible to differentiate between the "guided" and "unguided" lines (those formed from a PS domain aligned over an X-PS guide stripe vs. the

interpolated domains); in such cases the LER was binned and plotted separately. In all cases, LER measurements were only performed on continuous lines in large areas of defect-free assembly; images with alignment defects were excluded from this analysis.

5.4.2 Approach

In attempting to identify the root causes of LER in BCP DSA, we considered carefully the fundamental physics at play, beginning with an analysis of what LER represents in this system. In a lamellae-forming BCP film, the lines are individual phase-separated domains; the edges are the boundaries between the phases. Within this context, line edge roughness can therefore be understood as fundamentally related to the phase separation physics. Block copolymer systems self-assemble due to the chemical dissimilarity between the two blocks which is quantitatively represented by the Flory-Huggins interaction parameter χ (chi). The physics of phase separation and interfacial width are heavily influenced by this parameter, which is in turn a function of the chemistry of the BCP system. For these systems, chemistry is not limited to the molecular composition of the components but also their ratio and size distribution (symmetry and polydispersity). Furthermore, given the complex nature of macromolecular phase transitions, the thermal history of the system must be taken into account in order to identify equilibrium and quasi-equilibrium behavior. In chemoepitaxial directed self-assembly (DSA), the BCP thin film does not exist in isolation but instead interacts with and is directed by the chemical pattern, which can be defined by its chemical and geometric parameters. For the line-space patterns considered here, those parameters are the chemistry of the guide stripe and background regions, and the width (W) and spacing (L_S) of the former. Additionally, the LER of the final assembled BCP structures may be influenced by the spatial variation and edge roughness present in the chemical pattern itself. Thus, through this initial analysis, we have identified two main categories of potential root causes

of LER in our BCP systems: those stemming from factors intrinsic to the BCP film itself and those coming from the interactions of the film with the directing chemical pattern.

BCP film

5.4.3 BCP chemistry

In identifying and evaluating potential root causes of LER in BCP systems, we began by considering the composition of the BCP film and how that influences interfacial width and curvature. For BCP systems, phase separation behavior is most simply described by χN, the product of the Flory-Huggins interaction parameter χ (chi) and the degree of polymerization N. The relationship between χN and LER is shown in Figure 5.2 below and indicates that for increasing χN (and therefore increasing chemical dissimilarity between the two blocks), LER decreases significantly. This phenomenon can be understood as an effect of the sharpening of the interfacial width between the PS and PMMA domains due to the enthalpic penalty and resulting repulsion between the two blocks.[11]

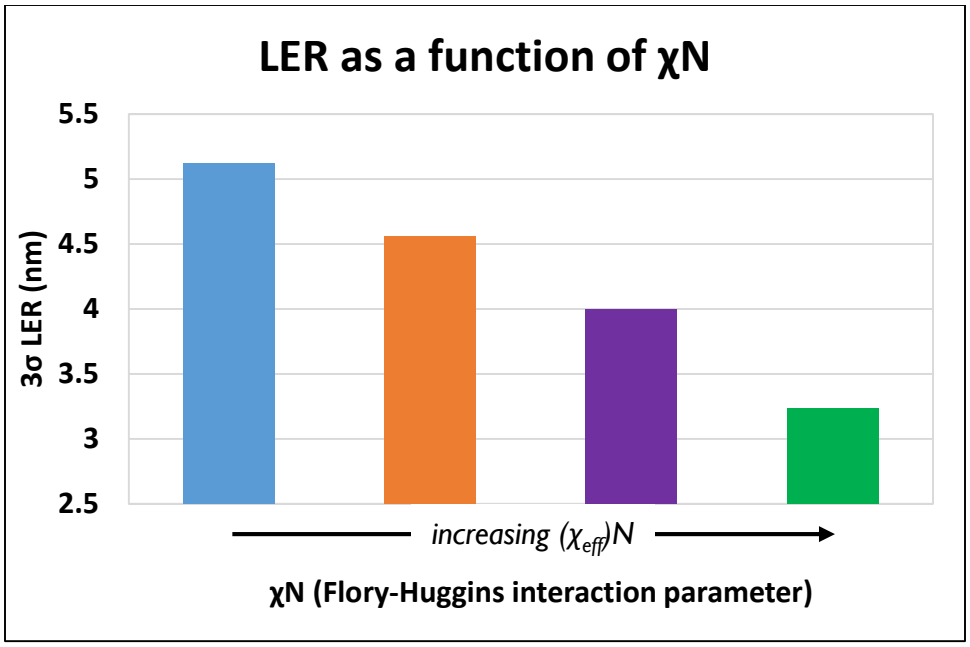

Figure 5.2: LER as a function of the Flory-Huggins interaction parameter χ (chi), a single order parameter measure of BCP chemistry. Roughness decreases as χ increases.

Block copolymer thin film composition is further described by the system's symmetry as well as its polydispersity. Symmetry describes how much a lamellae-forming system deviates from the perfectly symmetric case of equal volume fractions of both blocks.[12] The polydispersity index (PDI), used extensively to describe macromolecular and other systems, is a measure of uniformity in the size distribution of the individual polymer chains. The effect of these parameters is shown qualitatively in Figures 5.3 and 5.4, respectively. For a range of asymmetry in the BCP composition, lamellar structures are still observed but the LER is always slightly higher than for the symmetric (equal volume fraction) case. To investigate polydispersity, two BCP films with the same L_0 but different PDI were compared, with the LER for the lower PDI sample significantly lower than that of the higher PDI sample. This result can be understood when considering the interfacial physics in a polydisperse system. In such a system, the BCP chains are different lengths and therefore cannot line up perfectly, inducing curvature in the domains and their interfaces and thus causing higher LER in the system overall.[13-14]

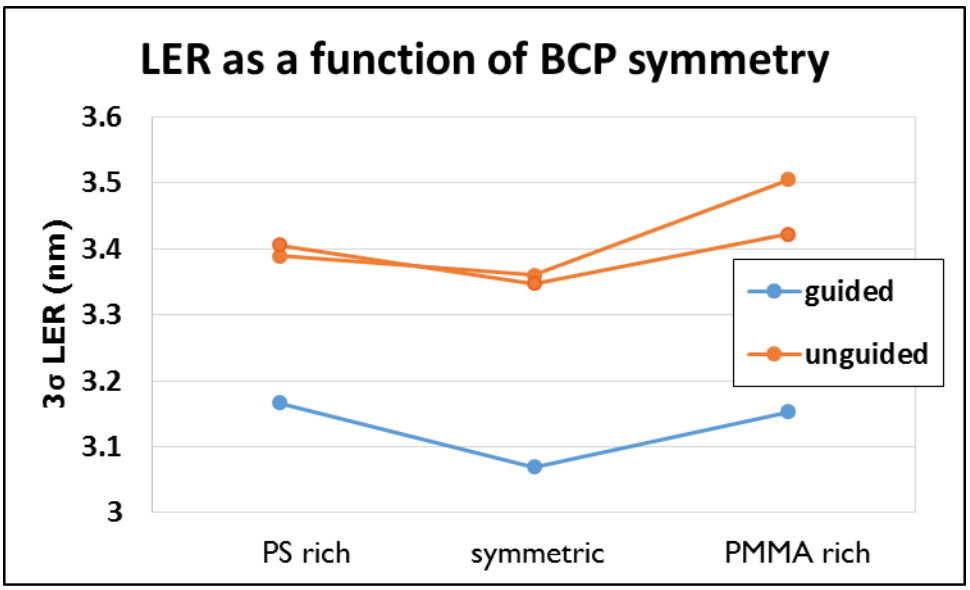

Figure 5.3: LER as a function of BCP symmetry. The symmetric (equal volume fraction of each domain) film yielded the lowest roughness, with asymmetric compositions showing slightly increased LER.

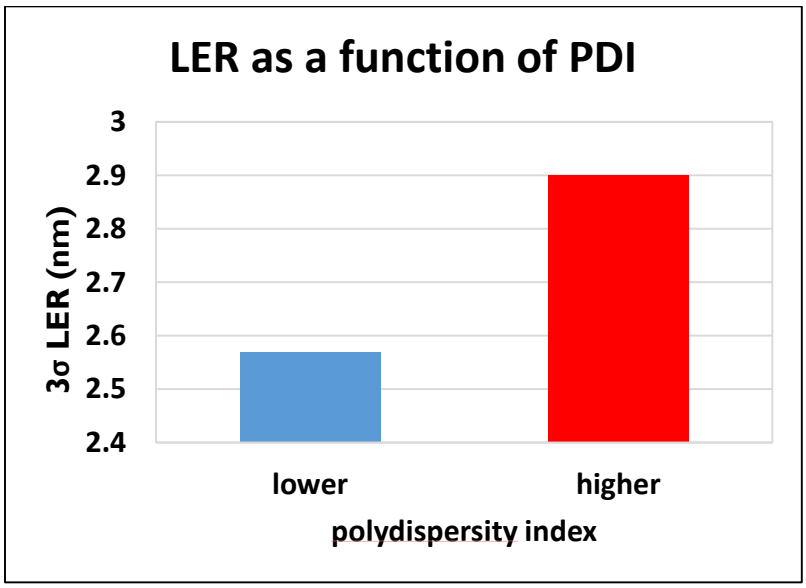

Figure 5.4: The effect of polydispersity on LER. Two systems with the same L_0 show markedly different roughness, with the lower PDI system exhibiting better performance.

5.4.4 BCP thermal history

Recent studies in BCP defectivity have identified thermal annealing as one way to reduce the count of misalignment defects, such as dislocation pairs.[8] Since these misalignment structures can be kinetically trapped states, they can relax to the defect-free aligned structures through additional annealing time or at elevated annealing temperatures. We tested the same conditions for LER, with the results shown in Figures 5.5 and 5.6 below. These graphs show that LER does not change with anneal time or temperature, indicating that the LER level is an intrinsic property of the particular BCP chemistry. Although additional annealing kinetics may help annihilate defects, once the BCP film achieves registration the LER does not change.

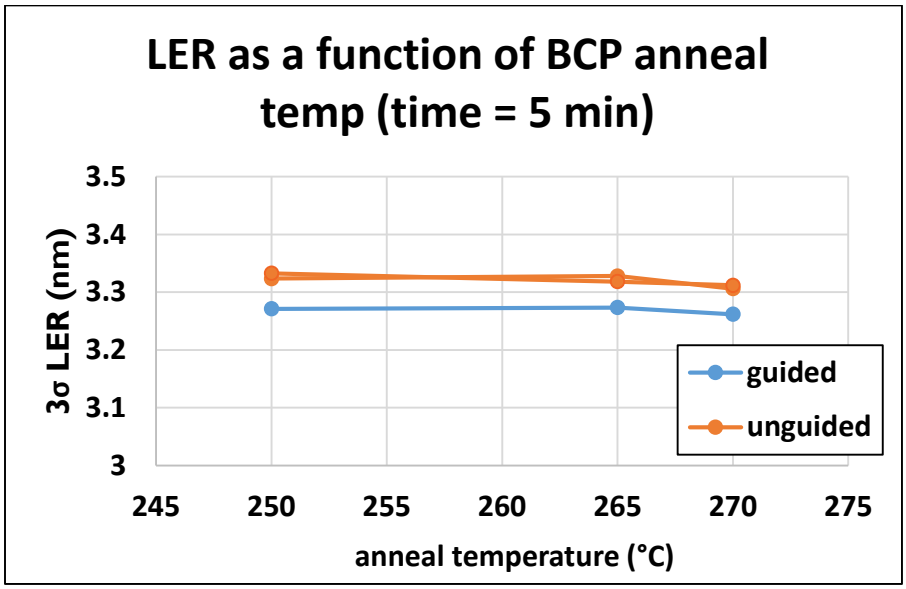

Figure 5.5: LER as a function of anneal temperature at a fixed time. Elevated anneal temperatures had no effect on roughness performance.

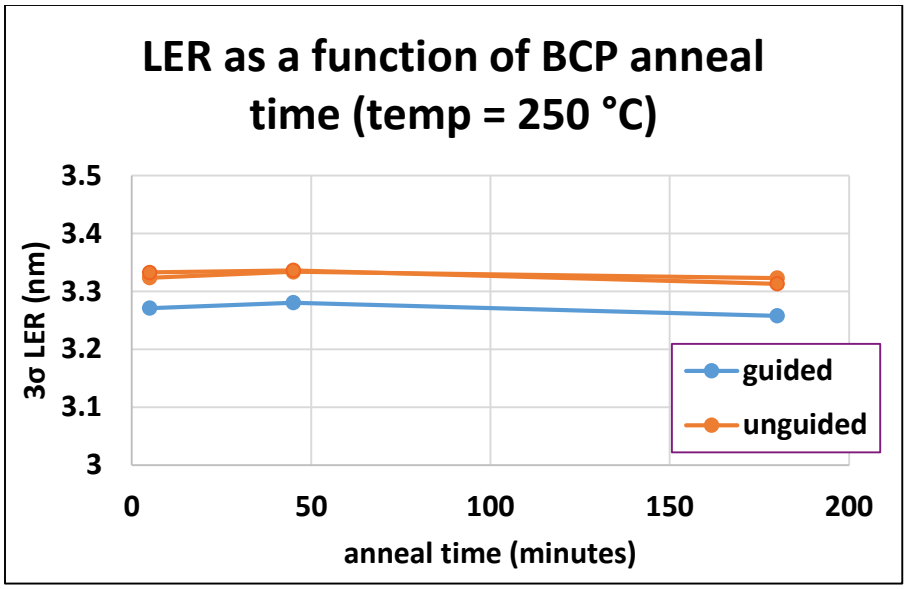

Figure 5.6: LER as a function of anneal time at fixed temperature. Once registration is achieved, annealing for longer times has no impact on edge roughness.

5.4.5 Impact of chemical pattern

Previous work has identified the salient features of the chemical patterns used in this flow as both geometric and chemical in nature.[1] In particular, the spacing or pitch (L_S) of the guide stripes, the width (W) of the guide stripes, the chemistry of the guide stripes, and the chemistry of the backfill brush are the defining features in this chemoepitaxial flow. To investigate LER as a function of each of these parameters, we generated four series of chemical patterns, each fixed in three variables and varying in the fourth. The impact of pattern geometry on LER is shown in Figures 5.7 and 5.8 below.

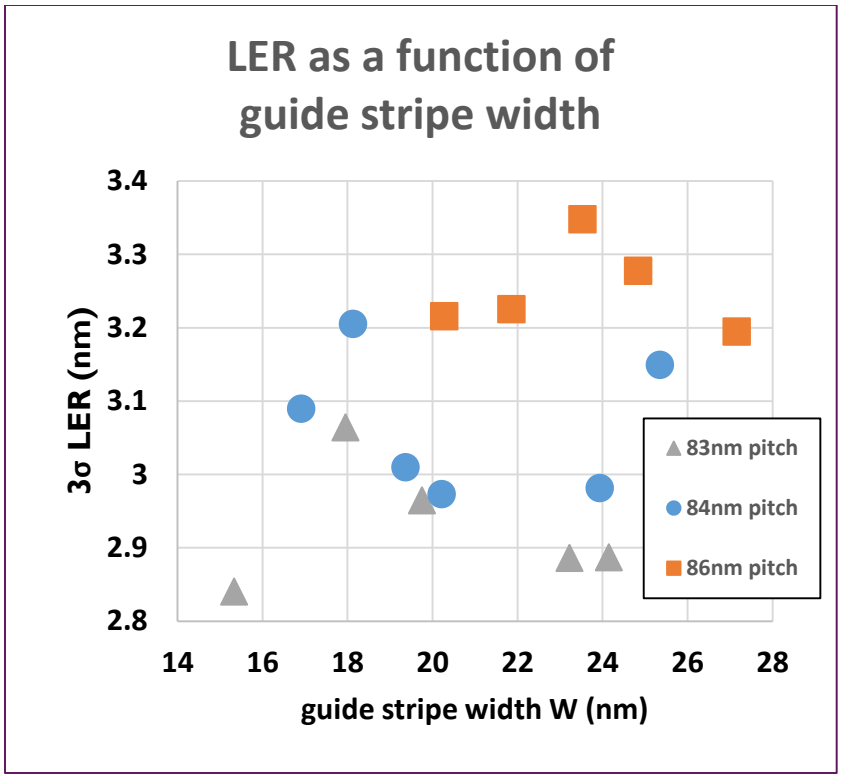

Figure 5.7: LER on chemical patterns with varying guide stripe width (W), at three different pitches. There is no correlation between LER and W.

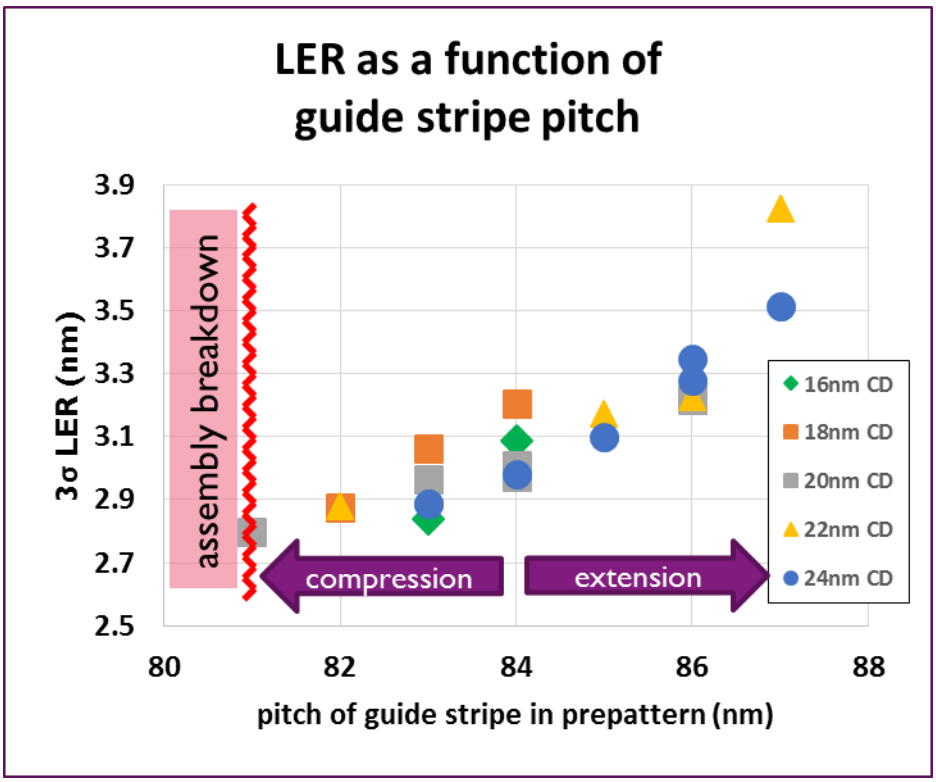

Figure 5.8: LER as a function of guide stripe pitch (L_S) at different guide stripe widths. LER decreased with tightened pitch, right up to the breakdown point where the BCP film no longer registers on the chemical pattern due to geometric mismatch.

As can be seen in Figure 5.7, guide stripe width has no effect on LER. In contrast, guide stripe pitch (Figure 5.8) does impact LER, with roughness lower at tighter pitches. For our system, we are using a BCP with a natural period (L_0) of 28 nm at 3x density multiplication, so a guide stripe pitch (L_S) of 84 nm is at the relaxed, equilibrium spacing of the domain. At broader pitches, the BCP domains are in extension, exerting stress on the domains and leading to a small additional degree of roughness along the line to relieve the stress. For pitches tighter than 84 nm, the BCP domains are in compression and the line edge roughness is diminished. However, other defect modes increase in frequency at these non-optimal pitches, so the benefit of the small decrease in LER is outweighed by the negative effect of higher defectivity. It is also possible that the additional defectivity is partially responsible for the decreased LER. For example, when disclination defects form, they provide sites of high interfacial curvature where polymer chains of abnormal length

(either longer or shorter than average) can reside with a lower enthalpic penalty. The effect on the system is to locally decrease the polydispersity, removing sources of curvature and therefore LER.

As an extension of our investigation of the impact of guide stripe pitch (L_S) on LER, we also considered density multiplication factor. In this resolution-enhancing flow, L_S is set by the pitch of the lithographic pre-pattern and is chosen to be an integer multiple of the natural period of the block copolymer L_0, where that integer is defined as the density multiplication factor. For the majority of this work, we used 3x as our density multiplication, but we also compared this setup to a higher density multiplication factor (4x), with the higher density multiplication factor showing noticeably larger LER (Figure 5.9). At higher density multiplication factors, a smaller fraction of the BCP domains are directly guided, allowing the system more flexibility to adopt locally curved interfaces and thus causing a higher degree of edge roughness.

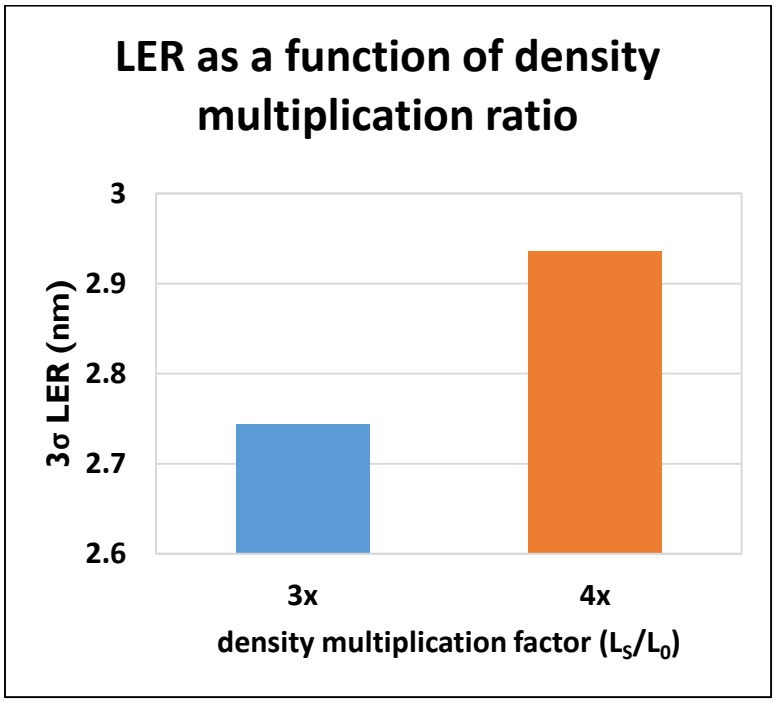

Figure 5.9: LER of the same BCP on chemical patterns with two different density multiplication factors. The lower density multiplication factor (3x) has a higher fraction of directly guided BCP domains and therefore shows better roughness performance than the higher density multiplication factor (4x).

We also looked at the effect on LER of pattern chemistry, both of the guide stripe and the backfill brush. To test the effect of guide stripe chemistry, we prepared samples with four different guide stripe materials, ranging in composition from 100% polystyrene (standard process) to lower styrene fraction (but still styrene-majority) materials. To test the impact of backfill brush chemistry, we prepared chemical patterns with brushes across a range of composition. The brushes were all poly(styrene-*random*-methyl methacrylate) (PS-*r*-PMMA) but ranged in composition from moderately majority styrene to moderately majority methyl methacrylate. The results are shown in Figures 5.10 and 5.11 below.

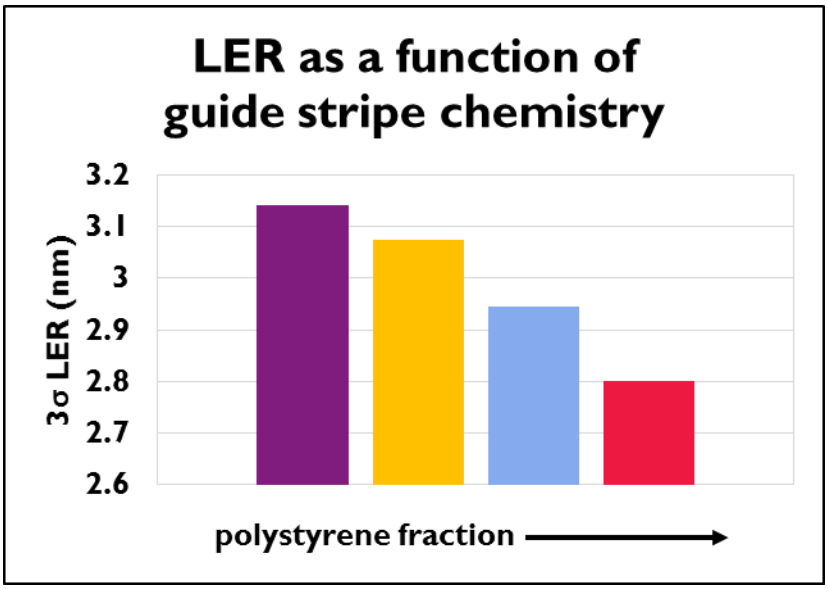

Figure 5:10: The impact of guide stripe composition (chemistry) on LER. At higher styrene fractions, the chemical affinity between guide stripe and guided domain was increased, resulting in a lower measured edge roughness.

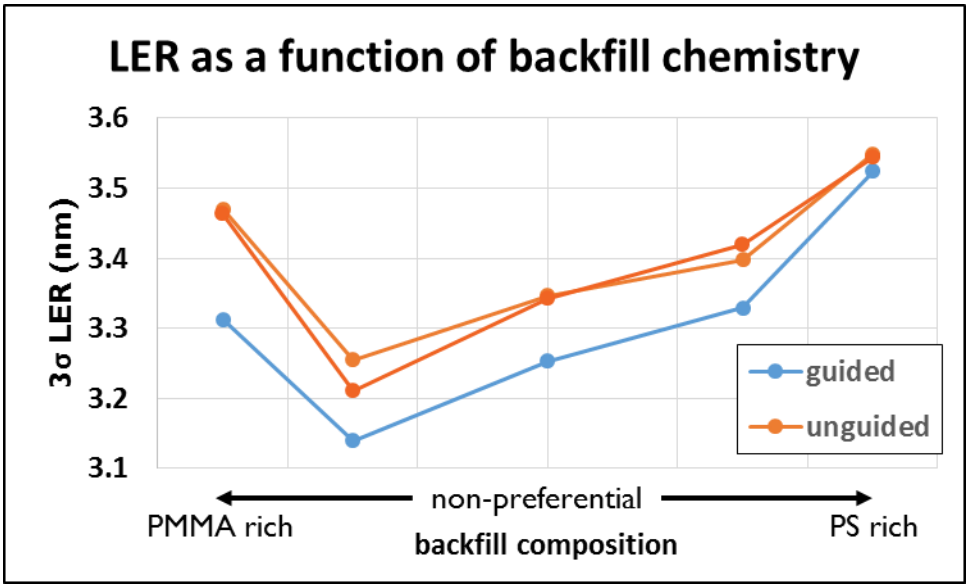

Figure 5.11: LER as a function of backfill chemistry. Roughness was minimized at a backfill composition slightly more PMMA-rich than the standard, non-preferential chemistry used in the process-of-record (POR) flow. This decrease in roughness was minimal (< 0.1 nm), however, and increased defectivity at this backfill composition negated any improved LER performance.

Compared to the baseline brush composition used in our standard process, a slightly more PMMA-preferential brush shows a slight reduction in LER, whereas all other cases showed worsened roughness performance. However, at this lower-LER brush composition, other defect modes such as registration defects increased significantly, more than offsetting any potential benefit from lower roughness. On the other hand, the trend present for guide stripe chemistry (Figure 5.10) showed promise as a way to decrease LER below current levels. When the styrene fraction of the guide stripe was decreased, LER increased significantly. To understand this result, we consider the equilibrium thermodynamics in directed self-assembly. At equilibrium, registration occurs because the enthalpic benefit of interaction between guide stripe and guided domains overcomes the entropic penalty of confining the BCP domains to that particular configuration. When the composition of the guide stripe matches the chemistry of the guided domain, that enthalpic benefit is maximized. Conversely, when the chemistry of the guide stripes is different from that of the guided domain, the enthalpic benefit of tight registration is weakened,

allowing relaxed domain curvature and therefore increased LER. For this data set, the lowest LER point is already observed at 100% styrene in the guide stripe so the styrene fraction cannot be increased, but there are other ways to improve the chemistry mismatch between the guide stripe and guided domain. Recent work has shown that the X-PS guide stripes generated in this flow undergo chemical modification through the processing steps, most notably the trim etch and brush grafting steps, and therefore do not represent strongly PS-preferential native styrene chemistry. Further development of the flow to reduce the chemical modification of the guide stripe could therefore be instrumental in reducing LER below its current measured value.

In addition to the above parameters, we also looked at roughness in the lithographic prepattern to see how that translated into roughness at the BCP level. To do so, we used three different off-axis illumination (OAI) settings to increase roughness in the exposure step, shown in the top row of Figure 5.12 below. Since the target features are line-space patterns, dipole illumination produces the lowest roughness in the photoresist, while quadrupole ("c-quad" on ASML scanners) is less optimal for these features and produces some roughness. Annular illumination is poorly suited for line-space arrays and produces the structures with the greatest LER at the lithography step. After processing, LER was again measured after PMMA removal, with representative results shown in the bottom row of Figure 5.12. (Measurements were also attempted after the trim etch step, but due to imaging constraints and poor material contrast it proved impossible to extract and measure edge profiles of the trim-etched lines.) In all cases, the LER was improved from PR to BCP, indicating that BCP DSA has a "healing" effect on edge roughness,[15] similar to the effect shown for placement accuracy in past work.[16-18] When LER in the lithographic prepattern exceeded 5 nm, a corresponding increase in LER in the BCP structures was observed. However, when the LER after lithography was below 5 nm, no further reduction in roughness in the BCP film was observed.

The small degree of roughness observed is innately present in the BCP system, seemingly due to the film's chemical composition, polydispersity, and other parameters described in the preceding sections, but is lower than the roughness of the prepattern. Further improvements in BCP LER performance must therefore come from the chemistry of the system rather than efforts aimed solely at improving the roughness of the chemical pattern.

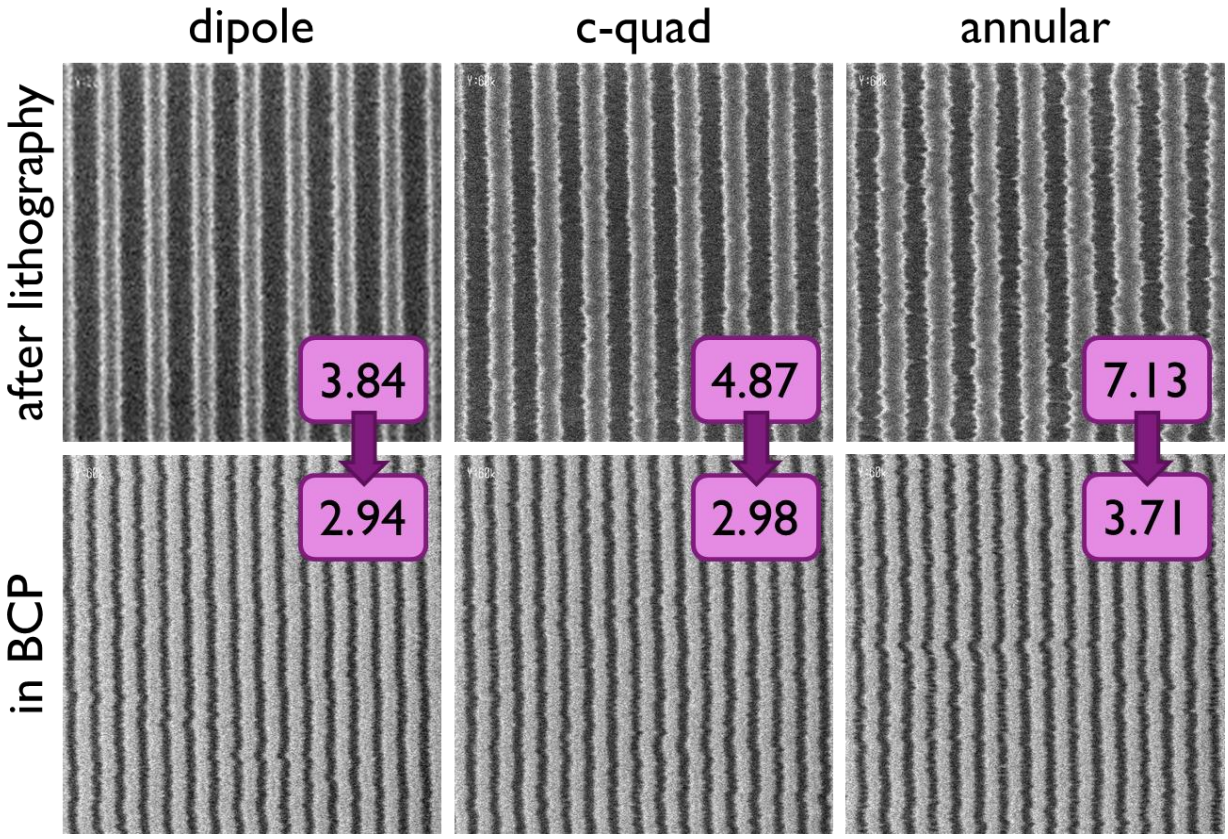

Figure 5.12: LER after lithography (top) and after PMMA removal (bottom) for three different off-axis illumination settings. For very rough lithographic pre-patterns, additional roughness was observed in the BCP structures. However, when the LER after lithography was below around 5 nm, no additional change was observed in the BCP structures regardless of how smooth the photoresist lines were.

Film thickness was one other factor considered for our study, but investigation into its impact on LER presented significant challenges. Ongoing work suggests that roughness varies through the film thickness, with a significantly lower roughness at the bottom of the film compared to the

top in some cases. At the same time, measuring LER through edge profile detection requires imaging at a set depth from the surface in order to have data sets that can be properly compared. Since deconvolution of the effects of imaging depth from thickness-induced roughness would be effectively impossible, this factor was not further investigated.

5.5 Summary and Conclusions

In this investigation, we built on many years of theoretical and experimental studies focused on elucidating the fundamental physics and thermodynamics at play in block copolymer phase equilibria in the presence of guiding chemical patterns. Through this knowledge, we were able to carefully consider the influence of various parameters in chemoepitaxial DSA on line-edge roughness in these BCP systems. Several factors contribute to LER in BCP DSA, but three parameters play a particular important role: the chemistry of the BCP film, described by the Flory-Huggins interaction parameter χ (chi); the polydispersity of the BCP system; and the strength of interaction between the guide stripe and guided domain. Each of these factors has a strong thermodynamic argument that both explains and is supported by the experimental evidence. To achieve the best roughness performance, BCP systems with high-χ chemistry and low polydispersity must be synthesized, with complimentary strong guiding substrates. Designer materials targeting these characteristics will provide an avenue to achieving industry tolerance for roughness and placement accuracy, and enable integration of BCP DSA into advanced patterning applications.

5.6 References

1. Liu, C.-C.; Ramirez-Hernandez, A.; Han, E.; Craig, G. S. W.; Tada, Y.; Yoshida, H.; Kang, H.; Ji, S.; Gopalan, P.; de Pablo, J. J.; Nealey, P. F., Chemical Patterns for Directed Self-Assembly of Lamellae-Forming Block Copolymers with Density Multiplication of Features. *Macromolecules* **2013,** *46* (4), 1415-1424.

2. Liu, C.-C.; Thode, C. J.; Delgadillo, P. A. R.; Craig, G. S. W.; Nealey, P. F.; Gronheid, R., Towards an all-track 300 mm process for directed self-assembly. *Journal of Vacuum Science & Technology B* **2011,** *29* (6).

3. Rincon-Delgadillo, P.; Craig, G.; Gronheid, R.; Nealey, P. F., Scale-up of a Chemo-Epitaxy Flow for Feature Multiplication Using Directed Self- Assembly of Block-Copolymers. *Journal of Photopolymer Science and Technology* **2013,** *26* (6), 831-839.

4. Delgadillo, P. A. R.; Gronheid, R.; Thode, C. J.; Wu, H.; Cao, Y.; Neisser, M.; Somervell, M.; Nafus, K.; Nealey, P. F., Implementation of a chemo-epitaxy flow for directed self-assembly on 300-mm wafer processing equipment. *Journal of Micro-Nanolithography Mems and Moems* **2012,** *11* (3).

5. Craig, G. S. W.; Nealey, P. F., Self-assembly of block copolymers on lithographically defined nanopatterned substrates. *Journal of Photopolymer Science and Technology* **2007,** *20* (4), 511-517.

6. Cushen, J.; Wan, L.; Blachut, G.; Maher, M. J.; Albrecht, T. R.; Ellison, C. J.; Willson, C. G.; Ruiz, R., Double-Patterned Sidewall Directed Self-Assembly and Pattern Transfer of Sub-10 nm PTMSS-b-PMOST. *Acs Applied Materials & Interfaces* **2015,** *7* (24), 13476-13483.

7. Gronheid, R.; Delgadillo, P. R.; Singh, A.; Younkin, T. R.; Sayan, S.; Chan, B. T.; Van Look, L.; Bekaert, J.; Pollentier, I.; Nealey, P. F., Readying Directed Self-Assembly for Patterning in Semi-Conductor Manufacturing. *Journal of Photopolymer Science and Technology* **2013,** *26* (6), 779-791.

8. Pathangi, H.; Chan, B. T.; Bayana, H.; Vandenbroeck, N.; Van den Heuvel, D.; Van Look, L.; Rincon-Delgadillo, P.; Cao, Y.; Kim, J.; Lin, G.; Parnell, D.; Nafus, K.; Harukawa, R.; Chikashi, I.; Polli, M.; D'Urzo, L.; Gronheid, R.; Nealeyg, P., Defect mitigation and root cause studies in 14 nm half-pitch chemo-epitaxy directed self-assembly LiNe flow. *Journal of Micro-Nanolithography Mems and Moems* **2015,** *14* (3).

9. Delgadillo, P. R.; Suri, M.; Durant, S.; Cross, A.; Nagaswami, V. R.; Van Den Heuvel, D.; Gronheid, R.; Nealey, P., Defect source analysis of directed self-assembly process. *Journal of Micro-Nanolithography Mems and Moems* **2013,** *12* (3).

10. Liu, C.-C.; Nealey, P. F.; Raub, A. K.; Hakeem, P. J.; Brueck, S. R. J.; Han, E.; Gopalan, P., Integration of block copolymer directed assembly with 193 immersion lithography. *Journal of Vacuum Science & Technology B* **2010,** *28* (6), C6B30-C6B34.

11. Bosse, A. W., Effects of segregation strength and an external field on the thermal line edge and line width roughness spectra of a diblock copolymer resist. *Journal of Vacuum Science & Technology B* **2011,** *29* (3).

12. Williamson, L. K., J.; Cao, Yi; Lin, Guanyang; Gronheid, Roel; Nealey, Paul F. In *Impact of BCP asymmetry on DSA patterning performance*, SPIE Advanced Lithography, San Jose, CA, San Jose, CA, **2015**.

13. Peters, A. J.; Lawson, R. A.; Nation, B. D.; Ludovice, P. J.; Henderson, C. L., Simulation study of the effect of molar mass dispersity on domain interfacial roughness in lamellae forming block copolymers for directed self-assembly. *Nanotechnology* **2015,** *26* (38).

14. Mahanthappa, M. K.; Schroeder, J. M. W.; Schmitt, A. L.; Schmitt, A. K.; Banik, S. M.; Im, K., Morphological consequences of block polydispersity in ABA triblock copolymers derived from ROMP-CT. *Abstracts of Papers of the American Chemical Society* **2011,** *241*.

15. Kim, S. K., Stochastic Simulation Studies of Line-Edge Roughness in Block Copolymer Lithography. *Journal of Nanoscience and Nanotechnology* **2014,** *14* (8), 6143-6145.

16. Stoykovich, M. P.; Daoulas, K. C.; Mueller, M.; Kang, H.; de Pablo, J. J.; Nealey, P. F., Remediation of Line Edge Roughness in Chemical Nanopatterns by the Directed Assembly of Overlying Block Copolymer Films. *Macromolecules* **2010,** *43* (5), 2334-2342.

17. Cheng, J. Y.; Rettner, C. T.; Sanders, D. P.; Kim, H. C.; Hinsberg, W. D., Dense self-assembly on sparse chemical patterns: Rectifying and multiplying lithographic patterns using block copolymers. *Advanced Materials* **2008,** *20* (16), 3155-3158.

18. Detcheverry, F. A.; Nealey, P. F.; de Pablo, J. J., Directed Assembly of a Cylinder-Forming Diblock Copolymer: Topographic and Chemical Patterns. *Macromolecules* **2010,** *43* (15), 6495-6504.

CHAPTER 6: THE USE OF LAYER-BY-LAYER DEPOSITED FILMS TO CONTROL BLOCK COPOLYMER DOMAIN ORIENTATION

6.1 Abstract

Alternating layers of poly(vinyl dimethylazlactone) (PVDMA) and branched poly(ethylene imine) (BPEI) were used to create amine-functional layer-by-layer (LbL) deposited films on various substrates. Polymer brushes of tunable composition were grafted to these films to create surfaces of controlled chemistry and surface energy. Grafting behavior kinetics were investigated both in the melt and from solution using ellipsometry. In the melt, grafting temperature is the dominant parameter: below T_g grafting does not occur, but above T_g grafting rapidly reaches saturation. In the solution phase grafting can occur at room temperature but the time scales are much longer; grafting rates can be accelerated through the use of polyfunctional chemical mats. Thin films of lamellae-forming block copolymer (BCP) were coated on the functionalized surfaces; through selection of the brush chemistry, BCP domain orientation could be controlled. Perpendicular assembly of poly(styrene-*block*-methyl methacrylate) domains was achieved on topographic surfaces coated with functionalized LbL films and grafted random copolymer brushes of 57% styrene composition.

6.2 Introduction

Block copolymer (BCP) thin films have attracted a growing degree of attention due to their ability to phase separate and self-assemble at the nanoscale.[1] By controlling the orientation of the phases, or domains, of the BCP thin film, commercially relevant structures can be produced for many applications, including membrane separation,[2] nanopatterning,[3] and energy storage.[4] The orientation of BCP domains in a thin film is a function of many factors including film thickness,

substrate roughness, and surface energies of the respective blocks.[5-7] However, even when these other factors are controlled, BCP domain orientation in a thin film is still dictated by the surface energetics – and therefore chemistry – of the supporting substrate.[6] In order to modify the surface energy of the substrate, it often must be coated with an additional layer of tunable chemistry. In one approach, developed by Mansky and expanded by others, polymer brushes of tunable composition are grafted to a supporting substrate.[8-9] Another representative approach uses thiol self-assembled monolayers on gold-coated surfaces.[10] In these and similar methods, the underlying substrate must be chemically functional to allow grafting or deposition of the layer with tunable chemistry.

A recent trend in manufacturing processing has been the increased emphasis on high-volume manufacturing (HVM) methods. One example of HVM is roll-to-roll (R2R) processing, where a flexible substrate is passed along rollers and coated, treated, or processed in a continuous manner. The substrate used for such processing must possess adequate mechanical strength and processing compatibility, but materials that meet these criteria may not have ideal or even any chemical functionality for coating with other films of tunable surface energy. Similarly, some three-dimensional structures cannot be coated with spin-casting or other approaches typically used for planar substrates. Layer-by-layer (LbL) deposited films provide an alternate approach to achieve tunable wetting behavior on these and other substrates.[11] These films are deposited using a cyclical process of alternating half-steps, where each half-step involves the self-limiting deposition of a layer of a particular polymer chemistry; alternating chemistries react to form bonds between the species and grow the LbL film.[12] Due to the nature of the deposition mechanism and self-limiting growth during each half-step, the films coat any substrate conformally and uniformly; the final thickness of the film is determined simply by the number of half-steps used in the process.

Due to their advantageous properties for a wide variety of thin-film applications, LbL films have been the subject of many past studies. Some have focused on the use of polyelectrolyte systems of polycations and polyanions, where electrostatic interactions hold the films together.[12] However, these films are not ideally suited for certain applications, since those interactions can be disrupted and the LbL films subsequently broken down by changes in pH, the presence of aqueous media, exposure to high temperatures, or other external factors.[13] Another class of LbL films uses covalently cross-linking polymers that possess complementary chemistry. One example of this last class that has been the subject of a number of recent studies is a polyazlactone/polyamine system.[14] Constrained azlactone groups undergo nucleophilic attack by primary amines in a 'click'-type ring-opening reaction, resulting in substantial, rapid crosslinking between polymers containing these two groups. LbL films fabricated using these materials have been shown to be tunably thick, have adequate structural integrity, and coat conformally and uniformly on a wide variety of materials and substrates including horsehair, cotton fiber networks, paper, and gauze.[15] Additionally, these LbL films are necessarily chemically functional: if the last half-step is coating by a polyazlactone, they are azlactone-functional and can react with primary amines, and the inverse is also true. Their chemical functionality was a motivation for several recent studies, where amines such as *n*-decylamine or D-glucamine were covalently bound to the LbL stack to produce substrates with tunable wetting behavior ranging from hydrophilic to superhydrophobic.[16]

The method here of using conformal LbL films to functionalize any substrate geometry or chemistry can be married with the approach outlined earlier of using grafted end-functional polymer brushes of tunable chemistry to control surface energetics, and the resulting combination offers an avenue to realize the benefits of both techniques simultaneously. By using amine-functionalized polymer brushes, we can graft a layer of tunable composition and therefore surface

chemistry on an azlactone-functional LbL film, opening up the possibility of directing the orientation of BCP thin films on a variety of flexible or topographic substrates. Herein we report efforts to characterize the grafting behavior of various amine-functional polymers and progress in directing the orientation of BCP domains on a non-planar substrate.

6.3 Experimental

6.3.1 Materials

Branched poly(ethylene imine) (BPEI, M_n = 10 000, M_w = 25 000; ratio of primary:secondary:tertiary amines = 1:1.2:0.76) and poly(vinyl dimethylazlactone) (PVDMA) were a kind gift from Dr. David Lynn at the University of Wisconsin, Madison. Amino-terminated polystyrene (PS-NH_2, M_n = 32 kg mol^{-1}, M_w = 33 kg mol^{-1}), amino-terminated poly(methyl methacrylate) (PMMA-NH_2, M_n = 30 kg mol^{-1}, M_w = 54 kg mol^{-1}), nonfunctional polystyrene (PS, M_n = 25 kg mol^{-1}, M_w = 26 kg mol^{-1}), poly(methyl methacrylate) (PMMA, M_n = 37 kg mol^{-1}, M_w = 38 kg mol^{-1}), and poly(styrene-*block*-methyl methacrylate) (P(S-*b*-MMA), M_n = 37-37 kg mol^{-1} for each block) were purchased from Polymer Source and used as received. Acetone, toluene, and chlorobenzene were purchased from Fischer Scientific and used as received. End-hydroxyl-functional poly(styrene-*random*-methyl methacrylate) (P(S-*r*-MMA), styrene fraction 0.57) was purchased from Polymer Source and the functionality was changed to end-amine in the procedure shown here:

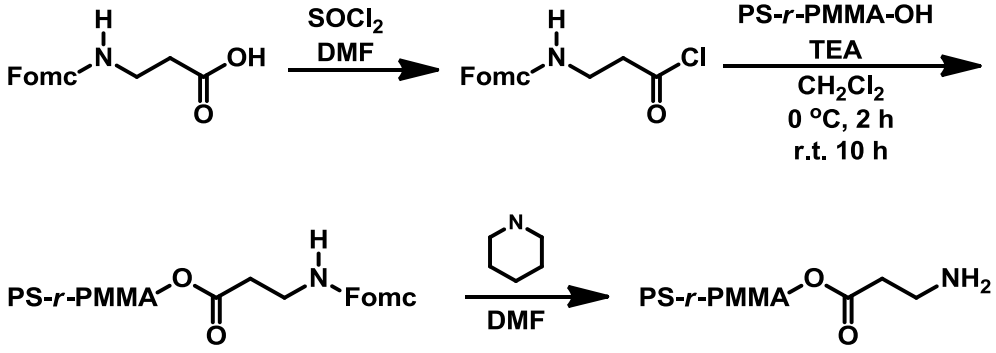

Prime silicon <100> wafers were purchased from WRS Materials and cleaned with piranha solution (3:7 v/v 30% H_2O_2:H_2SO_4) at 130 °C for 30 min, rinsed with deionized water, dried under N_2, and used immediately.

6.3.2 Layer-by-layer film deposition

Solutions of BPEI and PVDMA in acetone were prepared at concentrations of 20 mM with respect to the repeat unit. Silicon wafers were cleaned using piranha solution and used immediately. The wafers were cut into small strips (1/4" x 1") and dip-coated first in the solution of BPEI for 30 s, followed by two 30 s rinses in fresh acetone, and then in the solution of PVDMA for 30 s, followed by two 30 s rinses in fresh acetone. This process was repeated to build up a layer-by-layer deposited film with seven bilayers. The films were then dried under nitrogen and used immediately or stored under vacuum in a desiccator to prevent loss of azlactone functionality.

6.3.3 Brush grafting from the melt

Solutions of 1.5% (w/w) polymer in chlorobenzene were prepared and spin-coated on LbL-functionalized substrates at 3000 rpm for 30 s. Brushes were annealed at 160 °C under vacuum for 12 h unless otherwise explicitly noted.

6.3.4 Brush grafting from solution

Solutions of 1.5% (w/w) polymer in chlorobenzene were prepared, and LbL-functionalized substrates were submerged in these solutions at room temperature for various lengths of time. The substrates were immediately rinsed with pure chlorobenzene after removal from solution to prevent uneven drying and dewetting of the films.

6.3.5 Characterization

Static water contact angle measurements were obtained using a Dataphysics OCAH230L contact angle measurement system. A syringe dispensed 5 μL drops of deionized water, which

were measured after 0.3 s of stabilization. Film thicknesses were determined using a Gaertner LSE ellipsometer (632.8 nm, incident angle = 70°). Scanning electron microscopy images were obtained using a LEO 1550 VP field-emission SEM. Atomic force microscopy was performed on a Bruker Nanoscope IIIa Multimode 5 AFM in tapping mode.

6.4 Results and Discussion

6.4.1 Generation of layer-by-layer deposited films

Using a previously reported method, we fabricated samples coated with layer-by-layer deposited bilayer films of alternating branched poly(ethylene imine) (BPEI) and poly(vinyl dimethylazlactone) (PVDMA), as shown in Figure 6.1. These two chemistries are complementary: the constrained azlactone ring structures in the PVDMA pendant groups undergo nucleophilic attack by the primary amine groups of BPEI in a 'click'-type reaction, allowing formation of a heavily crosslinked system when these polymers are mixed. However, since neither polymer reacts with itself, this crosslinking can be controlled to make films of tunable thickness. In depositing these films, we always began with BPEI because its hyperbranched nature makes it "sticky" on the molecular level, enabling it to adhere to nanoscopic irregularities in the structural substrate and remain stuck to the substrate even after subsequent rinsing. We then submerged the samples in a solution of PVDMA and agitated the solutions to accelerate diffusion. PVDMA molecules in solution that come in contact with the adsorbed BPEI on the substrate undergo the 'click'-type reaction described above until the entire substrate is covered with a thin layer of PVDMA. At this point, no further reaction can occur, since the BPEI has effectively "saturated" with PVDMA; the film growth is thus self-limiting. The samples are removed from solution and rinsed to remove any physically adsorbed but unreacted polymer, leaving a complete bilayer of BPEI/PVDMA with the top chemistry being PVDMA. The samples are then submerged in a solution of BPEI and agitated

to drive a similar self-limited crosslinking reaction with BPEI. Past work has shown that self-limited saturation of each layer occurs in less than 5 seconds in an unagitated solution, but we used 30 second dips with agitation to ensure complete reaction. This method of alternately dipping the samples in solutions of BPEI and PVDMA, with rinses between each dip step is known as 'layer-by-layer' (LbL) deposition; the bilayer films produced can be built up in a linear manner to the desired thickness. Ellipsometric measurements show that each half-layer has a thickness of roughly 3.5 nm, with each bilayer therefore being roughly 7 nm thick; for all our experiments, we used films of seven bilayers, corresponding to an overall thickness of roughly 50 nm.

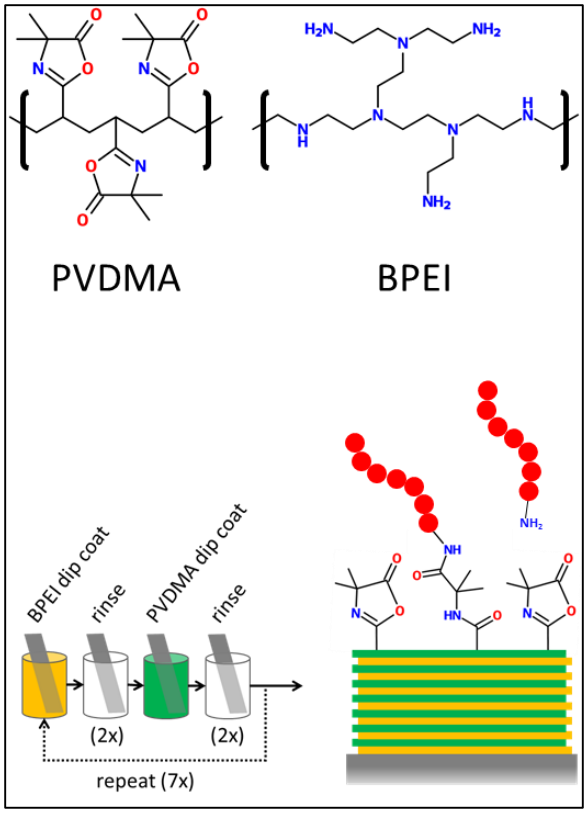

Figure 6.1: Top: Representative chemical structures of poly(vinyl dimethylazlactone) (PVDMA) and (hyper)branched poly(ethylene imine) (BPEI) used in this work. BPEI has a mix of primary, secondary, and tertiary amine groups. Bottom: Schematic of process used to generate functional LbL films. A clean substrate is dip-coated with a BPEI solution and rinsed, and then dip-coated with a solution of the complimentary PVDMA chemistry and rinsed. The process is repeated seven times to build up a bilayer film roughly 50 nm thick with top azlactone functionality. The azlactone group undergoes a 'click'-type ring-opening reaction with nucleophiles such as primary amines, enabling the grafting of end-amine functional molecules of any type to the substrate. Here we show a cartoon representation of a short polystyrene chain grafting to the functionalized LbL film.

By using PVDMA rather than BPEI as the final chemistry (i.e. an even number of layers, or equivalently an integer number of bilayers), we can control not only the thickness of the overall film but also the chemical functionality of its top surface. The constrained-ring azlactone functionality of the top layer is susceptible to attack from a number of nucleophilic species including water, necessitating use of dry solvents when possible and storage of samples under dry nitrogen or vacuum to preserve their functionality until use. More interestingly, however, these azlactone rings react with any primary amine, and past work has demonstrated how various end-

amine-functional molecules can be grafted to the LbL substrate to create surfaces of any desired chemistry. Other past work has used end-grafted polymer brushes of tunable composition to direct the domain orientation of block copolymer (BCP) thin films on planar substrates. Here we combine the ideas of LbL functionality with tunable composition of end-grafted polymer brushes, depositing the brushes from both the melt and solution. We discuss the results of each approach in turn and culminate with our efforts to direct the assembly of BCP structures on topographic substrates.

6.4.2 Deposition from the melt

Our first experiments sought to characterize deposition behavior of polymer brushes from the melt. In these experiments, substrates prepared as described above were spin-coated with end-amine-functional polystyrene (PS-NH_2) and poly(methyl methacrylate) (PMMA-NH_2) homopolymer brushes and thermally annealed. Thermal annealing of the samples was performed at 160°C (well above T_g of the polymer brushes) to give the brushes sufficient mobility to explore configuration space and graft to the LbL substrate. Other LbL films used as controls were coated with non-functionalized homopolymer PS and PMMA and thermally annealed with the same treatement. After annealing, the samples were rinsed to remove any ungrafted polymer, and the resulting films were characterized using water contact angle and ellipsometry; the results are shown in Figure 6.2.

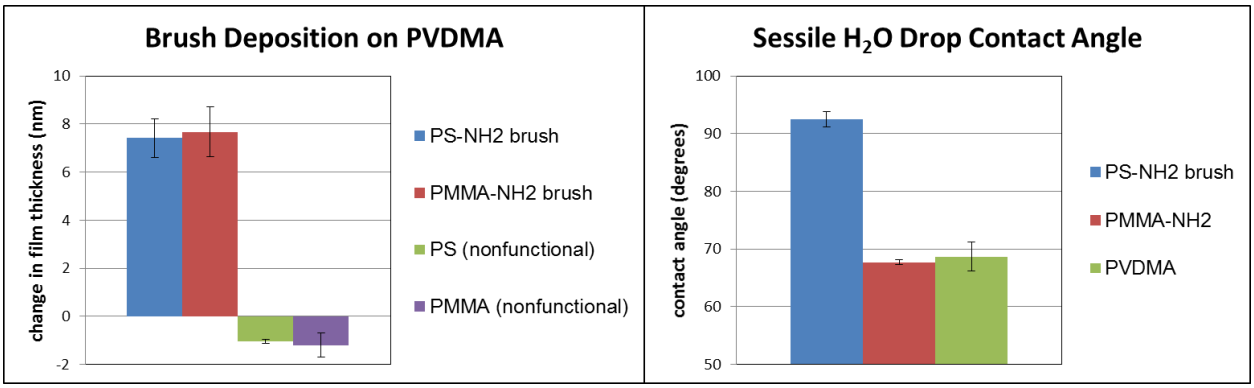

Figure 6.2: Ellipsometry (left) and goniometry (right) results characterizing brush deposition from the melt on LbL films. End-amine functional brushes clearly graft to the LbL film while nonfunctional polymers of the same chemistry and similar molecular weight do not. The water contact angle (WCA) of the LbL films does not change appreciably after grafting of PMMA-NH_2 but does change dramatically after grafting of PS-NH_2.

As can be seen from the ellipsometry results, both PS-NH_2 and PMMA-NH_2 brushes grafted to the LbL-coated substrates to a thickness of around 7 nm, which is the saturation thickness of a PS or PMMA brush of this particular molecular weight. Meanwhile, the non-functional homopolymers did not graft at all and were simply rinsed away after anneal. Indeed, there was a slight *decrease* in film thickness (~1 nm, or roughly 2% of the ~50 nm total thickness of the LbL film) after treatment with the non-functional homopolymers, indicating possibly that over time the LbL films become more tightly cross-linked. Since the motivation for this work is to control the wetting behavior of the LbL/brush system, we measured the sessile water contact angle (WCA) of each of the films in question. The contact angle of the PMMA-NH_2 brush was found to be 67°, which is that of a simple PMMA film. However, since the WCA of the native LbL film is roughly the same (68°), this result does not conclusively demonstrate that the wetting behavior of the system was changed. In contrast, the WCA of the PS-NH_2 brush was found to be 92°, the same as a simple PS film. This WCA is markedly different from that of the LbL film, demonstrating conclusively that the PS-NH_2 brush is grafted to and changes the wetting behavior of the LbL top surface. To further investigate the wetting behavior of the films, we cast a lamellae-forming PS-

block-PMMA BCP on each of the substrates at a thickness of 1.25 L_0 (~50 nm) and assembled it by thermal annealing, with the results shown in Figure 6.3. On the PS-NH_2 coated film, the BCP formed islands, indicative of a PS-wetting surface, but on the PMMA-NH_2 coated film, the BCP formed holes, indicative of a PMMA-wetting surface. These results further confirm our hypothesis that the wetting behavior of the LbL top surface can be changed by grafting an end-functional polymer brush to it, and the exact wetting behavior can be tuned by changing the composition of that brush.

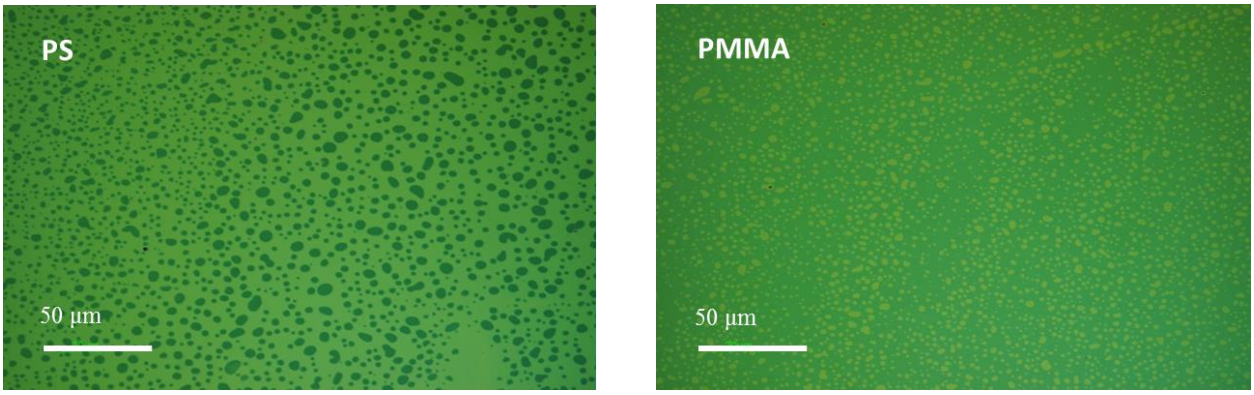

Figure 6.3: Formation of BCP islands (left) and holes (right) on LbL films coated with PS and PMMA brushes, respectively. These structures are indicative of strongly preferential surfaces.

Both the hole and island morphologies observed on the preferential substrates in Figure 6.3 form with the domains parallel to the substrate, but for many commercial applications, perpendicularly-oriented domains are preferable. For a lamellae-forming BCP, these vertical structures manifest as "fingerprint" morphology in top-down SEM images. In order for fingerprint to form on a given substrate, that surface must be sufficiently non-preferential to both blocks to allow the BCP to adopt this preferred configuration. While film thickness, surface energy of the blocks, substrate topography, and other factors play a role in determining how non-preferential the surface can be and still permit perpendicular assembly, there is generally a range of surface chemistries that comprise this non-preferential "window." For a P(S-*b*-MMA) block copolymer, a

surface treated with a random copolymer of styrene and methyl methacrylate (P(S-*r*-MMA)) can satisfy this condition when the fractions of each monomer are roughly equivalent. Though the exact numbers can vary from system to system, it has generally been reported that a styrene fraction between 0.45 and 0.65 in a random copolymer brush allows perpendicular assembly. Therefore, to induce perpendicular assembly on the LbL system, we grafted an end-amine functional P(S-*r*-MMA) brush with a styrene fraction of 0.57 by the same process as described above and assembled a BCP on the structure. As can be seen in Figure 6.4, the BCP assembled on this brush, grafted to an LbL film, adopts the fingerprint morphology indicative of a non-preferential surface.

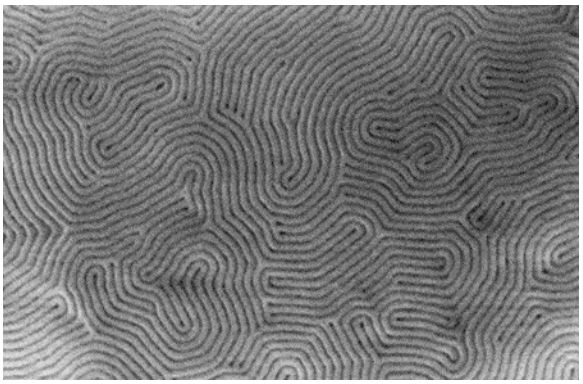

Figure 6.4: Fingerprint morphology observed on LbL film coated with a non-preferential random copolymer P(S-*r*-MMA) brush (styrene fraction 0.57).

To better understand the kinetics of brush grafting, we performed a series of experiments at various time scales, coating LbL samples with PS-NH_2 brushes and annealing them for various lengths of time at 160°C, then rinsing to remove ungrafted brush. The film thickness before and after grafting was measured with ellipsometry and the results are shown in Figure 6.5a. Note that in this curve, the horizontal (time) axis crosses the vertical (thickness) axis at a value of 12 nm to better illustrate the relevant behavior of the data trend. It can be seen that even at very short anneal times (3 minutes), the brush grafts to over 13 nm, close to the saturation thickness of 15 nm; saturation is itself reached after only 30 minutes of grafting. This saturation curve is much sharper

than that of an end-hydroxyl functional polystyrene brush (PS-OH) grafting to a SiOx substrate via dehydration, a process that has been used in much of our past work (see supplemental information). However, the difference is easily understood. Dehydration reactions are slow and take place at an appreciable rate only at elevated temperatures, requiring thermal annealing for long periods of time, since the grafting process is reaction kinetically limited. In contrast, the ring-opening 'click'-type reaction between a primary amine and the azlactone group is a fast, irreversible process even at room temperature, indicating that the grafting process is instead diffusion limited for the LbL films. While the grafting process is very fast at room temperature, polymer mobility and diffusion is quite suppressed. To test the effect of grafting temperature, a series of LbL samples was coated with PS-NH_2 brush, annealed for a fixed time of 120 minutes at a temperatures ranging from 70°C to 150°C, and rinsed to remove ungrafted brush. The difference in film thickness before and after grafting is plotted in Figure 6.5b, with a curve fit to the data shown to guide the eye. In this plot, brushes annealed at temperatures below T_g (~100°C) did not graft to a substantial thickness, while those well above T_g grafted to saturation thickness. These data provide further evidence that the grafting rate is limited by the mobility and diffusion of the polymer chains and therefore that operating above T_g is necessary for deposition from the melt.

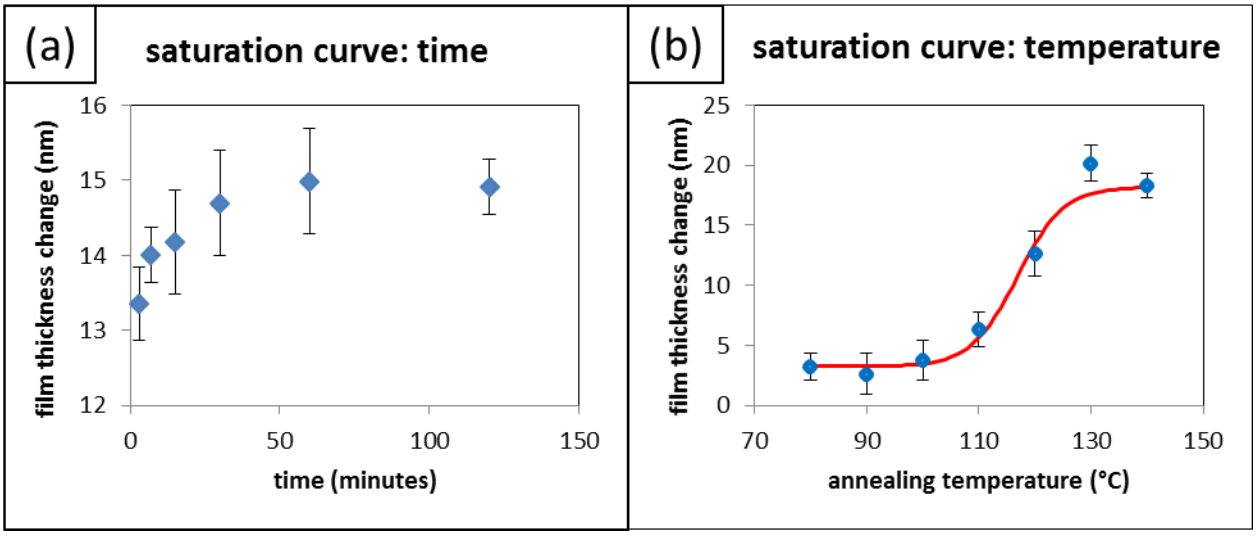

Figure 6.5: Film thickness increase from grafting a PS-NH_2 brush to an LbL film (a) for different times but fixed temperature of 160°C and (b) for different temperatures but fixed time of 120 minutes.

6.4.3 Deposition from solution

As we have shown in the preceding paragraphs, polymer brushes of tunable composition and wetting behavior can be grafted rapidly and irreversibly via a 'click'-type reaction, even at low temperatures. However, due to polymer mobility requirements, grafting from the melt requires operating at elevated temperatures, which may not be suitable for all applications. For example, primary amines can undergo a transesterification/amidation reaction with the side chains of a PMMA molecule, which complicated some of our initial experimental trials. One avenue to enhanced mobility at lower (or even room) temperatures is grafting brushes from solution instead of from the melt. In this approach, LbL samples are submerged in a solution of end-amine functional polymer brush, which diffuses through the solvent and grafts to the azlactone functionality of the LbL-coated substrate upon contact. This next section discusses our results employing this approach. In parallel with experiments from the melt, we submerged samples in a range of dilute polymer solutions where the polymer content was a mixture of PS-NH_2 and PMMA-NH_2 blended in various ratios. These ratios ran the full range from pure PS-NH_2 to pure

PMMA-NH_2 in 20% increments. The samples were allowed to stand for 24 hours to achieve grafting saturation, then rinsed, coated with a BCP thin film, and annealed. The films were then characterized using SEM and AFM, and representative images are shown in Figure 4.6. On the substrates that had been coated with pure PS or PMMA brushes, the films exhibited hole/island morphology (left side of Figure 6.6), in agreement with the behavior observed for the parallel experiment from the melt. Similarly, on the samples that had been left in solutions of primarily PS or PMMA, hole/island morphology was also observed. On the samples that were submerged in the solutions of the 40/60 and 60/40 mixtures of PS/PMMA, however, fingerprint structures were observed (right side of Figure 6.6), indicating that these substrates were sufficiently non-preferential to permit perpendicular assembly.

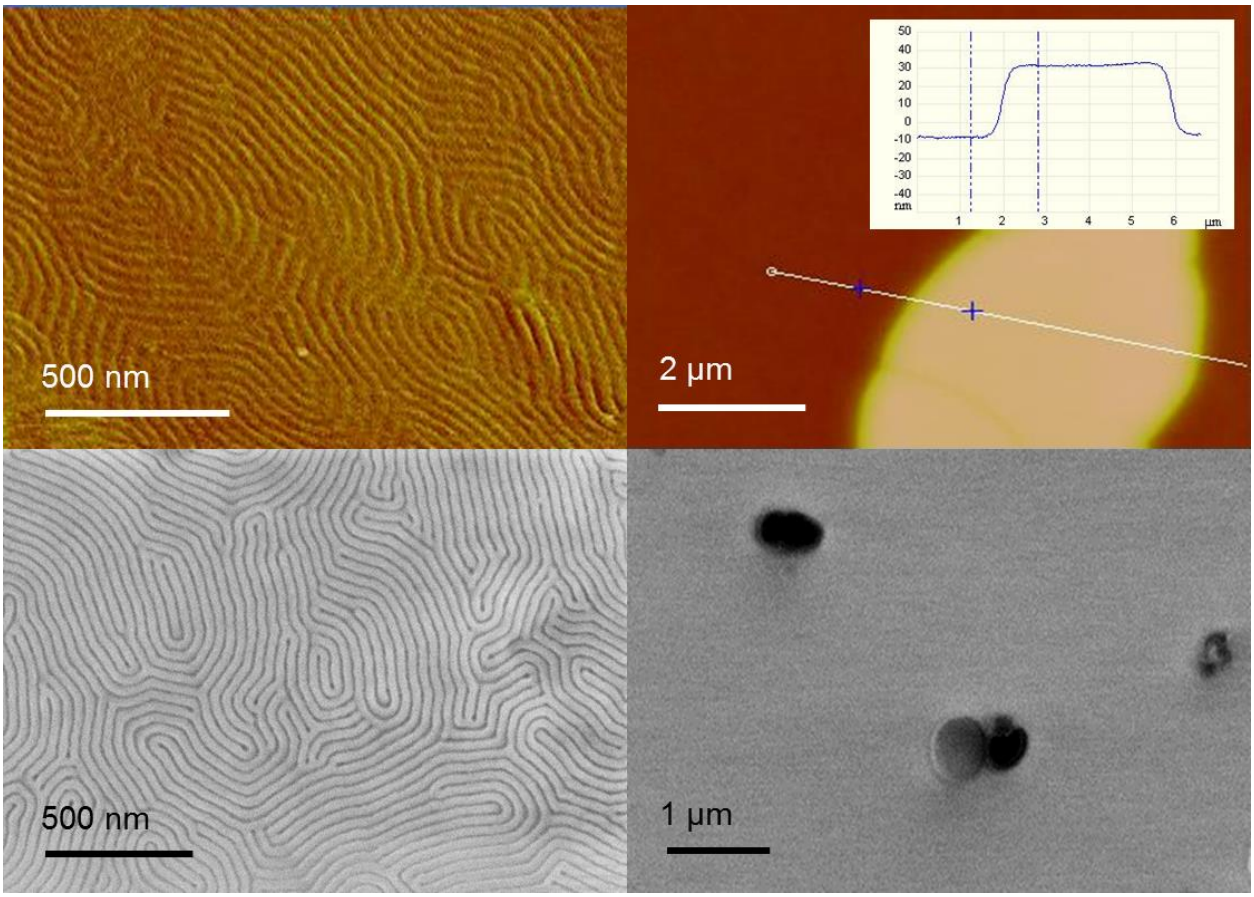

Figure 6.6: BCP assembly on LbL films coated with solutions of polymer brushes. The sample on the left was coated with a 40%/60% mixture of PS/PMMA brushes, whereas the sample on the right was coated with a solution of only PS brush. The inset confirms the formation of islands 40 nm in height.

Two points should be noted here, as this observation may appear initially to be in disagreement with past results. First of all, the non-preferential composition window appears to be much larger than previously reported for random copolymer brushes on planar substrates. However, it has also been reported that slight roughness or topography in a substrate can also induce perpendicular assembly. Since these LbL films have been shown to have a nontrivial degree of nanoscopic roughness, it is reasonable that the composition window supporting perpendicular assembly would be larger than for flat surfaces. The second point is that a similar approach of mixing homopolymer brushes and depositing from the melt was tried by Ji *et al.* but that effort was largely unsuccessful. In their work, the authors concluded that since PS and PMMA phase separate, a mixture of these

brushes graft in a highly inhomogeneous manner, creating large, irregular regions of primarily PS or primarily PMMA. Such a surface does not behave as a non-preferential substrate when a BCP is assembled on top of it; instead the BCP orients with domains parallel to the surface but wets with its PS or PMMA domain, depending on the local chemistry. To overcome the phase separation behavior, the authors introduced a large amount (as much as 85% by weight) of short copolymer chains into the PS/PMMA brush mixture to act as an emulsifying agent and prevent formation of large areas of principally one grafted chemistry and enable perpendicular assembly. In our system, however, the homopolymer brush blends grafted to form apparently homogeneous surfaces, even in the absence of an emulsifying agent. This seeming contradiction, however, is easily understood when we consider that when the polymer brushes are in solution, they do not phase separate to form domains of one chemistry or another. Instead, the brushes diffuse relatively unimpeded through the solution and irreversibly graft upon contact between the end-amine functionality and an unopened azlactone ring on the LbL surface. It is therefore possible to achieve a uniform surface of polymer brush chemistry that reflects the composition of the solution, even when the constituent solute molecules are species that would phase separate in the bulk, and furthermore to use this approach to make tunably non-preferential surfaces on LbL-coated substrates.

To determine the rate and mechanism for brush grafting, a set of LbL samples was placed in a solution of PS-NH_2 and several of them were removed at particular time intervals, rinsed to remove excess polymer, and evaluated using ellipsometry and water contact angle. The film thickness difference before and after grafting was plotted as function of time, with the results shown in Figure 6.7. The trend through time appears to asymptotically approach a saturation limit, indicated by the horizontal dashed line. When discussing how to mathematically fit the data, we consider a few simplifying assumptions that can aid in developing a model. First, the amount of polymer

brush in solution is large enough that even after grafting to saturation, the concentration remains effectively unchanged and can therefore be treated as constant through the experiment when the samples are first submerged in the solution, they by necessity experience some agitation simply because of the experimental setup. During agitation, the solution circulates rapidly over the LbL surface, and the frequency of collisions between polymer brush solute and the substrate is high, leading to a similarly high rate of brush grafting. Furthermore, during this initial period, only a few, isolated chains are grafted and therefore there is very little surface coverage by the brushes. The effect of the agitation combined with the relatively exposed substrate leads to an almost instantaneous grafting rate right at the beginning of the process. After the initial short time interval, we hypothesize that the system enters a second regime of grafting behavior, characterized by limitations on the grafting rate. These limitations come partly from the diffusion-limited kinetics of polymer chains coming in contact with the surface, but our assumption of an effectively constant concentration of polymers in solution means that this factor is similarly constant through time and therefore does not vary during the course of the experiment. A second limitation, however, is the availability or accessibility of grafting sites (unreacted azlactone groups) on the LbL surface. As brushes graft, they impede further grafting at adjacent sites; as the average brush film thickness grows, the accessibility of grafting sites further decreases. We predict that the rate of grafting is therefore proportional to the accessibility of the grafting sites, which is itself proportional to the film thickness. The rate of film thickness growth is therefore proportional to the film thickness, suggesting an exponential fit. However, the initial fast grafting regime contributes a nonzero brush thickness at effectively zero time, so we model the data with an offset exponential fit of the form:

$$l(t) = l_{sat} \cdot \left(1 - exp(-\alpha t)\right) + l_{off}$$

where α is a time constant, l_{off} is the offset thickness of the film from the rapid grafting at $t = 0$,

and l_{sat} is the additional thickness past offset to reach saturation. The values of these parameters are displayed in Table 6.1, and the fit is overlaid on the data in Figure 6.7.

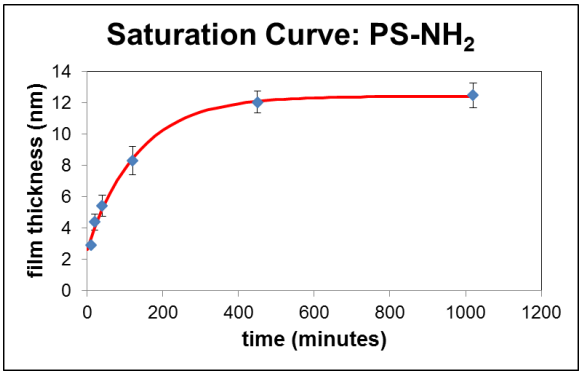

Figure 6.7: Saturation curve of end-functional polystyrene brush grafted from the melt. The overlaid red curve is an exponential regression fit. The coefficients for the curve are shown in Table 6.1.

$$l(t) = l_{sat} \cdot \left(1 - exp(-\alpha t)\right) + l_{off}$$

parameter	value
α (time constant)	7.5 x 10^{-3} min^{-1}
l_{off} (offset thickness)	2.6 nm
l_{sat} (added thickness)	9.8 nm
total brush thickness	12.4 nm

Table 6.1: Equation and parameters for exponential regression fit of data shown in Figure 6.7. The brush grafts to a thickness of 2.6 nm almost immediately (the "offset thickness") and then adds an additional 9.8 nm to reach the 12.4 nm saturation thickness.

As can be seen from these results, the grafting kinetics are diffusion limited and quite slow at the concentration of polymer solution used (1.5% w/w). To accelerate the grafting rate, experimental conditions can be adjusted. For example, by increasing the solute concentration or agitating the solution, the frequency of interactions between the end-functionality of the polymer brushes and the azlactone groups of the surface can be increased. Alternately, by increasing the number of primary amine groups on the polymer brush itself, additional functionality and therefore higher grafting rates can theoretically be achieved. To test this hypothesis, we synthesized a

random copolymer of styrene and 4-(aminomethyl)styrene, P(S-*r*-S(NH_2)). LbL samples were submerged in a solution of this polymer and a similar time study was conducted, where a few samples were removed at each time interval, rinsed to remove excess polymer, and measured with ellipsometry, contact angle, and BCP wetting behavior. The ellipsometric results are shown in Figure 6.8 and follow a trend similar to that observed in Figure 6.7, though with two notable differences. The first is that the first part of the curve is much steeper, suggesting that a much higher initial rate of grafting occurs with the polyfunctional styrene. The second difference is that while this polymer has a molecular weight similar to that of the end-functional PS, the saturation thickness is only about 3 nm, or 25% of the saturation thickness of the end-functional brush. Both differences have immediately intuitive explanations when we consider the grafting mechanism of a polyfunctional brush. In contrast with an end-functional brush, which can only graft when its primary amine end encounters an active azlactone group, the polyfunctional P(S-*r*-S(NH_2)) can graft at multiple points along the chain. Once one point is tethered to the surface, the other points have a much higher likelihood of also encountering the surface, producing a rapid grafting effect. Since the polymer is grafted at multiple points, however, it cannot adopt the entropically favored random coil configuration and instead lies tethered along the substrate. In contrast, the end-functional brush has only one point in contact with the surface, leaving the remainder of the polymer chain to stretch away from the substrate and giving rise to much thicker polymer brush films. In spite of the significantly lower thickness of the polyfunctional styrene, WCA and BCP assembly results (not shown) showed PS-wetting behavior on all samples, even at a brush thickness of only 2 nm. This results suggest that thin layers of polyfunctional polymers of tunable composition coated on LbL films can serve as a platform with highly controllable surface energy and wetting behavior, both for control of BCP assembly and other potential applications.

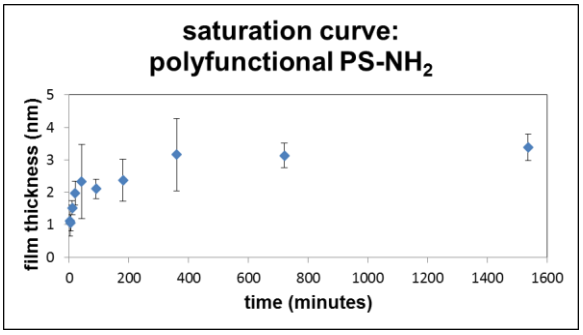

Figure 6.8: Saturation curve for poly-amine-functional PS grafted from solution. Saturation thickness for this film is around 3 nm.

6.4.4 Tunable surface energetics on topographic substrates

Much past work has focused on developing methods to tune surface energy and direct BCP assembly on planar substrates but LbL films provide an avenue to controlling the surface energetics of a broad range of three-dimensional shapes and topographic surfaces as well as flexible substrates. Furthermore, other work on controlling surface energies of topographic substrates has typically required use of that substrate's chemistry as a functional platform for grafting or other reaction, necessarily limiting the possible options to those with working chemical functionality. In contrast, LbL films can be treated to take on any desired chemistry, regardless of the functionality of the substrate upon which they are deposited. Previous studies have shown how these films conformally coat a diverse range of structures and can be functionalized to modify their chemistry in a broadly tunable manner. In extending that concept, we deposited LbL films using the dip-coat method described previously on topographic substrates. These samples consisted of lines and trenches with various spacing in a crosslinked PDMS matrix. The substrates were then coated with a film of end-functional P(S-*r*-MMA)-NH_2 with a styrene fraction of 0.57 and thermally annealed to provide polymer chain mobility. (We remind the reader that this polymer was described in earlier results, where it was used as a non-preferential brush to direct perpendicular assembly of a lamellae-forming BCP on a planar substrate.) After rinsing to remove

ungrafted polymer, we spin-cast a thin film of P(S-*b*-MMA) on the substrates and annealed them to allow the BCP to flow into the trenches and adopt its preferred orientation. The samples were characterized with AFM and the results are shown in Figure 6.9.

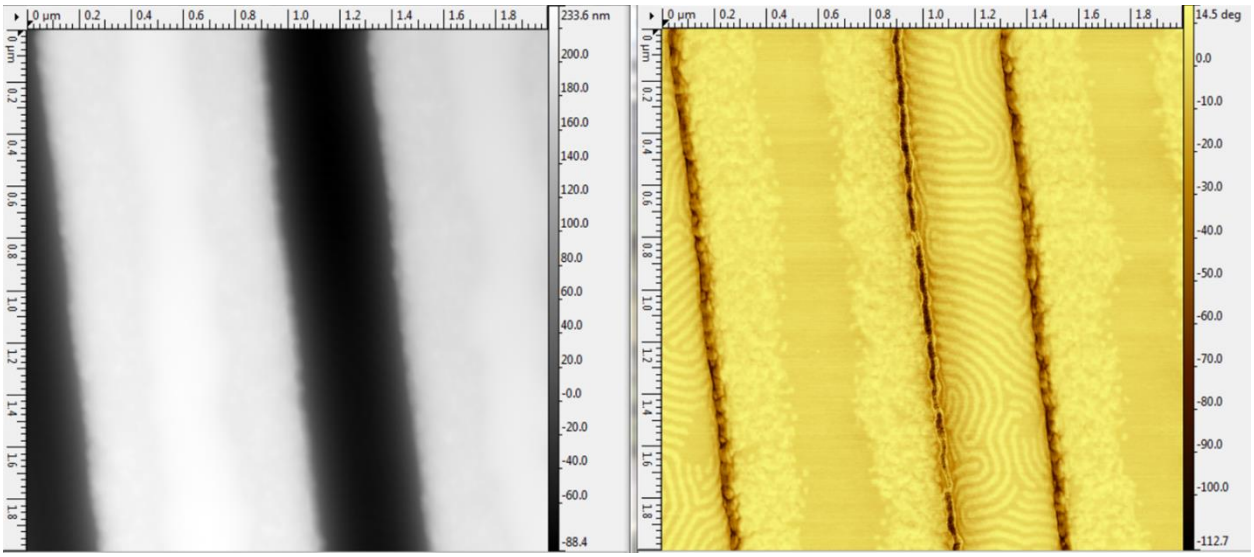

Figure 6.9: AFM height (left) and phase (right) images of a BCP film assembled on a LbL-coated topographic substrate. The topography of the substrate is preserved after LbL, brush, and BCP deposition, but the wetting behavior is modified to direct perpendicular assembly of the BCP lamellar domains.

As can be seen in the figure, the topography of the PDMS substrate is preserved after LbL deposition and brush grafting. Even after BCP deposition and anneal, the topography is preserved, indicating that the film does not completely fill the trenches, though it may reflow to some extent into them. Finally, the most important result is that the BCP domains orient perpendicularly to the non-preferential brush within the trenches, indicating that even on these topographic substrates the wetting behavior of the surface can be engineered and tuned to be non-preferential through the use of conformal LbL films and brushes of controllable composition.

6.5 Summary and Conclusions

In summary, we have demonstrated how polymer brushes can graft to layer-by-layer deposited functional films. We have also shown that by selection of the composition of the brush chemistry,

this technique can be used to control the surface energetics of the final LbL and brush film. The 'click'-type grafting reaction is very rapid, and the overall grafting kinetics are dictated by the frequency of interaction between complementary brush and LbL functionality, and by extension the mobility of the polymer brushes. Sufficient mobility can be achieved by depositing polymer brushes from solution or by operating above T_g if depositing brushes from the melt.

With this approach, we succeeded in directing the self-assembly of a BCP film on a topographic surface by tuning its surface energy, but without relying on the substrate's chemistry. Instead, all of the required chemical functionality was provided by the tunable properties of the brush grafted to the LbL films. Although in our work we used PDMS – which can be formed into a limitless variety of shapes – as our base structural material, this concept is broadly extendable to practically any substrate: flexible or rigid, planar or topographic, functional or inert. Furthermore, whereas our work has focused on orientational control of lamellar domains in BCP films, this approach can be extended to cylinder-forming BCP for membrane or separation applications or generalized to any class of self-assembling materials that requires control of surface energetics on topographic or flexible substrates.

6.6 References

1. Hamley, I. W., Ordering in thin films of block copolymers: Fundamentals to potential applications. *Progress in Polymer Science* **2009,** *34* (11), 1161-1210.

2. Hillmyer, M. A., Nanoporous materials from block copolymer precursors. In *Block Copolymers Ii*, Abetz, V., Ed. **2005**, pp 137-181.

3. Segalman, R. A., Patterning with block copolymer thin films. *Materials Science & Engineering R-Reports* **2005,** *48* (6), 191-226.

4. Orilall, M. C.; Wiesner, U., Block copolymer based composition and morphology control in nanostructured hybrid materials for energy conversion and storage: solar cells, batteries, and fuel cells. *Chemical Society Reviews* **2011,** *40* (2), 520-535.

5. Suh, H. S.; Kang, H.; Nealey, P. F.; Char, K., Thickness Dependence of Neutral Parameter Windows for Perpendicularly Oriented Block Copolymer Thin Films. *Macromolecules* **2010,** *43* (10), 4744-4751.

6. Suh, H. S.; Kang, H.; Liu, C.-C.; Nealey, P. F.; Char, K., Orientation of Block Copolymer Resists on Interlayer Dielectrics with Tunable Surface Energy. *Macromolecules* **2010,** *43* (1), 461-466.

7. Han, E.; Stuen, K. O.; Leolukman, M.; Liu, C.-C.; Nealey, P. F.; Gopalan, P., Perpendicular Orientation of Domains in Cylinder-Forming Block Copolymer Thick Films by Controlled Interfacial Interactions. *Macromolecules* **2009,** *42* (13), 4896-4901.

8. Mansky, P.; Russell, T. P.; Hawker, C. J.; Pitsikalis, M.; Mays, J., Ordered diblock copolymer films on random copolymer brushes. *Macromolecules* **1997,** *30* (22), 6810-6813.

9. Mansky, P.; Liu, Y.; Huang, E.; Russell, T. P.; Hawker, C. J., Controlling polymer-surface interactions with random copolymer brushes. *Science* **1997,** *275* (5305), 1458-1460.

10. Chaki, N. K.; Vijayamohanan, K., Self-assembled monolayers as a tunable platform for biosensor applications. *Biosensors & Bioelectronics* **2002,** *17* (1-2), 1-12.

11. Buck, M. E.; Lynn, D. M., Layer-by-Layer Fabrication of Covalently Crosslinked and Reactive Polymer Multilayers Using Azlactone-Functionalized Copolymers: A Platform for the Design of Functional Biointerfaces. *Advanced Engineering Materials* **2011,** *13* (10), B343-B352.

12. Decher, G., Fuzzy nanoassemblies: Toward layered polymeric multicomposites. *Science* **1997,** *277* (5330), 1232-1237.

13. Lynn, D. M., Peeling back the layers: Controlled erosion and triggered disassembly of multilayered polyelectrolyte thin films. *Advanced Materials* **2007,** *19* (23), 4118-4130.

14. Buck, M. E.; Lynn, D. M., Azlactone-functionalized polymers as reactive platforms for the design of advanced materials: Progress in the last ten years. *Polymer Chemistry* **2012,** *3* (1), 66-80.

15. Buck, M. E.; Schwartz, S. C.; Lynn, D. M., Superhydrophobic Thin Films Fabricated by Reactive Layer-by-Layer Assembly of Azlactone-Functionalized Polymers. *Chemistry of Materials* **2010,** *22* (23), 6319-6327.

16. Buck, M. E.; Lynn, D. M., Functionalization of Fibers Using Azlactone-Containing Polymers: Layer-by-Layer Fabrication of Reactive Thin Films on the Surfaces of Hair and Cellulose-Based Materials. *Acs Applied Materials & Interfaces* **2010,** *2* (5), 1421-1429.

CHAPTER 7: CONCLUDING REMARKS

The contributions outlined in this work towards deepening our understanding of block copolymer thermodynamics will continue to have an impact as BCP DSA moves to the full commercial integration. As process tolerances tighten, an ever more rigorous evaluation of the fundamental science at play will be necessary, and this in a world undergoing a massive paradigm shift. Technological advances in data collection, mining, and analysis have opened up a brand new field for exploration, allowing even further integration of experimental setup and simulation analysis. The novel approach described in Chapter 4 of identifying the fractional alignment of an assembled BCP film is limited in its current applicability but can easily be extended to high-throughput metrology of these systems. This approach provides near-real time feedback on qualitative trends of assembly behavior and kinetics even when the system is coarsely aligned, allowing evaluation of systems where single-defect metrology tools are impractical or impossible to use.

Similarly, the analysis of root causes of LER in Chapter 5 has identified many important trends which are already being used by materials suppliers to target specific performance metrics in their manufacturing processes. At the ever-shrinking dimensions of the nanotechnology world, a more rigorous analysis of the data, complete with deconvolution of high-, medium-, and low-frequency roughness modes and their potentially independent root causes will be necessary. New imaging tools and processes currently under development will also enable evaluation of roughness at different levels through the BCP film thickness, yielding additional insight into the assembly behavior and how LER can be mitigated and reduced.

Furthermore, with the identification of the role of guide stripe chemistry – both the strength of interaction with the directly guided stripe (Chapter 4) and designed interaction with the sidewall

chemistry (Chapter 3) – in BCP assembly behavior, a new parameter space has been identified for process exploration and optimization. In the world of self-assembling materials, the emphasis has primarily been on the materials themselves and less so on the methods used to direct their assembly. As we have demonstrated, clever tricks can be employed to achieve a sort of bottom-up self-alignment in chemical pattern fabrication, and further creativity will enable yet more complex and device-targeted substrate geometries and chemistries. The ongoing partnership with theoretically informed simulation experts will be strengthened with our latest experimental results showing BCP morphology as a function of chemical pattern geometry and chemistry (Chapter 2), enabling more accurate simulations and in turn providing predictive models for advantageous experimental – and ultimately commercial – process conditions. The exploration of this nanoworld will never be complete, but the steps we have taken will hopefully enable future generations of researchers with improved scientific understanding and more successful technological endeavors.